ENERGY HARVESTING IN A ROTATING TIRE ENHANCING NON-LINEAR VIBRATION

（非線形振動を励起させることによる回転する

タイヤ内でのエナジーハーベスティング）

張　云順

Contents

Abstract

A model for energy harvesting from a rotating automotive tire is exploited by application of the principle of stochastic resonance to enhance energy harvesting efficiency. A bistable response characteristic can be obtained by recourse to a small harvester comprising a magnetically repellant configuration, in which an instrumented cantilever beam can flip between two physical response states, when suitably excited by the rotation of a car wheel into which it is fitted. The rotation of the wheel creates a periodic modulation which enables stochastic resonance to take place, and as a consequence of this for energy to be harvested from road noise transmitted through the tire. A concisely mathematical model of the harvesting system is presented based on a series of experimental tests, and it indicates that a ten-fold increase in harvested energy is feasible over a comparable monostable case. In practice, the suggested application for this harvester is to provide electrical power for a tire pressure monitoring system.

For the case of actual wheel rotation, the present study investigates the effectiveness of a piezoelectric energy harvester, with the application of stochastic resonance to optimize the efficiency of energy harvesting. It is hypothesized that the energy harvester is subjected to on-road noise as ambient excitations while the wheel rotates at variable speeds, and meanwhile a tangentially acting gravity force as a periodic modulation force that can stimulate stochastic resonance. For a laboratory experiment, the energy harvester was miniaturized with a bistable cantilever structure, and the on-road noise was measured for the implementation of a vibrator. A validation experiment revealed that the energy harvesting performance of system was improved to capture powers, which were approximately 12 times that of the captured under only on-road excitation and 50 times that of the captured under only the periodic gravity force.

Moreover, through the investigation of up-sweep excitations with an increasing rotational frequency, it is confirmed that stochastic resonance is effective in improving the performance of the energy harvester, with a certain bandwidth of vehicle speeds. Furthermore, it is found that the ability of the energy harvesting can be enhanced over a wider rotational frequency under considering the combination of stochastic resonance and the high energy orbit phenomena of the bistable systems. An actual-vehicle experiment validates that the prototype harvester using stochastic resonance is capable of improving power generation performance for practical tire application.

On the other hand, nonlinear energy harvesters have already been exhibited to draw energy from ambient vibration owing to their particular dynamic characteristics, in which are feasible to desirable responses for broadband excitations of bistable and monostable systems. However, due to coexistence of the lower energy orbit, it is still a challenging topic that is how to achieve

the stability of the high energy orbit oscillating to improve the valid broadband of the excitations. This study also focuses on proposing a stiffness tunable energy harvester for rotational applications.

As the rotationally angular velocity gradually increases, the tensile stress to the cantilever beam is also self-adjusted with the increscent centrifugal force, causing the potential barriers of bistable type to become shallow, so that the cantilever beam has the ability to maintain the high energy orbit motion from bistable hardening type to monostable hardening behavior. From the implemented results, the valid bandwidth of angular frequency can be improved from 26 rad/s–132 rad/s to 15 rad/s–215 rad/s, under the case of the effect of centrifugal force on nonlinear vibrating behavior. In an actual-vehicle experiment, it is simultaneously demonstrated that the centrifugal force can significantly promote the performance of nonlinear energy harvesters in the tire applications.

Nomenclature and Abbreviations

B	Magnetic flux density
C , C_P	Electrostatic capacitance
D	Power intensity of ambient vibration
D_i	Amplitude of diode
E , E_K	Kinetic energy
E_b	Activation energy
E_1, E_2, E_3, E_t	Dissipated energy
E'	Young's modulus
F	Amplitude of harmonic force
F_R, F_t'	Resultant restoring force
F_M	Repulsive magnetic force
F_H	Tangential component of magnetic force
$F_M{}'$	Nonlinear spring force
F_c	Centrifugal force
F_t	Tangential centrifugal force
G	Gravity
G'	Transfer function
H	Centrifugal distance
I , I_b	Equivalently action
I''	Moment of inertia
L	Length
M	Particle mass
$\mathbf{M}_f$, $\mathbf{M}_c$	Magnetization amplitude
M_{fx}, M_{cx}	Magnetization amplitude in *x* direction
M_{fy}, M_{cy}	Magnetization amplitude in *y* direction
N	Ambient noise
P	Instantaneous power
P'	Dynamic force

R	Total resistance
R_{op}	Internal impedance of transducer
R_L	External load resistance
R_S	Internal impedance of sensor
T_c	Centripetal centrifugal force
U , U_d	Dimensional displacement amplitude
U_0 , U_M , U_0'	Potential energy
V	Voltage response
Z	Gravity acceleration
a	Linear coefficient
$\boldsymbol{a}$	Acceleration
a' , a''	Negative and positive equivalent linear stiffness
b	Nonlinear coefficient
$b_{n'}$	Amplitude of the first sampling point
$b_{n'+p}$	Amplitude of the last sampling point
c	Damping coefficient
c_m	Mechanical damping coefficient
c_e	Electrical damping coefficient
d	Distance between two magnets
$f(t)$	Linear amplification
f_H	Resultant force
g	Gravity acceleration
$g(t)$	Linear attenuation
i	Direction of current
j	Imaginative symbol
j'	Steady-state current
k	Spring constant
k'	Nonlinear spring coefficient
Δk	Equivalent stiffness coefficient

$k_B T$	Power intensity of ambient vibration
l	Center axis of vibration
l'	Centrifugal distance
m	Seismic mass
$\mathbf{m}_c$	Magnetic dipole moment vector
n_0	Population inside initial domain
n'	Number of the first counting point
p_1 , p_2 , p_3	Average generated power
p_0 , p	Stationary probability density
p'	Number of the last counting point
r	Radius
t	Real-time
u	Relative displacement
u'	Steady state solution
$\dot{u}'$	Velocity of steady state solution
$\ddot{u}'$	Velocity of steady state solution
v , $\boldsymbol{v}$	Velocity
v_S	Tangential speed
v_c	Centripetal speed
v'	Volume of the magnet
w	Transverse displacement
x_T , x , x_0	Relative displacement
y_c	Centripetal displacement
β^{-1}	Power intensity of ambient vibration
γ , γ'	Jump down frequency
δ	Replacement symbol
θ	Deflection angle
θ'	Electromechanical coupling coefficient
ω	Angular velocity of harmonic force

ω_b	Boundary frequency
ω_{cc}	Determination frequency
ω_n , ω_0	Resonance of nonlinear system
ω_{SR} , $\omega_{SR}{}'$	Frequency of stochastic resonance
ϖ_d	Positive solution of jump-down frequency
ψ	Replacement symbol
κ , κ^+ , κ^-	Escape rate
μ	Permeability of free space
ϑ	Static linear shape
Φ	Replacement symbol
μ_0	Initial phase angle
τ	Total experiment time
$\triangle U$	Activation energy
ς	Damping coefficient
ξ	Ambient noise

Acknowledgements

I sincerely appreciate to my supervisor Dr. Kimihiko Nakano, Associate Professor in The University of Tokyo for his helpful guidance, positive encouragement, and academic suggestion over the past three years. His enthusiasm and attitude to details will continue to influence my academic career in the future.

I greatly thank Professor Yoshihiro Suda, Professor Shinichi Warisawa, Professor Beom Joon Kim, and Associate Professor Takeshi Oishi. As referees of my dissertation, all of their valuable comments and constructive suggestions are helpful to complete my research and improve the dissertation.

I deeply wish to thank Dr. Rencheng Zheng, the Project Associate Professor of the K. Nakano Laboratory. He strenuously supported me in my experiments and enthusiastically helped me so much not only in my research but also in my daily life. I also want to convey my sincere thanks to Professor Matthew P. Cartmell, University of Strathclyde, for his valuable assistance and productive discussions.

I appreciate Dr. Tsutomu Kaizuka, the Research Associate of the K. Nakano Laboratory, and he gave me much advice about experimental design and helped me to carry out the experiments. I also appreciate Dr. Keisuke Shimono, Dr. Kenji Ejiri, the previous Project Researchers of K. Nakano Laboratory, and Dr. Dongxu Su, the Degree Recipient of K. Nakano Laboratory for their helpfully technical assistant.

I express my gratitude to the staffs of the Central Workshop of the Institute of Industrial Science, The University of Tokyo, who are Mr. Yoshihiro Itakura, Mr. Kentarou Shikada, and Mr. Etsuo Yatagai. Thanks to them for the important suggestions and assistance during the process of the equipment manufacturing.

I also would like to express my gratitude to Ms. Atsuko Hasegawa, the Secretary of the K. Nakano Laboratory, for his warmly encouragement and care on my daily life as well as the research activities.

Meanwhile, I want to thank to Mr. Bo Yang, Mr. Zheng Wang, Mr. Antonin Joly, and all the other members of the K. Nakano Laboratory, they gave me their help with their kindness in my research and daily life.

Last but not least, I can never forget the support from my parents and two sisters during this unforgettable period of my study abroad. I appreciate them from the bottom of my heart.

February 6, 2017

Yunshun Zhang

Chapter 1

Introduction

1. Introduction

1.1 Background

A primary motivation for the creation of energy harvesters is to avoid the regular replacement of batteries within electrical sensing and instrumentation systems, particularly if they are remotely located. Vibration energy harvesting has been a rich field for research for a considerable time [1][2][3], and designs based on linear systems are popular because of their functional simplicity albeit a little limited due to high efficiency only around resonance [4][5][6]. Meanwhile, effective designs were also proliferated for harvesting of thermal energy [7][8][9] and human motion [10][11][12]. Efficient harvesting of road vibration through vehicle is of great interest [13] within vehicle-fitted harvester of electromagnetic [14][15], electrostatic[16], and piezoelectric [17][18]. With the references to vehicle environments, it is still a key point to maximize the relatively narrow operating bandwidth of the running speeds.

Currently, several general approaches are proposed in order to widen the bandwidth, by tuning the resonant frequency of the linear harvester during operation, conducting the frequency-up conversion, implementing multi-mode oscillators, and employing nonlinear oscillators with bistable systems to widen the bandwidth. Although these methods are equally applicable to rotational systems, the use of nonlinear bistable systems to achieve automobile vibration power generation has shown real potential for broadening bandwidth of energy harvesting [19][20]. However, the theory of stochastic resonance has not so far been successfully applied to rotational automobile tires, noting that they can produce a larger vibrational response than for a typical resonance, when a weak periodic force and a noise excitation are input into a nonlinear bistable system [21].

As a conclusion, the energy of road noise excitation is trapped in the frequency bandwidth of 5 Hz–1 kHz for different tires, different road conditions as well as different driving speeds[22]; thereby, a novel model must be sensitive to the broadband vibration for stimulating the phenomenon of stochastic resonance. Therefore, in view of the principle of stochastic resonance, a novel model is derived to demonstrate that tire rotation can make the phenomenon of stochastic resonance occur, which is different from the previous studies where a weak external periodic force was manually added [23][24]. This system can be autonomously self-exciting from a combination of gravitational effects and the rotation of the tire, thereby without consuming extra energy. When the energy harvester device is mounted on a rotating tire the road noise excitation coupled with the periodic rotational force caused by the tire revolution and gravitational effect of the magnetic end mass, provide the necessary external effect of the magnetic end mass, and the necessary external conditions for the occurrence of stochastic

resonance. Besides that this fabricated energy harvester has dimensions much smaller than applied in previous studies, enabling it to be possibly quite widely applied in the automotive field. Moreover, instead of a typically low frequency of 3 Hz as encountered for stochastic resonance, this study shows that power harvesting can be enhanced by stochastic resonance at a higher frequency of 15.6 Hz.

Meanwhile, stochastic resonance as a physical phenomenon has recently been proposed to explain the periodicity of Earth's glaciation, where the output response can be greatly amplified with a certain probability by adding noise to a weak periodic signal [25]. In recent years, this phenomenon has attracted considerable attention for information transmission and detection [26][27][28][29], biological neuro analysis [30][31][32][33], and image processing [34][35][36][37]. In the mechanical engineering field, it has been theoretically investigated whether stochastic resonance can be applied to improve the efficiency of energy harvesting [38]. Consequently, an experimental study has realized the one-degree-of-freedom behavior of stochastic resonance in a bistable vibrating energy harvester [24][39]. Nevertheless, in the rotational environment of an automobile wheel, such behavior coexists with the two-degree-of-freedom motion of the wheel rotation and vibration.

In this study, ideal white noise and a periodic force were employed to simulate rotational wheel motion, and the energy harvesting efficiency is improved by the realization of stochastic resonance. By application of the on-road noise measured for low-speed automobile wheels, a mathematical model of vibration energy harvesting is presented for the simulation analysis of stochastic resonance. Furthermore, a macro-scale energy harvester is fabricated, and only displacement response is studied to know its dynamic performance. However, it is still unclear for their harvesting effectiveness in a real-world environment.

Therefore, considering on-road noise and periodic acceleration by gravity for vehicle traveling on a paved road, the present study also focuses on the effectiveness testing of a piezoelectric energy harvester on vehicle tires using stochastic resonance, and the energy harvesting characteristics are comprehensively investigated through simulation and laboratory experimental analyses. It shows that the appearance of stochastic resonance is not limited to a constant rotation frequency but can be maintained under varying frequencies, indicating that more energy can be harvested with a bandwidth for rotational systems. Moreover, the bandwidth can be further broadened by combining the stochastic resonance and high energy orbit oscillation.

The nonlinearity of the system that can improve the performance of the energy harvester over a wider bandwidth is presented for enhancing energy harvesting over that of the conventional linear energy harvester [40][41][42]. It is classified into bistable [43][44], monostable hardening , and monostable softening cases [45][46]. Through adjusting the parameters of the

above nonlinear systems, the systems can appear an enhanced high-energy orbit motion over a certain frequency range. Meanwhile, because of the existence of unstable and low-energy orbits, it is necessary to stabilize the high-energy orbit all the time by the adjustability of system parameters, with a widely variable frequency of environment excitations.

A nonlinear energy harvesting model that is considered to apply to rotational environments, which is different from the previous researches of this study that the centrifugal force is not exploited. The linear stiffness of this system can be tuned to achieve the sustained high-energy orbit oscillating by stimulating the system of bistable into monostable hardening type under considering the increasingly centrifugal force effect. In comparison to a passive self-tuning linear and pendulum energy harvesters adopted to rotational motion [47][48][49], the apparent advantage in the nonlinear section is specifically analyzed in this study.

1.2 Tire Rotating Energy Harvesting

With the increasing requirements of advanced driving assistance systems, researchers have developed a tire-pressure monitoring system that can provide the driver with the tire condition via wireless transmission [50][51][52]. However, because it is inconvenient to replace or recharge the batteries of a monitoring system, there is a desire to establish an effective energy harvesting system [53].

1.2.1 Piezoelectric

Several researchers have attempted to exploit the piezoelectric energy harvesters for rotating environments. Specifically, a linearly piezoelectric energy harvester using a cantilever beam has been proposed, where the centrifugal force is used to stimulate the natural frequency of the energy harvester system matching the rotational frequency [54]. A linear MEMS energy harvester using tire shock excitations was proposed for automotive applications; however, it can extract more energy only in the case of high-speed driving, and the energy harvesting efficiency depends on the concave-convex condition of the road surface [55]. A nanogenerator layer was attached on the inner surface of the tire, and the energy was harvested by the bending of the piezoelectric film; however, the energy harvesting performance was investigated using a bicycle tire instead of a real vehicle tire also it would cost too high for fabricating or replacing the piezoelectric film [56][57][58] as shown in Figure 1.1. Moreover, a linear energy harvester was presented to optimize the frequency band of operation based on a feedback loop control system [59].

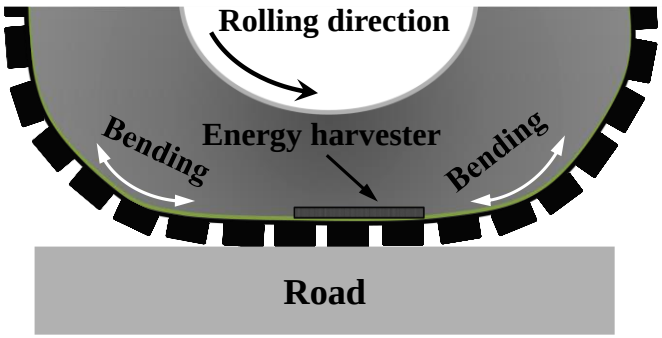

Fig. 1.1. Tire energy harvesting using the bend deformation during vehicle movement.

Nonlinear systems have a small structure, which can improve the performance over a wider bandwidth for harvesting more energy compared with a conventional linear system; therefore, they have also been used for rotational energy harvesting. Figure 1.2 demonstrates an offset pendulum with a nonlinear bistable restoring spring structure that has been developed to improve the operational bandwidth of the system considering the effects of gravity [60]. However, the cited studies ignored the effects of road noise on the dynamic performances of the harvesting systems as well as the large centrifugal acceleration on the stiffness of the beam; also the power density is still at a relatively low level around 0.42 $\mu W/cm^3$ under low driving speeds.

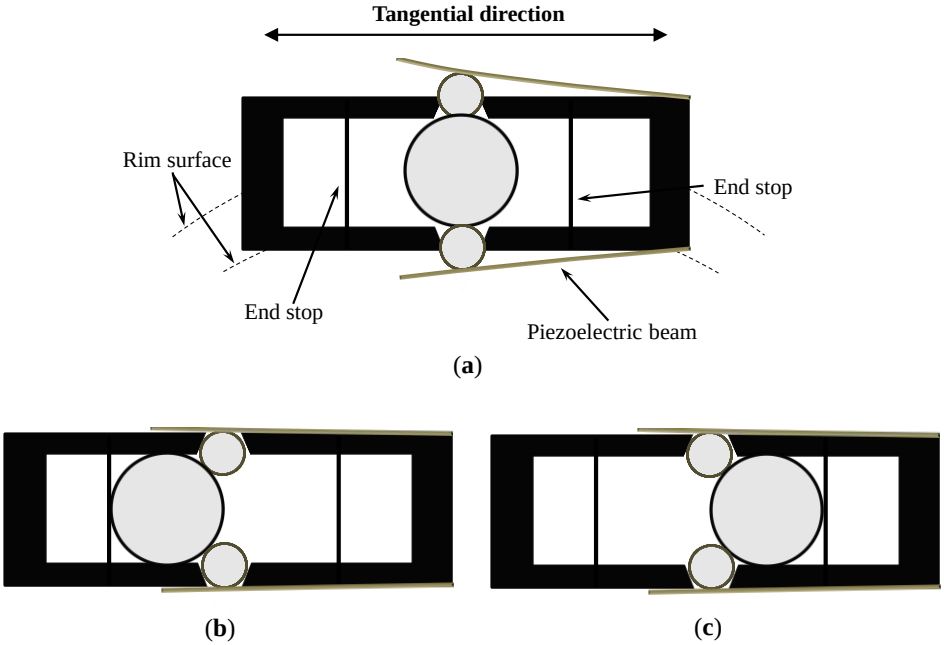

Fig. 1.2. Illustration of the nonlinearly bistable tire energy harvester: (**a**) unstable state with maximum deflection; (**b**) stable state on un-deflected position; and (**c**) another stable state on un-deflected position.

1.2.2 Electromagnetic

Electromagnetic as a conventional approach which makes use of the relative motion between magnets and coils, has been investigated by many researchers [61][62]. The magnets often linearly or rotationally move through the stationary coils, which is different from the above introduced piezoelectric energy harvesters that often take the form of cantilevers. One approach is to utilize inertial type, using which a levitated magnet is urged past the fixed coil among the energy harvester that is mounted on the tire wheel as a result of tire contact with road surface [63]. The advantages of this type of energy harvesters are its design simplicity and it is easy to parametrically determine it in such a Watt that its resonance frequency matches the frequency of the external excitation [64].

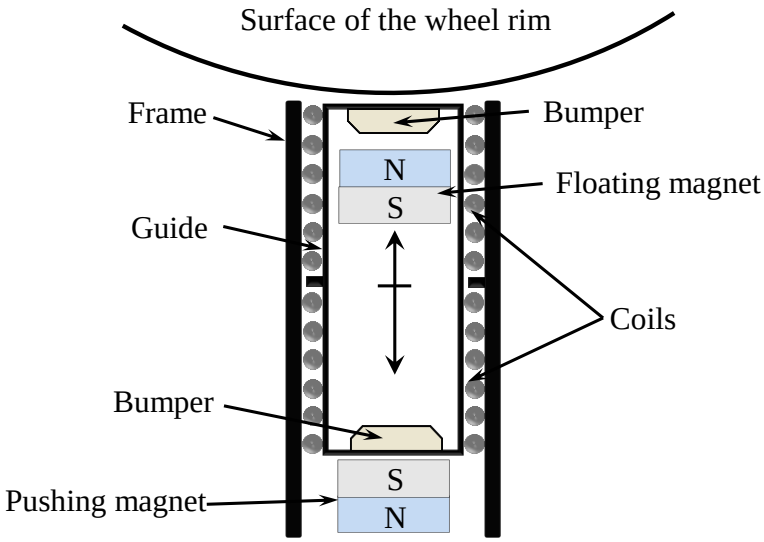

Fig. 1.3. A schematic layout of the nonlinear energy harvester.

In order to broaden the operational frequency of tire rotation, a natural frequency adjustable electromagnetic device to collect energy was proposed by [65], which is applied for a spinning wheel while the vehicle travels around a certain bandwidth of speeds. The rotating wheel produces a centrifugal force while the proof mass is subjected to a tension force from one side spring and an extrusion force by another spring, which causes the variation of the specific spring constants. Hence, the natural frequency of the spring-mass system can be adjustable by the centrifugal force of the wheel rotating. Other researchers also presented a new non-resonant micro-energy harvester based on the combination of the free and impact vibration to increase the operational frequency [66]. Additionally, a suspended energy harvester has also been developed; its natural frequency varies because of variations in the transverse gravity force

during plate rotation, then the harvester mean power of the harvester was improved to 30 μW with extrapolated power density of 0.94 μW/cm^3 under the condition of low-frequency rotating [67].

Furthermore, a nonlinearity system is presented and its configuration is shown in Figure 1.3. The energy harvester is mounted to the surface of the wheel rim, it is subjected to the radial acceleration which resulted from centrifugal force, contact zone and changes its shape, and the preload from the pushing magnet. An analysis of different nonlinearities of the system at different vehicle speeds and a study on the combined effect of softening and hardening behavior of the device are performed and discussed [68].

1.2.3 Electrostatic

The electrostatic energy harvester captures power by the variable capacitor while it is driven by the environmentally mechanical vibrations. As the capacitance decreases, the charge will move from the capacitor to a storage device or to the external resistance load resulting in the conversion of the electrical energy. The classification of the electrostatic energy harvesters are mainly defined by the varying overlap area and the gap between electrode fingers, as the configuration shown in Figure 1.4 [69]. Although, a few devices can realize the output power of 4.28 μW level with a high power density of 0.079 μW/mm^3 by using the electrostatic energy harvesters. Nevertheless, its real-world application on rotating tire can deliver an average power of 3 μW around low speed of 30 km/h, then can be increased linearly as the speed increases, which is sufficient for powering the electrical requirement of tire pressure sensors [70].

However, because the risk of the contact between the electrodes of the capacitor [71], and the fact that electrostatic energy harvester require an initial voltage charged action or at least in a while before the beginning of energy harvesting, which makes them unsuitable as the main power source for the tire application.

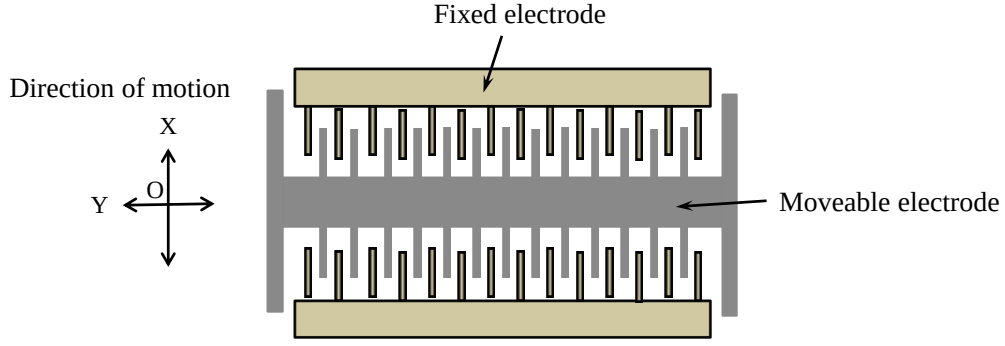

Fig. 1.4. A schematic layout of the electrostatic energy harvester.

1.3 Broadening Frequency Bandwidth

In this section, the descriptions of the typical and novel approaches for widening the operational bandwidth of the excitations in this field are briefly introduced in the following parts, including the resonant frequency tuning, multi-frequency converter array, frequency-up conversion, and nonlinear approach.

1.3.1 Linear Resonant Frequency Tuning

As the typical linear energy harvester can only effectively deliver the electric power when its natural frequency is equal to the input vibration frequency, self-tuning frequency methods that can enable the energy harvesting system to adjust to the variable input frequencies are exploited to increase the functionality of energy harvesting over time. Since the square of the nature resonance frequency is directly proportional to the spring constant and inversely proportional to proof mass, the modification of the frequency therefore focus on the ways to adjust the spring constant and the proof mass characteristics of the harvester. For instance, some researchers have proposed the varying position of proof mass that can self-tune the nature frequency of the systems [72][73]. Figure 1.5 shows the schematic of the mass-type self-tuning resonance frequency. However, the rapidly real-time response of the proof mass is difficult to control.

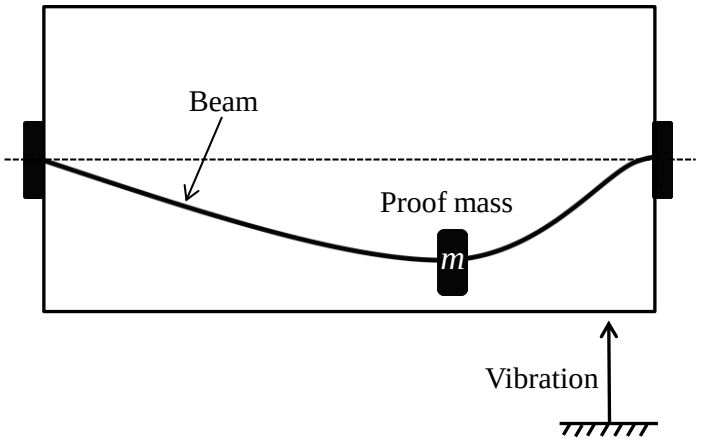

Fig. 1.5. Schematic of the mass-type self-tuning resonance frequency.

The frequency also can be tuned by the changeable effective stiffness of the beam through piezoelectric actuators [74], and a magnetic force [75]. For piezoelectric methods the frequency of main beam is altered electrically by applying mechanical preloads actuator through piezoelectric actuators as shown in Figure 1.6, and the stiffness of the beam can also be changed

by varying the distance of the permanent magnets. Although the consumed power for tuning processing is only the level of micro-Watt [76], it becomes difficult for tuning the energy harvester automatically to follow the frequency of external excitations.

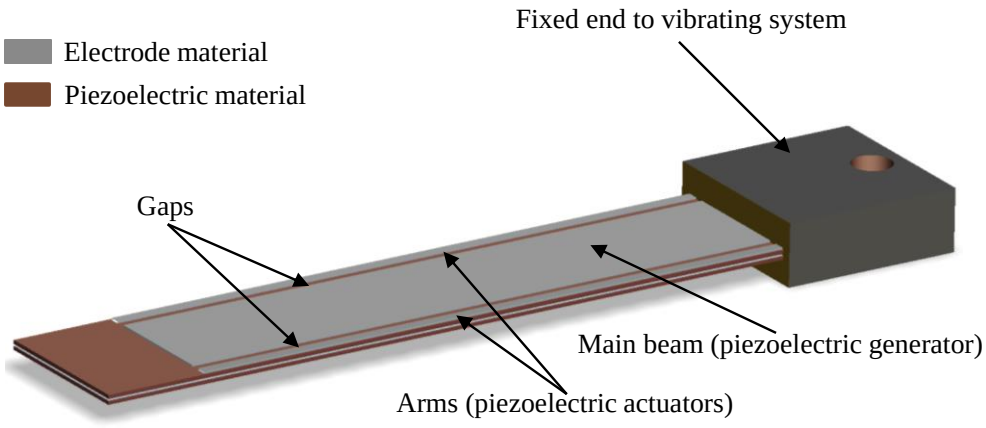

Fig. 1.6. Configuration of the stiffness tunable generator based on piezoelectric actuators.

1.3.2 Multi-Frequency Converter Array

In this method, the response bandwidth is broadened by designing a harvester that comprises of several small fabrications of beams and masses; each of them has different natural frequency due to the diverse dimensions of the components. That is why it is named multi-frequency converter array. As the variation of the external frequency, the harvesters can still keep some of the beams reach its natural frequency, causing a wide operational frequency range [77][78].The different beams and tip masses are used to assemble the array of harvesters, and the operational bandwidth can be increased only if the number of the arrayed devices is added, which will enlarge the volume of the harvester. Therefore, the power density is reduced to a low lever.

1.3.3 Frequency-up Conversion

In practice, a large part of the ambient vibration happens at a low frequency, for example vehicle body, human motion, and rotational tires. Therefore, the frequency-up conversion is adopted for the amplification of the response of the harvester.

Previous study, a device made of polyethylene terephthalate which consists of two slender bridges and cantilever beams at the center of the bridges and a proof mass mounted on the bridge at the center, is proposed as the up-conversion system. When the excitation applied to the buckled bridge exceeds the threshold acceleration value, the rapid transition between two

equilibrium states generates a highly accelerated excitation of the buckled bridge, thereby causing the attached beams to vibration freely at the natural resonance frequency independent of the input frequency[79]. However, in the most cases, the vibrational amplitude of the ambient excitation cannot always appear adequately large over wide range of frequency, which leads to the excitation source that is too weak to stimulate the bridge for transiting between equilibrium states going on all the time. Other related researches was presented in the literatures [80], a two-stage cantilever beam and a mass-spring system with mechanical energy transfer teeth as the fabricated parts of the energy harvester that can intermittently transfer its primary vibrating energy to one or more secondary vibrating beams. However, in this case, the problem is that the more vibrating energy will dissipate because of the impact between transfer teeth and beams.

1.3.4 Nonlinear Approach

Many researchers have recently exploited the nonlinearity systems as a means to extend the coupling between the excitation and a harmonic oscillator to a wider broadband of the frequency for enhancing the transduction of vibrating energy harvesters. The most common approaches to the design of such systems introduce a nonlinear restoring force based on the using of the magnetic or mechanical forces [81][82][83]. According to the type of nonlinearity, the nonlinear energy harvesters can be generally classified into monostable, bistable cases and more than two stable states named multi-stable in this dissertation. In the condition of certain harmonic excitation, both the bistable and the hardening-type monostable nonlinearities can provide enhanced energy harvesting over that of the conventional linear energy harvester.

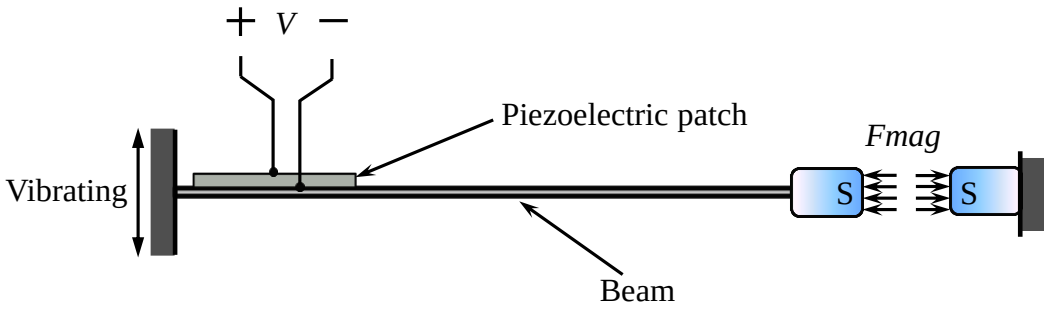

Fig. 1.7. Schematic of the bistable piezoelectric energy harvester.

More recently, the intentional introduction of piezoelectric beam-type design has been an expressly interesting and promising topic that is being received more attention due to its simple construction and the characteristic of the efficient energy harvesting. As one of the

representative configuration shown in Figure 1.7, a magnet is attached to the end of the beam while another one is fixed in the reference frame. The restoring force can be adjusted by altering the distance between two magnets, when the distance is kept on the certain value, the beam can show the behavior of the nonlinearity meanwhile have two stable states. By the parameter design, the response of the beam can be induced a jump-up action owing to the effect of the high orbit of the bistable system [41].

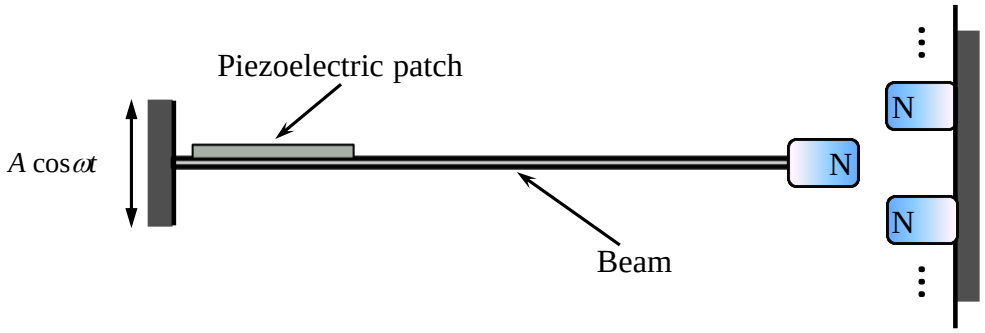

Fig. 1.8. Schematic of the multi-stable piezoelectric energy harvester.

The Figure 1.8 depicts that the stable states will be increased to multiple type when the magnets are added two or more, therefore, with regard to the same deflection of the beam at the end position of the beam, the potential wells of the multi-stable energy harvester (TEH) would be much shallower than that of the bi-stable energy harvester (BEH). Therefore, the BEH needs lager kinetic energy to carry out the high-energy orbit motion. In other words, the TEH may need low excitation level to jump through potential wells than the BEH. Hence, the TEH is more suitable to harvest more ambient energy for a wider frequency of the excitation [84].

Another is the monostable energy harvesting system that comprises a cantilever beam on which two piezoelectric patches are attached at the root of the beam and a magnetic mass fixed at the end of the beam as shown in Figure 1.9. The magnet interacts with two other fixed magnets by the same polarity, and by altering the distance of the magnets the harvester exhibits a softening nonlinearity or a hardening type [85]. Although the nonlinear systems demonstrate their superior properties in many respects, it is still difficult to optimize the structures and find suitable sources of vibration over a wide range of the practical applications due to the complexity of nonlinearity systems.

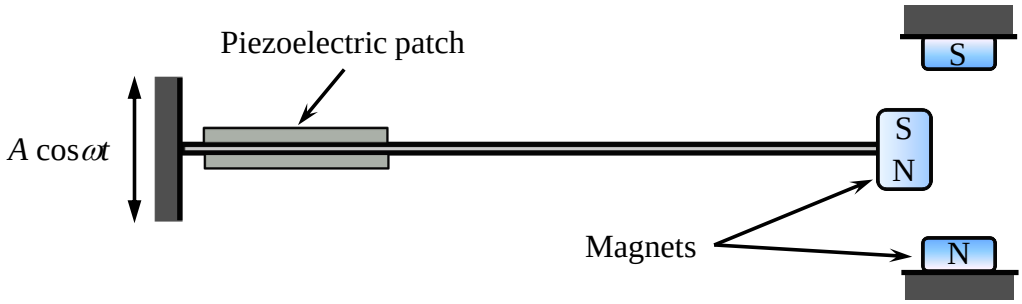

Fig. 1.9. Schematic of the monostable piezoelectric energy harvester.

1.4 Objective and Structure

This dissertation primarily focuses on widely enhancing tire energy harvesting in a rotating tire by nonlinearly vibration systems. The main objectives of this dissertation are highlighted as follows:

(1) Attempt to take advantage of the nonlinear characteristics for harvesting the vibrational energy from the source of rotating gravity combined with ambient road noise excitation on the automobile tires.

(2) Investigating the approaches by theoretical as well as numerical analyses.

(3) Validating the proposed approaches for improving the performance of energy harvesting under a broadening bandwidth of frequency on the basis of laboratory tests.

(4) Achieving the nonlinear vibration on the application of the rotating tires by actual-vehicle experiments.

In Chapter 1, the background of this researcher including the existing methods for tire energy harvesting which relies on the types of piezoelectric, electromagnetic, and electrostatic are introduced by enumerating the typical model structures. Meanwhile, Chapter 1 summarizes the principles of broadening the frequency bandwidth of the excitations covering frequency tuning frequency, multi-frequency converter array, frequency-up conversion, and nonlinear approach.

As presented in Chapter 2, the dynamics characteristics of the nonlinearities are analyzed, which includes the principles of the theory of bistable, monostable and stochastic resonance. The existing challenges of nonlinear vibration on the tire rotational circumstances are also offered.

The main efforts of Chapter 3 are concentrated upon the methodologies of enhancing energy harvesting. Using the unique dynamic characteristics of the rotating tire provides the necessary conditions for the stimulus of stochastic resonance, by which the mechanical output of the amplitude can be improved to a highly vibrational level. The efficient bandwidth can be further

broadened under considering the combination of stochastic resonance with the high energy orbit oscillation. However, owing to the existence of the low energy orbit, how to maintain the stability of the high energy orbit for a wide range of driving speeds becomes an important challenge. Consequently, in Chapter 3, proposing an approach using centrifugal force of tire rotating for tuning the stiffness of the cantilever ensures that the high energy orbit oscillation can be stabilized for a wider bandwidth rather than jumping down the low energy orbit.

In Chapter 4, by the numerical analyses and simulation investigations, the occurrence of stochastic resonance is feasible under both simulating condition and measured on-road noise excitation. And the valid bandwidth is possible to be enlarged to a wider range by combining stochastic resonance with high energy orbit motion, and stabilizing the high energy orbit motion by transferring the initial system from the behavior of bistable to monostable.

In Chapter 5, the experiment study including the laboratory as well the actual-vehicle experiments, are carried out for the validation of the effectiveness of the proposed nonlinear systems that the power harvested is enhanced by a mW level from a rotating tire by the particular nonlinear vibration or the mixture of different types of nonlinear characteristics.

In Chapter 6, the discussions regarding the coexistence of three different nonlinear oscillating phenomena of stochastic resonance, high energy orbit motions of bistable and monostable, are furthered for confirmation of the combined nonlinear vibrations. After that, the design of the rectifier circuit and the comparison with other energy harvesting strategies are discussed in the end.

In Chapter 7, it concludes the details and significances of this research.

Chapter 2

Energy Harvesting from Nonlinear Vibration

2. Energy Harvesting from Nonlinear Vibration

2.1 Nonlinear Systems

In this chapter, the basic dynamics and its characteristics are introduced for the monostable and bistable Duffing oscillators under harmonic excitations, which will be used for the theoretical derivation in the following chapters.

2.1.1 Monostable Energy Harvester

The motion Equation of a monostable piezoelectric beam-based harvester under a harmonic excitation can be obtained as

$$m\ddot{x}_T + c\dot{x}_T + ax_T + bx_T^{\,3} = F\sin\left(\omega t + \mu_0\right), \qquad (2.1)$$

$$\left(a > 0, \quad b > 0 \; or \; b < 0,\right)$$

where x_T is the relative displacement, and m is the seismic mass which is coupled with a restoring force with cubic nonlinearity and an energy transducer with damping coefficient c, excited by a harmonic force $F\cos\left(\omega t + \mu_0\right)$, t is the real time, F is the amplitude of harmonic force, ω is the angular velocity of harmonic force, and μ_0 is the initial phase angle between the excitation and the response. The symbol of a is the linear coefficient term of the nonlinear system, the negative value represent the bistable type, or else the system reflects the monostable behavior. The symbol of b is the nonlinear coefficient term of the nonlinear system. The positive and negative nonlinearity of b indicate a hardening and softening characteristics, respectively. As presented in Figure 2.1 with the same displacement the potential energy of hardening type is higher than linear, and softening is lower than linear type.

To obtain the response of the oscillator, the frequency-amplitude relationship needs to be investigated. The approach to obtain the analytical solution of the Equation is the method of harmonic balancing method (HBM). It is assumed that the steady state solution of Equation (2.1) is of the form

$$u' = B + U\cos\omega t, \qquad (2.2)$$

so that the corresponding the response of the velocity and acceleration is written by

$$\dot{u}' = -\omega U \sin \omega t \,, \tag{2.3}$$

then

$$\ddot{u}' = -\omega^2 U \cos \omega t \,. \tag{2.4}$$

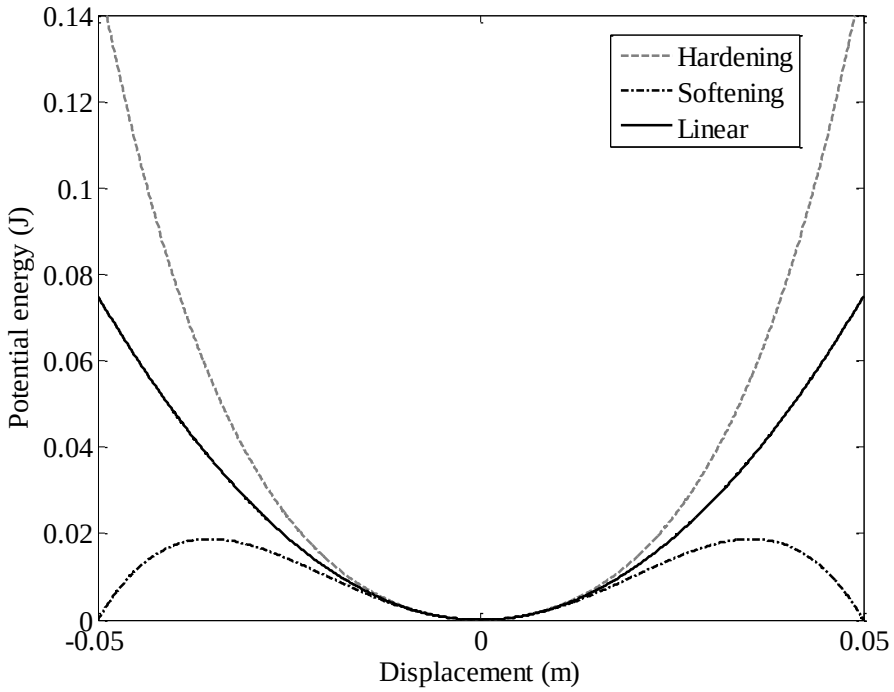

Fig. 2.1. Potential energy diagrams for the three cases: hardening, softening, and linear types.

Submitting the Equations (2.2), (2.3) and (2.4) into the Equation (2.1), it is arranged to

$$-m\omega^2 U \cos \omega t - c\omega U \sin \omega t + aU \cos \omega t + bU^3 (\cos \omega \mathrm{t})^3 = F \sin\left(\omega t + \mu_0\right). \tag{2.5}$$

The term of *b* is equally transformed using elementary trigonometric relations. By ignoring the super harmonics, it gives as

$$bU^3 (\cos \omega \mathrm{t})^3 = \frac{3}{4} bU^3 \cos \omega t + \frac{1}{4} bU^3 \cos(3\omega t) \,. \tag{2.6}$$

Substituting the Equation (2.6) into Equation (2.5), the re-arranged frequency-amplitude Equation is shown as

$$\left(-m\omega^2 U + aU + \frac{3}{4}bU^3\right)\cos\omega t - c\omega U \sin\omega t = F\sin\mu_0 \cos\omega t + F\cos\mu_0 \sin\omega t\,, \tag{2.7}$$

by equating the coefficient terms of the $\cos\omega t$ and $\sin\omega t$, the following relationships are given

$$-m\omega^2 U + aU + \frac{3}{4}bU^3 = F\sin\mu_0\,, \tag{2.8a}$$

$$-c\omega U = F\cos\mu_0\,. \tag{2.8b}$$

Squaring the Equations (2.8a) and (2.8b) respectively, and summarizing them to obtain

$$\frac{9}{16}b^2U^6 - \frac{3}{2}b\left(m\omega^2 - a\right)U^4 + \left[\left(m\omega^2 - a\right)^2 + c^2\omega^2\right]U^2 - F^2 = 0\,. \tag{2.9}$$

The Equation (2.9) expresses the frequency-amplitude relationship of the nonlinear monostable hardening type. Based on the solutions of the sixth order polynomial of the frequency-amplitude equation, the frequency and velocity amplitude curve of the monostable hardening type can be drawn as shown in Figure 2.2. The initial black curve represents the high energy orbit, as the frequency of the excitation is increased, the response of the beam will rise along the high energy orbit until the peak point. After that the beam jumps down the low energy orbit and keep the low level vibration. The red curve shows the unstable characteristics of this monostable system. Figure 2.3 by increasing the linear and nonlinear stiffness to stabilizing the high energy orbit motion, therefore the operational bandwidth can be further improved for energy harvesting.

However, the expressions of the jump-down point of the oscillator should be derived, which are necessary for the high-energy orbit stabilization. Solving Equation (2.9) for the positive solutions obtains the jump-down and jump-up frequency expressions as

$$\varpi_d \approx \sqrt{\frac{3\delta U^2}{4} + 1 - 2\psi^2 \pm \frac{\sqrt{1 - 4\psi^2 U^2\left(1\text{-}\psi^2\right) - 3\delta\psi^2 U^4}}{U}}\,, \tag{2.10}$$

where ϖ_d are expressed as the positive solution of jump-down and jump-up frequency, and the amplitude of jump-down frequency is greater than the one of jump-up frequency, defining the

$\delta = bF^2/a^3$, $\psi = c/2m\omega_n$. Assuming the $\psi^2 << 1$, the Equation (2.10) can be simplified to

$$\varpi_d \approx \sqrt{\frac{3\delta U^2}{4} + 1 + \frac{\sqrt{1 - 4\psi^2 U^2 - 3\delta\psi^2 U^4}}{U}} . \tag{2.11}$$

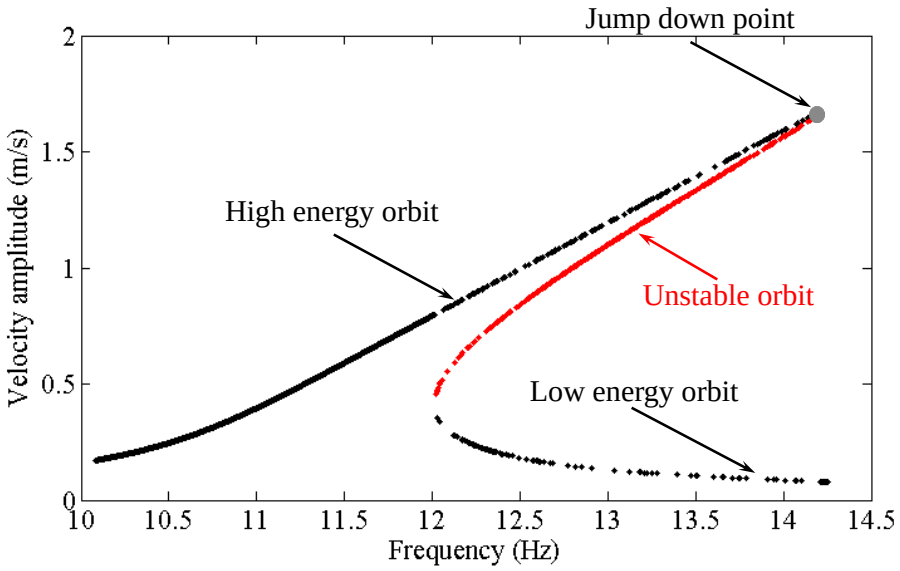

Fig. 2.2. Frequency-amplitude response curve of monostable hardening system.

The jump-down frequency can be regarded as the resonance point of the nonlinear monostable oscillator and in the case of the frequency of the external excitation approaching to the jump-down frequency; the response amplitude becomes the maximum. The relationship among δ , ψ , and U can be obtained by the approach presented by [86][87] as

$$1 - 4\psi^2 U_0^{\,2} - 3\delta\psi^2 U_0^{\,4} = 0 , \tag{2.12}$$

then re-arranging the Equation (2.12) yields

$$U_d \approx \sqrt{\frac{2}{3\delta}\left(\sqrt{1 + \frac{3\delta}{4\psi^2}} - 1\right)} . \tag{2.13}$$

Substituting the Equation (2.13) into Equation (2.11), the jump-down frequency Equation γ can be expressed in the non-dimensional form as

$$\varpi_d \approx \sqrt{\frac{1}{2}\left(\sqrt{1+\frac{3\delta}{4\psi^2}}+1\right)}. \tag{2.14}$$

The dimensional expression of jump-down frequency is yielded by substituting the equation of its natural frequency of nonlinear system $\omega_n = \sqrt{a/m}$ into Equation (2.15) as

$$\gamma = \omega_n \varpi_d, \tag{2.15}$$

Substituting Equation (2.14) into Equation (2.15) and considering the relationships of $\delta = bF^2/a^3$, $\psi = c/2m\omega_n$ obtain the specific dimensional expression of jump-down frequency as

$$\gamma = \sqrt{\frac{1}{2m}\left(\sqrt{a^2+\frac{3mbF^2}{c^2}}\right)+\frac{a}{2m}}. \tag{2.16}$$

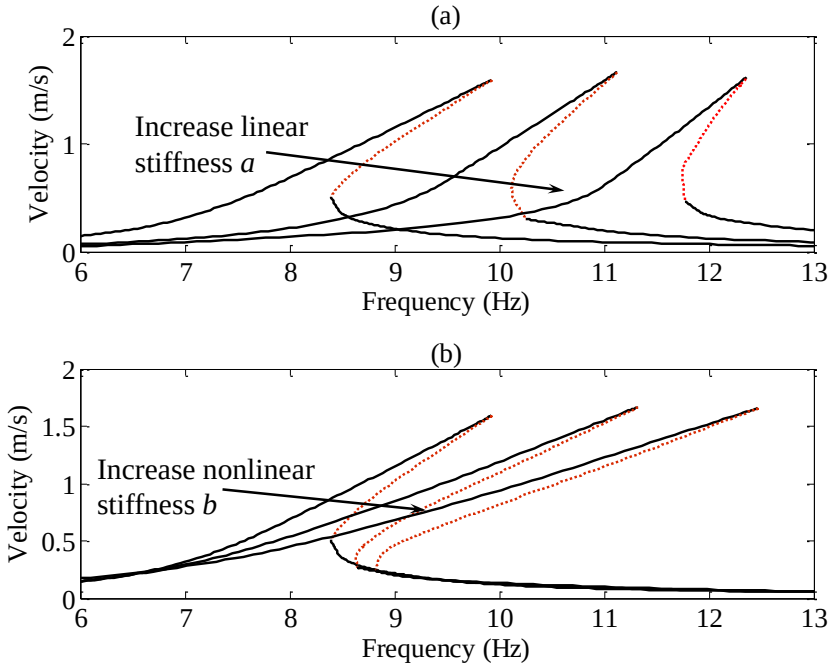

Fig. 2.3. Variable characteristics of the monostable system with the incensement of the linear and nonlinear stiffness.

2.1.2 Bistable Energy Harvester

The motion Equation of bistable oscillator can be expressed in dimensional form as

$$m\ddot{x}_T + c\dot{x}_T - ax_T + bx_T{}^3 = F\sin\left(\omega t + \mu_0\right), \quad (a>0,\quad b>0), \tag{2.17}$$

where *a* is the negative amplitude and *b* is the positive amplitude. Potential energy of the system can be governed as

$$U_0(x_T,t) = -\frac{1}{2}ax_T{}^2 + \frac{1}{4}bx_T{}^4, \tag{2.18}$$

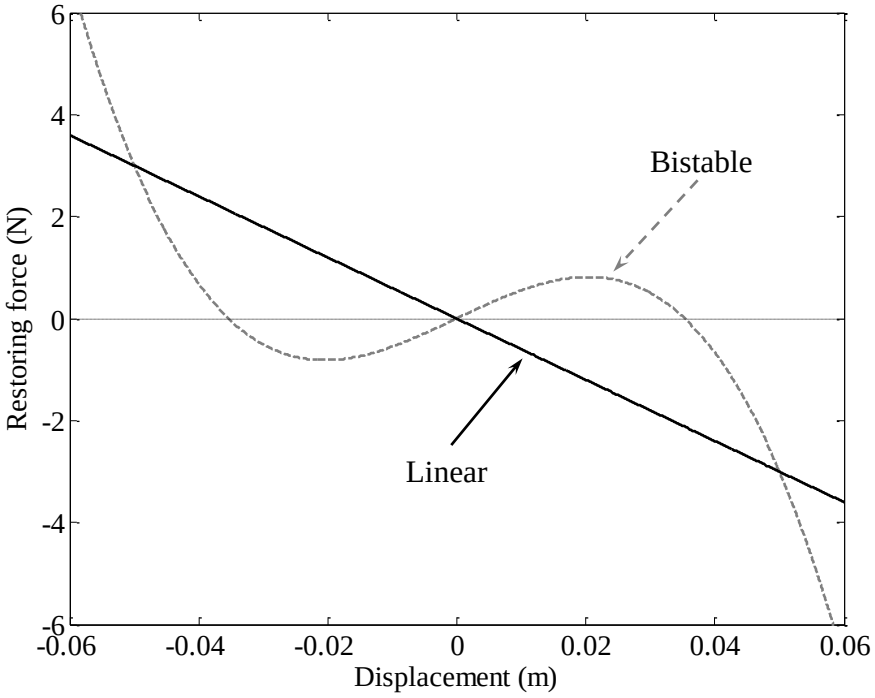

Fig. 2.4. Comparison of restoring force under two case of linear and bistable systems.

Differentiating Equation (2.18), the fitted polynomial expression of restoring force of bistable system can be given

$$F(x_T,t) = ax_T - bx_T{}^3. \tag{2.19}$$

As shown in Figure 2.4, in the case of the typical linear system, it has only one stable point around the equilibrium position. Otherwise, in the case of the bistable system, there are two stable states also the restoring force decreasing linearly.

Using the HBM the same with the monostable case, the frequency-amplitude response equation of bistable can also be obtained, which can be expressed as

$$\frac{9}{16}b^2U^6-\frac{3}{2}b\left(m\omega^2+a\right)U^4+\left[\left(m\omega^2+a\right)^2+c^2\omega^2\right]U^2-F^2=0\,. \tag{2.20}$$

Based on the solutions of the sixth order polynomial of the frequency-amplitude equation, the frequency-amplitude response of bistable system is described as shown in Figure 2.5, from which it can be observed that because of the stabilization of the high energy orbit the efficient bandwidth of the frequency can be broadened to a wider range.

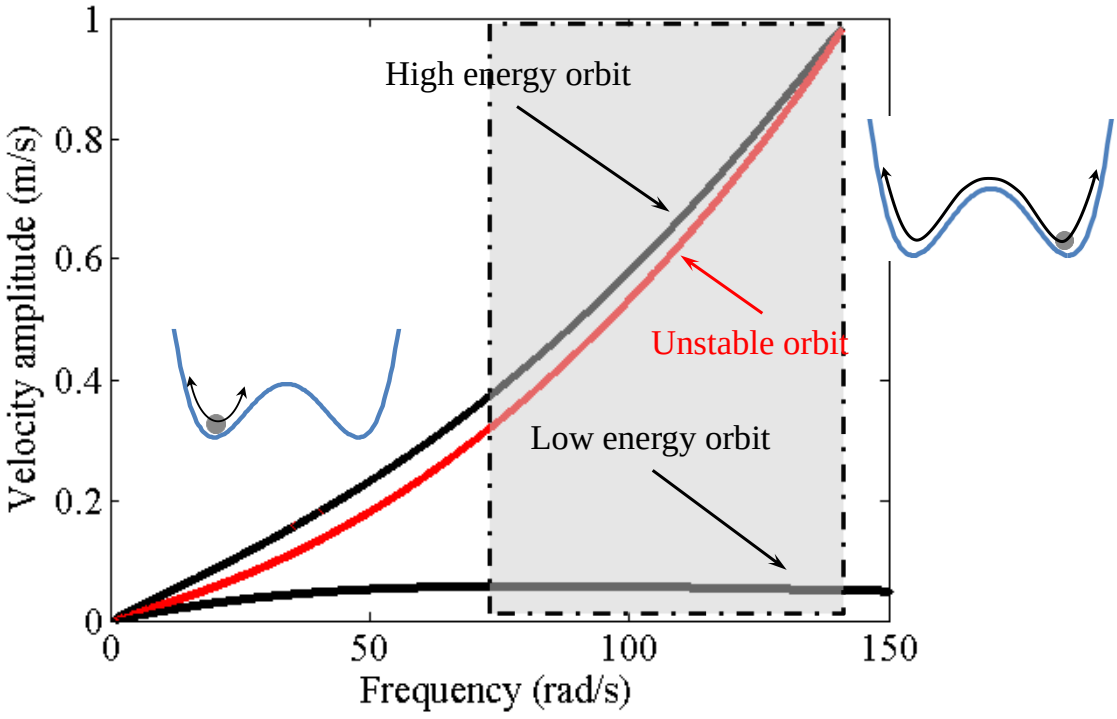

Fig. 2.5. Effective bandwidth of frequency-amplitude response curve of bistable system.

2.2 Stochastic Resonance

In this research the investigation of stochastic resonance is carried out under weak damping rather than overdamped condition. The frequency of stochastic resonance is mainly determined

based on the Kramers rate theory [88]. This theory is then specifically further elaborated by [89][90]. Kramer's model initially presented for a chemical reaction consists of a classical particle of mass *M* moving in a one-dimensional asymmetric double-well potential seeing Figure 2.6. Based on the definition of the Kramers theory, the escape rate κ is expressed by the ratio of

$$\kappa = \frac{j'}{n_0}. \tag{2.21}$$

In this Equation, the j' is the steady-state current if the particles are continuously fed into the domain of attraction, and then subsequently are captured by an observer in the neighboring domain of the attraction. The symbol of n_0 denotes the population inside the initial domain of attraction that usually is normalized to one particle and is defined as

$$n_0 = \int p_0(x)\,dx, \tag{2.22}$$

In Equation (2.22), $p_0(x)$ represents a stationary probability density inside the initial domain of attraction.

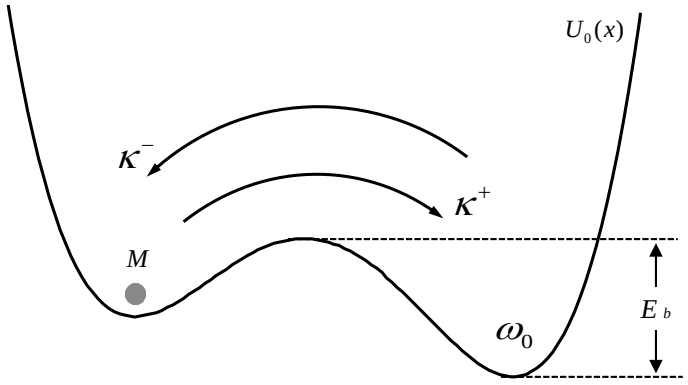

Fig. 2.6. Potential energy with two metastable states, Escape occurs via the transition rate of κ^+ and κ^-, and E_b is the activation energy between two potential wells.

The Newton's Equation of motion of the particle in the form of a Langevin Equation can be written as

$$M\ddot{x} = -U_0'(x) - \varsigma M\dot{x} + \xi(t), \tag{2.23}$$

where the x is the displacement from the equilibrium position, ς is a constant damping coefficient, and $\xi(t)$ denotes ambient noise. The time evolution of the probability density $\partial p(x, \dot{x} = \upsilon, t)$ of the particle transition to the energy barrier is governed by the Klein-Kramers Equation [88][91] as

$$\frac{\partial p(x,\upsilon,t)}{\partial t} = \left[-\frac{\partial}{\partial x}\upsilon + \frac{\partial}{\partial \upsilon}\frac{U'(x) + M\varsigma\upsilon}{M} + \frac{\varsigma k_B T}{M}\frac{\partial^2}{\partial \upsilon^2} \right] p(x,\upsilon,t), \tag{2.24}$$

The symbols of $k_B T$ here is regarded as the power intensity of the ambient vibration. In the case of weak friction, the energy, or equivalently action is almost constant and is given as

$$I(E) = \oint p\, dq\,. \tag{2.25}$$

Then, yields a diffusion Equation for the probability density of the action [92] as

$$\frac{\partial p(I,t)}{\partial t} = \varsigma \frac{\partial}{\partial I} I \left[1 + \frac{2\pi k_B T}{\omega(I)}\frac{\partial}{\partial I} \right] p(I,t), \tag{2.26}$$

where $\omega(I)$ is the angular frequency at the action I,

$$\frac{\partial E}{\partial I} = \frac{\omega(I)}{2\pi}. \tag{2.27}$$

Then the diffusion of the action given in Equation (2.26) can be immediately transformed into a diffusion equation with respect to energy E,

$$\frac{\partial p(E,t)}{\partial t} = \varsigma \frac{\partial}{\partial E} I(E)\left[1 + k_B T \frac{\partial}{\partial E}\right] \frac{\omega(E)}{2\pi} p(E,t). \tag{2.28}$$

As soon as the particle has acquired an energy which is larger than the barrier height of E_b, the particle can escape from the well. The energy that is captured by the particle is defined as the $I_b = I(E_b)$. In this case the steady-state current is obtained by the stationary probability density,

$$j' = -\varsigma I\left[1 + \frac{2\pi k_B T}{\omega(I)} \frac{\partial}{\partial I}\right] p(I), \quad 0 < I < I_b. \tag{2.29}$$

Imposing an immediate absorption at $I = I_b$, that is $p(I = I_b) = 0$, one finds with $\beta = (k_B T)^{-1}$ from Equation (2.29).

$$p(I) = j'\beta\varsigma^{-1} \exp\left[-\beta E(I)\right] \times \int_I^{I_b} \frac{\exp\left[\beta E(I')\right]}{2\pi I'} \omega(I')\, dI'. \tag{2.30}$$

Substituting Equation (2.30) into Equation (2.22), integrating it with respect to I, yields

$$n_0 = \int_I^{I_b} j'\beta\varsigma^{-1} \exp\left[-\beta E(I)\right] \times \int_I^{I_b} \frac{\exp\left[\beta E(I')\right]}{2\pi I'} \omega(I')\, dI' dI. \tag{2.31}$$

Substituting Equation (2.31) into Equation (2.21) the rate is given as

$$\kappa^{-1} = n_0 / j' = \beta\varsigma^{-1} \int_I^{I_b} \exp\left[-\beta E(I)\right] \times \int_I^{I_b} \frac{\exp\left[\beta E(I')\right]}{2\pi I'} \omega(I')\, dI' dI. \tag{2.32}$$

In generally, the ambient vibration is too weak to excite the particle to transit from the potential well, because the ambient vibration energy is smaller than the potential energy of the wells. Hence, it can be defined that $k_B T = \beta^{-1} = D < E_b$, owing to the relationship as presented in Equation (2.27), the rate is reduced to

$$\kappa^{-1} = \frac{2\pi}{\varsigma\omega_0 \beta I(E_b)} \exp(\beta E_b). \tag{2.33}$$

Hence, for the weak damping, the Kramers rate is obtained as

$$\kappa = \varsigma\beta I\left(E_b\right)\frac{\omega_0}{2\pi}\exp\left(-\beta E_b\right), \tag{2.34}$$

which is valid expression for the transmitting rate if the intensity of the noise satisfies the following conditions:

$$\frac{k_B T}{E_b} < 1, \text{ and } \varsigma I\left(E_b\right) < k_B T. \tag{2.35}$$

Then the expression of the Equation (2.34) can be re-considered as

$$\kappa < \frac{\omega_0}{2\pi}\exp\left(-\beta E_b\right). \text{ (Hz)} \tag{2.36}$$

Due to existence of the double potential wells, the frequency of stochastic resonance can be expressed by

$$\omega_{SR} = \kappa\pi < \frac{\omega_0}{2}\exp\left(-\frac{E_b}{D}\right). \text{ (rad/s)} \tag{2.37}$$

2.3 Challenges on Rotational Energy Harvester

Through the above analysis of the nonlinear system, it can be clearly found that it has several advantages to improve the energy recovery. First of all, one of the main reasons is that it can achieve a broadband energy harvesting through a relative simple structure. Then, because there has no restriction of the stroke of the nonlinear energy harvesters compared many linear systems that results in the dynamic responses of the vibrating body can be maintained at a high level. Finally, the enhanced responses improve the performance of energy harvesting for widely applications.

However, due to the complexity of the dynamic characteristics of nonlinear systems, although it has been discussed by many researchers in theoretical investigations and laboratory experiments, it is still difficult to realize the application of the advantages of the nonlinear system to the actual environments, especially in the energy harvesting field. As the first challenges of this study is how to exploit nonlinear systems to the actual vehicle tires, and can

fully demonstrate their characteristics.

In addition, by using the currently available tire vibration power generation technologies, only a few micro-Watts of harvested power can be provided to power just one or two sensors, e.g. MEMS devices with a relatively high power density. With the increasing requirements of advanced driving assistance systems, a tire-pressure monitoring system that can provide the driver with the tire condition via wireless transmission is integrated with a growing number of sensors. Consequently, another challenge of this study is to improve the current stage of power generation for self-sufficient power so that it can guarantee more and more sensors working.

Chapter 3

Methodology for Rotation-Induced Energy Harvesting

3. Methodology for Rotation-Induced Energy Harvesting

3.1 Bistable System under Rotating Circumstances

In this section, the dynamic characteristics of the bistable system under rotating circumstances are introduced for presenting the basic principle utilized in this study. As indicated in Figure 3.1(1), the bistable system is mounted on the surface of the rolling rim of wheel, and has two stable points which can ensure the beam vibrating with constantly large amplitude. It is assumed the beam at the side of right stable point as the initial state, while the tire rotates ninety degrees to reach the case of (2), owing to the kinetic energy of the proof mass greater than the potential well height, the beam most probably begins to break the initial one potential well vibrating to drop down another stable point.

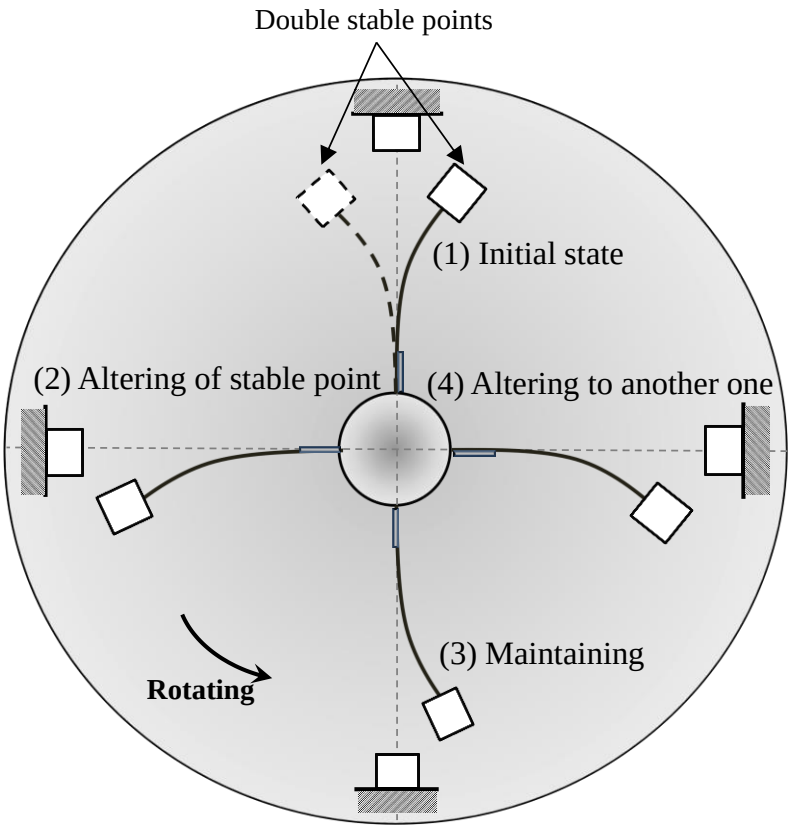

Fig. 3.1. Characteristics of the double stable points with the tire rotating: (1) initial state, (2) altering of the stable point, (3) maintaining previous state, and (4) altering to another one.

After that the dynamic of this beam is maintained the changeless stable to rotate through position (3) until reaching to the case of (4), the beam is altered to another one and keep this

kind vibrating to return the initial state. Therefore, per one cycle of rotation the beam can be realized to vibrate through potential wells for two times with amplified amplitude, which is hence considered to be an effective structure to enhance tire rotation-induced energy harvesting.

3.2 Modelling for Simulated Tire Rotation

3.2.1 Mathematical Analysis

A bistable mechanism is created through positioning a magnetic end mass attached to a cantilever beam and another permanent magnet with the same polarity on the frame depicted schematically in Figure 3.2. The cantilever beam is excited by noise excitation and there is an interaction between the elastic force and magnetic force of the beam, generating a nonlinear response by adjusting the distance d between the two magnets, after which the system can show bi-stability. Due to the configuration of the two magnets, a repulsive magnetic force will act between them. If the magnetic force and gravity of the magnet end mass are taken into consideration then this may induce a deflection angle in the beam of θ, a lateral end mass defection of x_T, and a centripetally generated displacement of y_C.

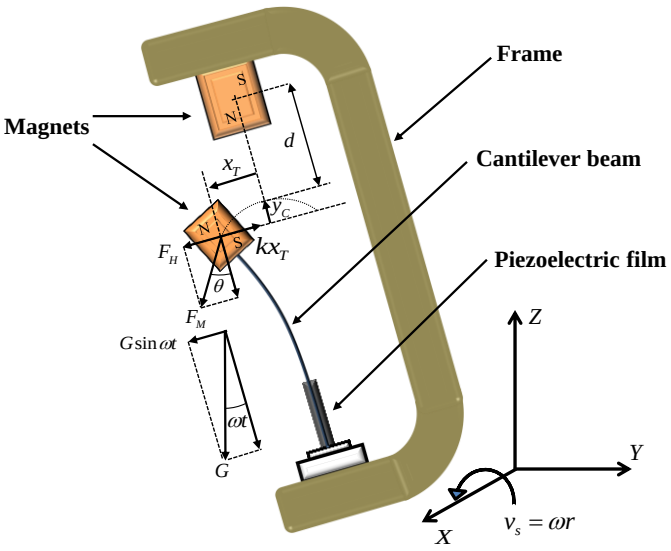

Fig. 3.2. Schematic of the energy harvesting device based on rotational environment.

When the power harvester revolves around the axis of X, due to the variation in the distance d between the two magnets, the repulsive magnetic force F_M and the tangential component F_H also change to make the mechanism vibrate between two stable states. kx_T is the restoring

force of the cantilever beam. F_H can be derived from Equation (3.2) using a dipole model [93][94] and expanded into a Taylor series, which the details can be found at the next section, calculated around $y_M = 0$ and truncated to Equation (3.3) as

$$F_H = F_M \sin\theta, \tag{3.1}$$

$$\begin{aligned} F_H = & \frac{\mu v^2}{4\pi}\left\{\frac{3\left[M_{cy}\left(dM_{fx}+x_T M_{fy}\right)+M_{cx}\left(dM_{fy}+3x_T M_{fx}\right)\right]}{\left(d^2+{x_T}^2\right)^{5/2}}\right\} \\ & -\frac{\mu v^2}{4\pi}\left\{\frac{15x_T\left(x_T M_{fx}+dM_{fy}\right)\left(x_T M_{cx}+dM_{cy}\right)}{\left(d^2+{x_T}^2\right)^{7/2}}\right\} \end{aligned}, \tag{3.2}$$

$$\begin{aligned} F_H \approx & \left(\mu v^2\frac{9M_{cx}M_{fx}-12M_{cy}M_{fy}}{4\pi d^5}\right)x_T \\ & -\left(\mu v^2\frac{75M_{cx}M_{fx}-90M_{cy}M_{fy}}{8\pi d^7}\right){x_T}^3 \end{aligned}, \tag{3.3}$$

where v' and μ are the volume of the magnets and the permeability of free space. $\mathbf{M}_f = (M_{fx}, M_{fy})$, $\mathbf{M}_c = (M_{cx}, M_{cy})$ are the magnetization strength amplitudes of permanent magnet attached on the frame and the magnetic end mass, respectively. When considering the centripetal force resulting from revolution of the frame, it becomes necessary to take into account the effect of gravity G of magnetic end mass. Therefore, the resultant force of the tangential direction f_H can be expressed as

$$f_H = F_H - kx_T + G\sin\left(\omega t + \mu_0\right). \tag{3.4}$$

When the frame with a radius of r revolves at the angular velocity of ω with the speed of v_S, the total kinetic energy of the end mass will be defined by E_K as

$$E_K = \frac{1}{2}m\left[\left(\dot{x}_T + v_S\right)^2 + {\dot{y}_C}^2\right]. \tag{3.5}$$

Thereby, according to the thin beam theory, the restoring coefficient of the beam, with the Young's modulus and the moment of inertia of E' and I'', is given as

$$k = E'I''\int_0^l \left(\vartheta''\right)^2 dx, \tag{3.6}$$

where $\vartheta(x)$ is a static linear shape function of the cantilever beam. Assuming $x_T(t) = w(L,t)$, where L is the length of the beam, the following equation can be derived as

$$w(x,t) = \vartheta(x)w(L,t) = \left(\frac{3x^2}{2L^2} - \frac{x^3}{2L^3}\right)x_T(t), \tag{3.7}$$

where w is the transverse displacement of the beam and $w'' = d^2w/dx^2$. Assuming the transverse deflection is insignificant, y_C is given by

$$y_C = \int_0^L \left[\sqrt{1+\left(\frac{dw}{dx}\right)^2} - 1\right]dx = \int_0^L \frac{1}{2}\left(\frac{dw}{dx}\right)^2 dx = \frac{1}{2}\left[\int_0^L \left(\vartheta'\right)^2\right]{x_T}^2. \tag{3.8}$$

According to Equations (3.4), (3.5) and (3.8), Lagrange's Equation can be given by

$$\frac{d}{dt}\left(\frac{\partial E_K}{\partial \dot{x}_T}\right) - \frac{\partial E_K}{\partial x_T} = F_H - kx_T + G\sin\left(\omega t + \mu_0\right). \tag{3.9}$$

The Equation of motion of the system is derived as

$$\begin{aligned} &m\ddot{x}_T + c\dot{x}_T + \left(k - \mu v^2 \frac{9M_{cx}M_{fx} - 12M_{cy}M_{fy}}{4\pi d^5}\right)x_T + \\ &\frac{\mu v^2\left(75M_{cx}M_{fx} - 90M_{cy}M_{fy}\right)}{8\pi d^7}{x_T}^3 = N(t) + G\sin\left(\omega t + \mu_0\right) \end{aligned}, \tag{3.10}$$

where c is the viscous damping coefficient, the term of $\mu v^2\left(9M_{cx}M_{fx}-12M_{cy}M_{fy}\right)/4\pi d^5$ is the linear coefficient of the two magnets, and $\mu v^2\left(75M_{cx}M_{fx}-90M_{cy}M_{fy}\right)/8\pi d^7$ is the nonlinear coefficient of the two magnets. When $k-\mu v^2\left(9M_{cx}M_{fx}-12M_{cy}M_{fy}\right)/4\pi d^5=-a$ and $\mu v^2\left(75M_{cx}M_{fx}-90M_{cy}M_{fy}\right)/8\pi d^7=b$ $(a>0,\ \ b>0)$, the Equation (3.10) can be transformed into

$$m\ddot{x}_T+c\dot{x}_T-ax_T+bx_T{}^3=N(t)+G\sin\left(\omega t+\mu_0\right). \tag{3.11}$$

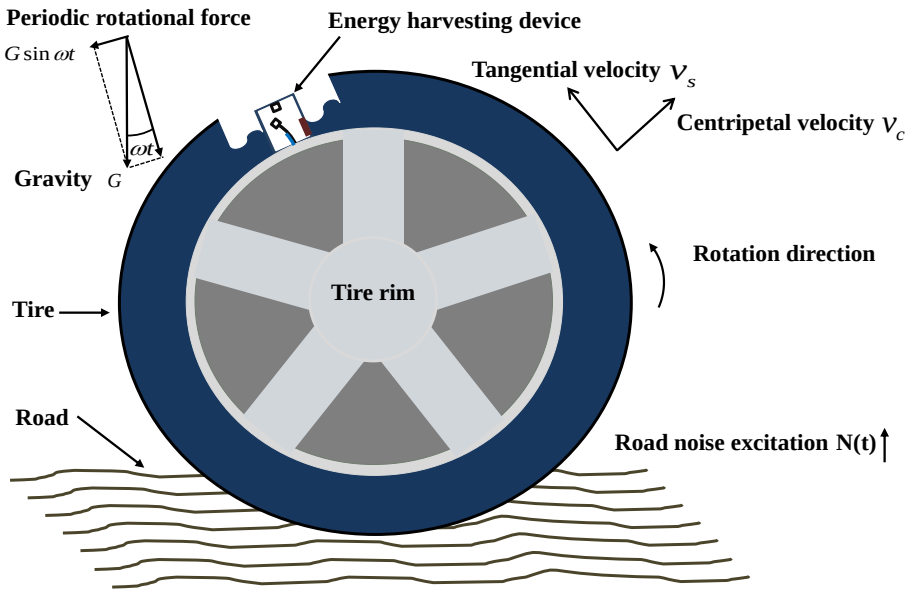

Fig. 3.3. Energy harvesting device mounted on a rotating tire.

From Equation (3.11), the periodic force can be generated automatically from the centripetally induced motion of the magnetic end mass. The noise excitation $N(t)$ is expressed as $N(t)=\sqrt{2D}\xi(t)$, in where D denotes intensity of the noise $\xi(t)$ that is a zero-mean, one-variance Gaussian white noise. Therefore, in the environment of tire rotation as shown in Figure 3.3, the energy harvesting device was mounted on rim of the rotating tire at the counterclockwise direction with angular velocity of ω. The vertical road noise excitation $N(t)$ is produced by the interaction of the tire and road surface. The tangential velocity of v_s is also presented in Figure 3.3, while the centripetal velocity is defined as v_c. The periodic rotational

force $G\sin\omega t$ is autonomously offered from the gravitational effect of the magnetic end mass and the rotation of the tire, where G is the gravity of the magnetic end mass. Hence, the proposed energy harvester model is capable of being utilized under the vehicle tire rotation environments.

3.2.2 Stochastic Resonance Frequency

In the presence of tire rotation, the standard potential energy Equation can be transformed from Equation (3.12) into Equation (3.13) as

$$U(x_T,t) = -\frac{1}{2}ax_T{}^2 + \frac{1}{4}bx_T{}^4, \tag{3.12}$$

$$U(x_T,t) = -\frac{1}{2}ax_T{}^2 + \frac{1}{4}bx_T{}^4 - G\sin\left(\omega t + \mu_0\right)x_T. \tag{3.13}$$

As shown in Figure 3.4, in the absence of tire rotation, the double potential wells remain symmetric. The minima are located at x_0. These are separated by double potential barriers with the heights given by ΔU. The detailed expression is calculated as

$$x_0 = \pm(a/b)^{1/2},\ \ \Delta U = a^2/(4b). \tag{3.14}$$

Hence, in the case of tire rotation, the double potential wells are asymmetrically tilted up and down, periodically raising and lowering the potential wells [89]. The height of the potential well becomes

$$U_0{}' = a^2/(4b) - G\sqrt{a/b}\sin\left(\omega t + \mu_0\right), \tag{3.15}$$

Differentiating Equation (3.12) with respect to x_T leads to

$$F_M{}' = -ax_T + bx_T{}^3, \tag{3.16}$$

where $F_M{}'$ is the nonlinear spring force. After differentiating $F_M{}'$ the nonlinear spring

coefficient k' can be given as follows

$$k' = -a + 3bx_T{}^2 . \tag{3.17}$$

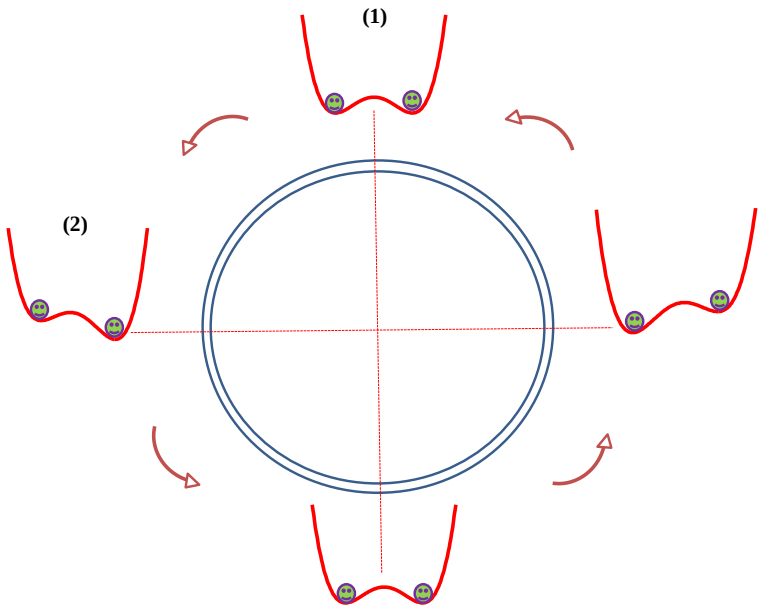

Fig. 3.4. Cyclic variation of the double potential wells with the tire rotation: (1) symmetric and (2) asymmetric conditions.

Also, the equilibrium points of two potential wells can be calculated by Equation (3.14), Substituting x_0 into Equation (3.17), the nonlinear spring coefficient $k' = 2a$ can be obtained, then the resonance angular velocity of the bistable system is given

$$\omega_0 = \sqrt{\frac{2a}{m}}, \text{ (unit: Hz).} \tag{3.18}$$

Substituting Equations (3.14) and (3.18) into Equation (2.37) as governed in Section 2.2 yields the standard expression of stochastic resonance as

$$\omega_{SR} < \sqrt{\frac{a}{2m}} \exp\left(-\frac{a^2}{4bD}\right), \text{ (unit: rad/s),} \tag{3.19}$$

where D is the intensity of the road noise excitation. With the tire rotation, the height of potential wells periodically vary, substituting Equations (3.15) and (3.18) into Equation (3.20)

yields

$$\omega_{SR} < \sqrt{\frac{a}{2m}} \exp\left(\frac{G\sqrt{a/b}\sin(\omega t + \mu_0) - a^2/(4b)}{D} \right). \tag{3.20}$$

Due to the influence of the term of $\sin \omega t$, it can result in that the frequency fluctuates up and down around a certain value. It means that there is existence of a certain operating frequency bandwidth corresponding to the calculated value, due to the effect of the periodic modulation force.

According to the general model of a vibration energy harvester the damping coefficient c is composed of the mechanical damping coefficient c_m and the electrically induced damping coefficient c_e. Therefore, the motion Equation can be described by rearranging Equation (3.11) as

$$m\ddot{x}_T \dot{x}_T + (c_e + c_m)\dot{x}_T^{\,2} - ax_T \dot{x}_T + bx_T^{\,3}\dot{x}_T = N(t)\dot{x}_T + G(\sin \omega t + \mu_0)\dot{x}_T . \tag{3.21}$$

Then, Equation (3.21) can be transformed to

$$\frac{d}{dt}\left(\frac{1}{2} m\dot{x}_T^{\,2} + \frac{1}{4} bx_T^{\,4} - \frac{1}{2} ax_T^{\,2} \right) + (c_e + c_m)\dot{x}_T^{\,2} = N(t)\dot{x}_T + G\sin(\omega t + \mu_0)\dot{x}_T . \tag{3.22}$$

Equation (3.22) represents the fact that the instantaneous power into the system is equal to the instantaneous power dissipated by damping plus the time rate of change of the sum of the kinetic and potential energies. In the left side, the terms of $1/2\, m\dot{x}_T^{\,2}$ is the kinetic energy of the system, and $1/4\, bx_T^{\,4} - 1/2\, ax_T^{\,2}$ presents the potential energy. $(c_e + c_m)\dot{x}_T^{\,2}$ is the instantaneous power absorbed by damping, $c_e \dot{x}_T^{\,2}$ is considered as the instantaneous power that can be converted to electricity, and $c_m \dot{x}_T^{\,2}$ is the unavoidably lost power in mechanical damping. In the right hand side terms, $N(t)\dot{x}_T$ is the input power from the road ambient vibration, and $G\sin \omega t \dot{x}_T$ is power drawn due to the periodic force caused by the rotation of the tire and gravity of the magnetic end mass. Therefore, the net instantaneous power that can be harvested by this system can be given by

$$P = c_e \dot{x}_T^{\,2} . \tag{3.23}$$

3.3 Modelling for Real-World Tire Rotation

3.3.1 Modified Stochastic Resonance Frequency

Figure 3.5 shows that a macro-scale energy harvester can be attached to a wheel rotating counterclockwise with angular velocity ω. The vertical on-road noise $N(t)$ is produced by the interaction of the rotating tire and the road surface.

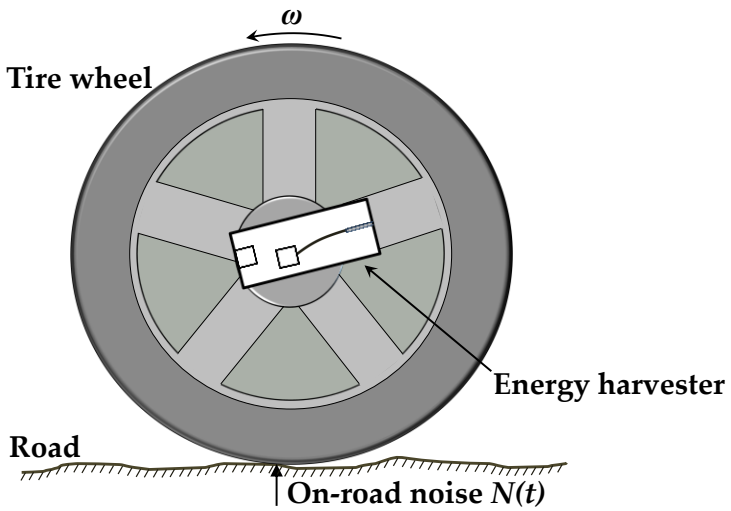

Fig. 3.5. Illustration of the energy harvester attached to the center of a wheel.

To eliminate the effect of the centrifugal forces, the center of the cantilever tip mass is located at the rotational center of the wheel due to the sensitivity of cantilever beam stiffness to centrifugal force, as shown in Figure 3.6.

To obtain the restoring force between the two magnets of the energy harvester, a mathematical model is first derived for the interaction forces of the magnets. The dipole model is used to represent the interaction forces, and the potential energy of the movable tip magnet can be defined as

$$U_M = -\mathbf{m}_c \cdot \mathbf{B}, \tag{3.24}$$

where $\mathbf{m}_c$ is the magnetic dipole moment vector of the fixed permanent magnet, defined by $\mathbf{m}_c = \mathbf{M}_c v'$. $\mathbf{B}$ is the magnetic flux density, $\mathbf{M}_c = (M_{cx}, M_{cy})$ denotes the magnetization strength amplitudes of the permanent magnet bonded to the frame in terms of its vertical and horizontal components, and v is the volume of the magnets.

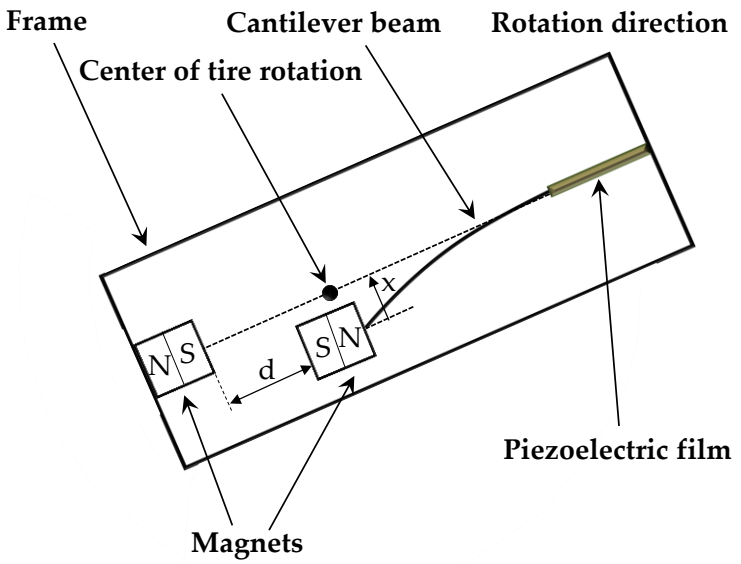

Fig. 3.6. Diagram of the nonlinear tire-induced energy harvesting configuration.

Then, the potential energy of the magnetic end mass is expressed as

$$U_M = \frac{\mu v^2}{4\pi}\Phi(x), \tag{3.25}$$

where μ is the permeability of free space and x is the vibrational displacement of the end magnet. The function $\Phi(x)$ is defined as

$$\Phi(x) = -\frac{3\left(dM_{cy} + xM_{cx}\right)\left(dM_{fy} + xM_{fx}\right)}{\left(d^2 + x^2\right)^{5/2}} + \frac{M_{fy}M_{cy} + M_{fx}M_{cx}}{\left(d^2 + x^2\right)^{3/2}}, \tag{3.26}$$

where d is the lateral separation of the two magnets. Note that $\mathbf{M}_f = (M_{fx}, M_{fy})$ denotes the magnetization strength of the magnetic tip mass in terms of its vertical and horizontal components; the two magnets should have opposite polarity, indicating repulsion.

The restoring forces are obtained from the spatial derivative of the potential energy as

$$F_M(x) = \frac{\mu_0 v^2}{4\pi}\Theta(x), \tag{3.27}$$

where $\Theta(x)$ is expressed as

$$\Theta(x)=\frac{3\left[M_{cy}\left(dM_{fx}+xM_{fy}\right)+M_{cx}\left(dM_{fy}+3xM_{fx}\right)\right]}{\left(d^2+x^2\right)^{5/2}}-\frac{15x\left(xM_{fx}+dM_{fy}\right)\left(xM_{cx}+dM_{cy}\right)}{\left(d^2+x^2\right)^{7/2}}. \quad (3.28)$$

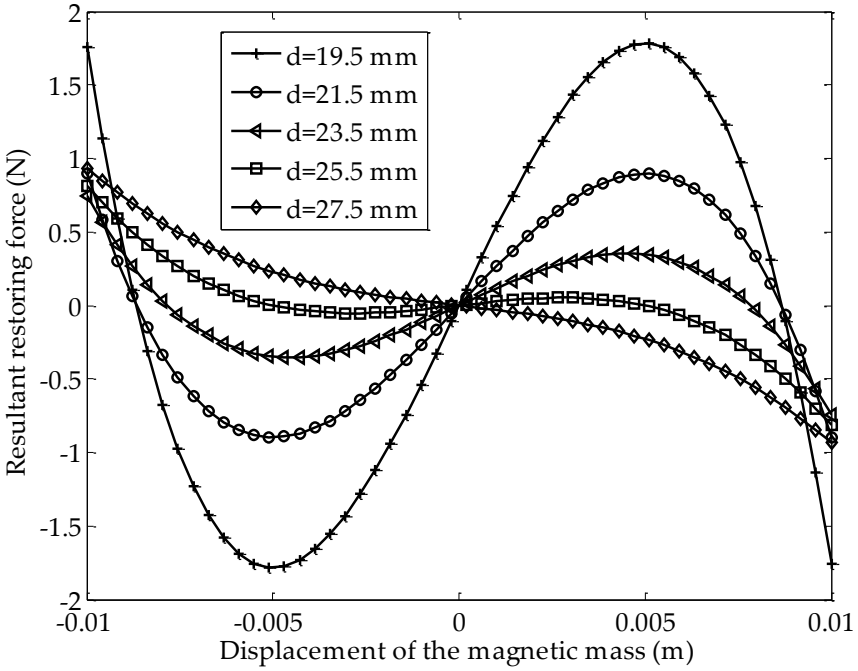

Fig. 3.7. Resultant force versus the distance between the two magnets.

By substituting Equation (3.28) into (3.27), the restoring forces of the magnetic end mass can be derived, and the resultant restoring force of the beam is expressed as follows

$$F_R(x)=F_M(x)-kx, \quad (3.29)$$

where k is the spring constant of the beam. As shown in Figure 3.7, with the distance between the two magnets increasing from 19.5 to 25.5 mm, there are two stable states, and the distance between the two stable points gradually becomes small. When the separation of the magnets exceeds 25.5 mm, the cantilever beam cannot be stimulated as being bistable, and it becomes a monostable system around the equilibrium position.

Equation (3.29) can be further expressed in Taylor series, calculated around x = 0 and simplified as follows

$$F_R(x)=\left(\mu_0 v^2\frac{9M_{cx}M_{fx}-12M_{cy}M_{fy}}{4\pi d^5}-k\right)x-\left(\mu_0 v^2\frac{75M_{cx}M_{fx}-90M_{cy}M_{fy}}{8\pi d^7}\right)x^3. \quad (3.30)$$

Based on the Duffing dynamic expression of Equation (3.11), the resultant restoring force of beam can be given as

$$F_M{}' = ax - bx^3 . \tag{3.31}$$

Due to the relation of $F_M' = F_R(x)$, Equations (3.32) and (3.33) are derived by employing the corresponding constant terms of Equations (3.30) and (3.31), respectively.

$$a = \mu_0 v^2 \left(\frac{9M_{cx}M_{fx} - 12M_{cy}M_{fy}}{4\pi d^5} \right) - k , \tag{3.32}$$

$$b = \frac{\mu_0 v^2 \left(75M_{cx}M_{fx} - 90M_{cy}M_{fy} \right)}{8\pi d^7} . \tag{3.33}$$

In the case of weak friction, the Kramers rate can be modified by substituting Equations (3.32) and (3.33) into (3.19), the Kramers rate can be presented as a function of the distance between the two magnets *d*.

3.3.2 On-Road Noise Measurement

The experimental environment shown in Figure 3.8 features a smooth paved road and electric vehicle (Coms, ZAD-TAK30-DS, Toyota Auto Body Co., Ltd., Aichi, Japan). To measure the road noise, a wireless acceleration sensor (MVP-RF3-J, MicroStone Corporation, Nagano, Japan) with a response frequency of 1 Hz –1000 Hz is installed on the front suspension of the vehicle. In low speed range conditions where the vehicle travels on a smooth paved road, it indicates that the power spectral density of the accelerations remains identical by analyses of the measured signal. Therefore, the measured acceleration under 20 km/h is selected as the input condition for simulation study, and then the intensity of the on-road noise can be derived with $D = 1.22 \times 10^{-4}$ (N).

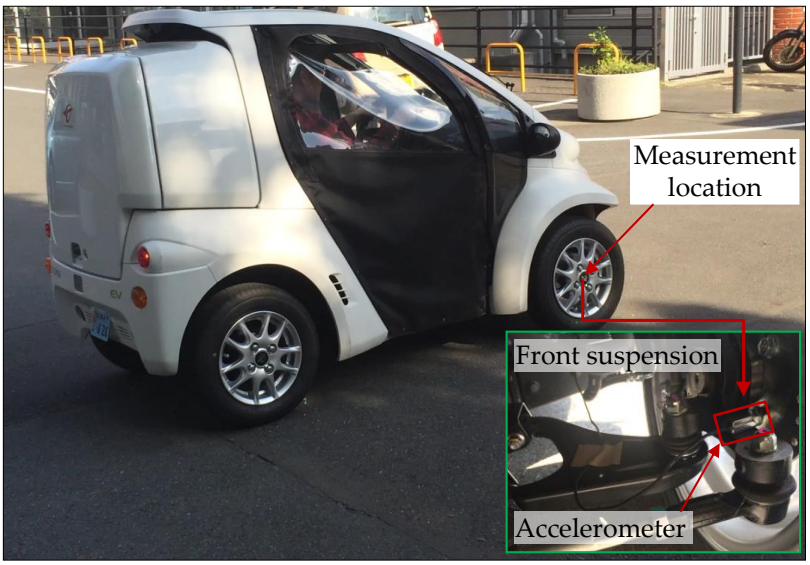

Fig. 3.8. Paved road testing and on-road noise measurement on front-wheel suspension.

3.4 Combination of Stochastic Resonance and High Energy Orbit Oscillations

As described in Section 2.1.2, for harmonic excitation of the $F\sin(\omega t+\mu_0)$, the symbol of F can be here considered as the gravity fore of G, due to only its gravitational acting, especially at the lower frequency filed when one potential well motion of nonlinear bistable system is dominant influence under periodical force excitation as shown in Figure 3.9. Before the activation of two potential wells oscillating, the one potential well vibrating always exists for reducing the effective bandwidth of the bistable system. By exploiting energy of the on-road noise *N(t)*, the low level motion of one potential well can be activated to the high level motion of two potential wells owing to the stimulus of stochastic resonance. Thereby, this approach is considered as a promising combination of two phenomena of stochastic resonance and high energy orbit oscillation, by which the effective bandwidth can be broadened for further improving the performances of bistable systems.

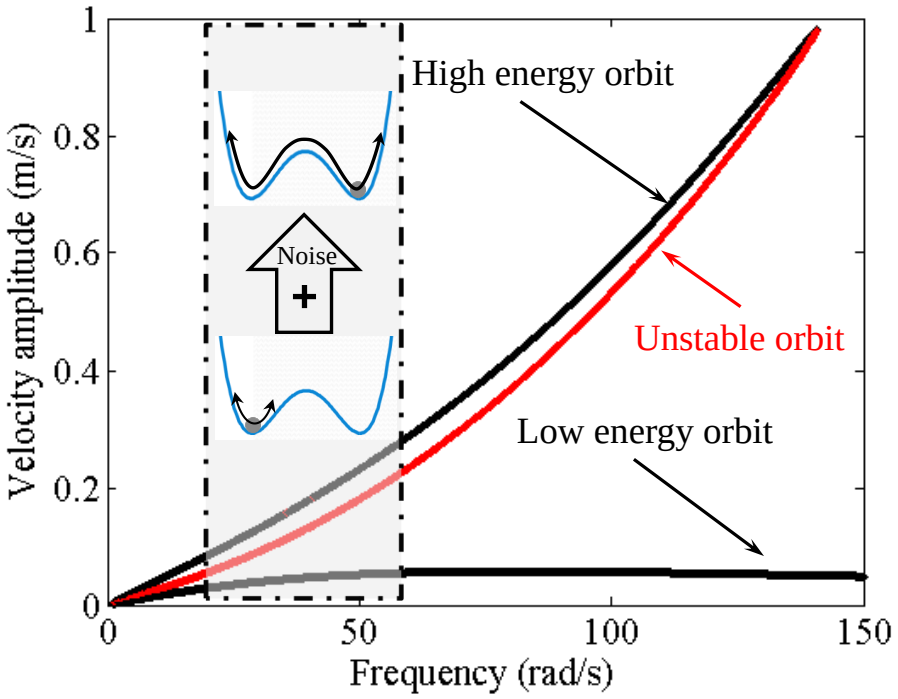

Fig. 3.9. Needed to be improved bandwidth of frequency-amplitude response curve of bistable system under the excitation of periodically gravitational acceleration of 9.8m^2/s.

3.5 Stability of High Energy Orbit Oscillating Using Centrifugal Force

In the most case of the real-world rotational environments, centrifugal acceleration caused from the proof mass is large enough even higher than the gravity acceleration as the driving speed increases. This section presents the active effect of centrifugal force on the rotational nonlinear energy harvesting field by analyzing the centrifugally rotating dynamic of the energy harvester as depicted in Figure 3.10(a).

The energy harvester comprises a cantilever beam pasted piezoelectric film and two magnets with the same polarity, one of which is attached on the pointed end of the beam, and another one is fixed at frame of energy harvester. The proposed nonlinear energy harvester is radially oriented, at a distance of *r* from the center axis of rotation *o*, as shown in Figure 3.10(b).

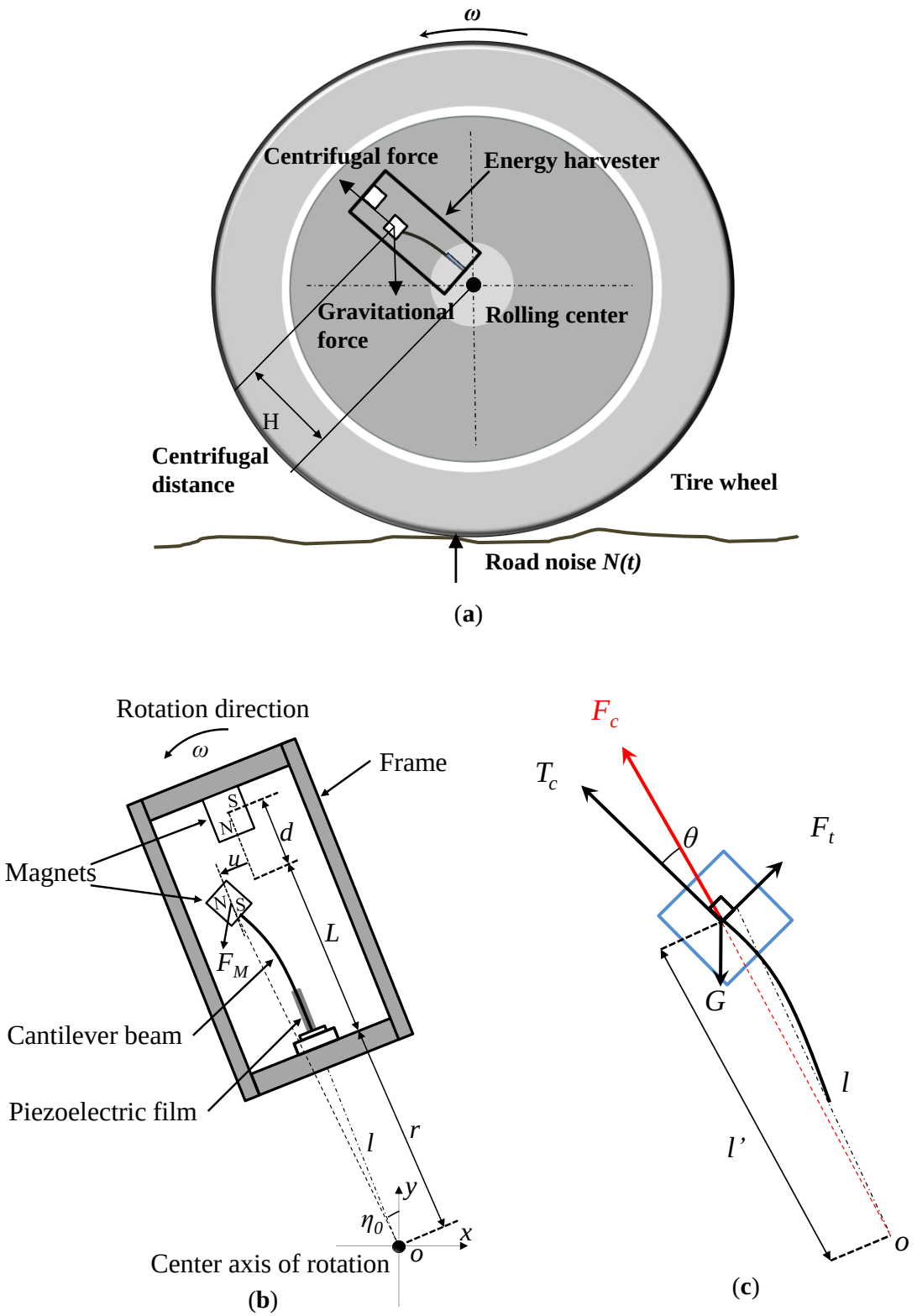

Fig. 3.10. (**a**) Tire rotating model conserving centrifugal force; (**b**) schematic of tire-induced energy harvesting model; and (**c**) equivalent force analysis of magnetic tip mass generated owing to centrifugal force effect.

While the device model rotates on the anticlockwise direction with the angular frequency of ω, as analyzed in Figure 3.10(c) the tensile stress generated from the centrifugal force of the tip mass is yielded as

$$F_c(t) = m\omega^2 l'(t), \tag{3.34}$$

in which m is the tip mass, l' is the distance from the center axis of rotation to center of gravity of the tip mass, and the l' can be expressed as

$$l'(t) = \sqrt{(L+r)^2 - u(t)^2}, \tag{3.35}$$

where L is the length of the beam, r is the distance from the root of the beam to the center axis of rotation, and u is the vibrational amplitude of the cantilever beam at the tip position, by rearranging the Equation (3.35), the approximate distance of Equation (3.35) is obtained as

$$l'(t) \approx (L+r)\left[1 - \frac{1}{2}\left(\frac{u(t)}{L+r}\right)^2\right], \tag{3.36}$$

in Equation (3.36), due to the amplitude of cantilever beam at tip position is insignificant compared to the distance of $L+r$, leading to $(u(t)/(L+r))^2 \approx 0$, thereby, the truncated Equation of centrifugal force can be written as

$$F_c(t) = m\omega^2 (L+r). \tag{3.37}$$

Then tangentially component of the centrifugal force is resolved as

$$F_t(t) = m\omega^2 (L+r)\sin\theta(t), \tag{3.38}$$

where θ is the angular of the direction of centrifugal force to the direction of centripetal component T_c. Assuming θ is tiny, the Equation (3.38) is described as

$$F_t(t) = m\omega^2 (L + r)\theta(t). \tag{3.39}$$

With the existence of the repulsive force of magnets, a dynamic force of *P'* is loaded on the tip position of cantilever beam as

$$P(t)' = \frac{3E'I''}{L^3} u(t), \tag{3.40}$$

in which *E'* is its Young's Modulus, *I''* is the moment of inertia. The static deflection of the cantilever beam is generated as

$$w(x) = \frac{L^3}{3E'I''}\left(1 - \frac{3x}{2L} + \frac{x^3}{2L^3}\right) P(t)'. \tag{3.41}$$

x is the distance from the tip position of cantilever beam to the point of the load force *P'*. Hence, the deflection angular $\theta(t)$ at the tip positon of the cantilever beam, by differentiating the static deflection with respect to *x*, is given as

$$\theta(t) = -\left.\frac{\partial w(x)}{\partial x}\right|_{x=0} = \frac{L^2}{2E'I''} P' = \frac{3}{2L} u(t), \tag{3.42}$$

Substituting the Equation (3.42) into Equation (3.39), tangential component of the centrifugal force is obtained as

$$F_t(t) = \frac{3m\omega^2 (L + r)}{2L} u(t). \tag{3.43}$$

When gravity force of tip mass is also included, the specific expression of the tangentially resultant force of tip mass is given as

$$F_t(t)' = \frac{3m\omega^2 (L + r)}{2L} u(t) - G\sin(\omega t + \eta_0). \tag{3.44}$$

In Equation (3.44), G is the gravity force of tip mass, η_0 is the initial angular of center axis of beam to the vertical aixs of y. Therefore, the motion Equation of the bistable oscillator can be expressed in dimensional form as

$$m\ddot{u} + c\dot{u} + (k - \frac{F_M}{d})u + bu^3 = -F_t(t)', \tag{3.45}$$

where c is the viscous damping coefficient, k is the stiffness of the cantilever beam. When harvester model revolves around the center axis of rotation, as the variation of the distance d between the two magnets, the repulsive magnet force F_M changes to make the mechanism vibrate between two stable states and constant of b is the nonlinear coefficient of two magnets. While substituting Equation (3.44) into Equation (3.45), and integrating the linear polynomials, the rearranged dynamic motion equation under rotational system can be governed as

$$m\ddot{u} + c\dot{u} + \left[k + \frac{3m\omega^2(L+r)}{2L} - \frac{F_M}{d} \right] u + bu^3 = G\sin(\omega t + \eta_0). \tag{3.46}$$

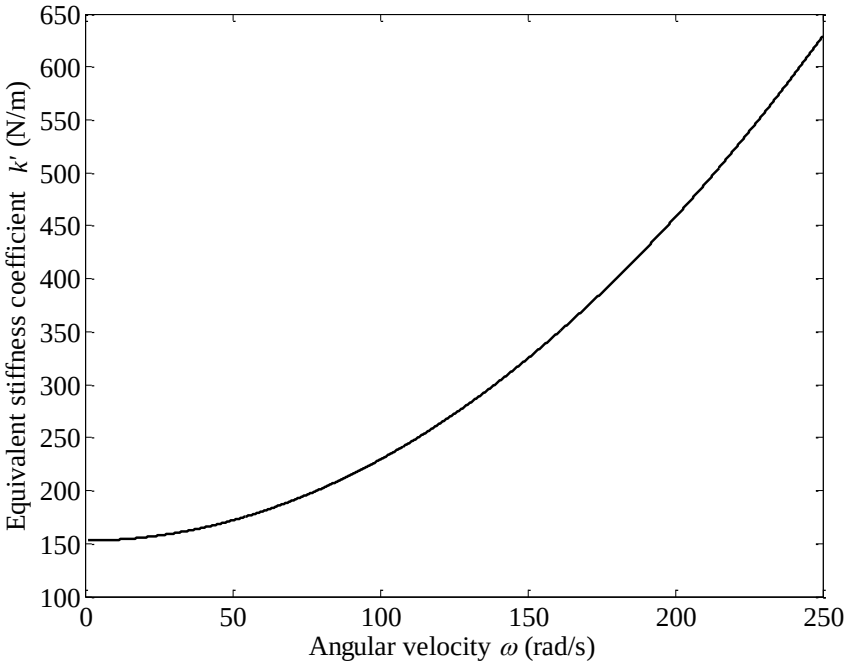

Fig. 3.11. Equivalent stiffness coefficient as a function of ω.

Hence, the expression of equivalent stiffness coefficient of cantilever beam Δk under rotational circumstance is given as

$$\Delta k = k + \frac{3m\omega^2 (L+r)}{2L}. \tag{3.47}$$

By setting the parameter values, k=152.7 (N/m), m=8×10^{-3} (kg), and L=4.2×10^{-2} (m), the equivalent stiffness coefficient as an function of ω is plotted as Figure 3.11, which indicates that as the angular velocity is increased up to 250 rad/s, the equivalent stiffness coefficient is self-tuned from 152.7 N/m to 628.9 N/m. From the third term coefficient of Equation (3.46), by centrifugal distance $H=L+r$, the equivalent linear stiffness expression of system leads to

$$a' = \frac{3m\omega^2 H}{2L} + k - \frac{F_M}{d}, \ (a' < 0). \tag{3.48a}$$

$$a' = \Delta k - \frac{F_M}{d}. \tag{3.48b}$$

It is assumed that the linear coefficient of the magnets F_M/d=212.7 (N/m), nonlinear stiffness coefficient of the magnets b=4.8×10^6 (N/m^3), the linear coefficient of system as a function of ω is depicted as Figure 3.12. It demonstrates that when the angular velocity is smaller than 88.7 rad/s, the value of system linear stiffness coefficient is negative and after that the coefficient declines to positive. Then, based on Equations (3.46) and (3.48), the potential energy of system is obtained under the condition of the centrifugal force on the cantilever beam as

$$U_0'(x,t) = \frac{1}{2}a'u^2 + \frac{1}{4}bu^4. \tag{3.49}$$

As shown in Figure 3.13, with the variation of angular velocity ω, when it is smaller than 88.7 rad/s, the system remains the bistable state, and when ω exceeds 88.7 rad/s, the performance of system is tuned to monostable hardening type behavior. Therefore, the jump-down expression can be given by substituting Equation (3.48) into Equation (2.14b)

$$\gamma' = \sqrt{\frac{1}{2m}\left(\sqrt{\left(\frac{2aL-3m\omega^2 H}{2L}\right)^2+\frac{3mbF^2}{c^2}}\right)+\frac{2aL-3m\omega^2 H}{4mL}}\,. \tag{3.50}$$

The steady state solution of Equation (3.46) is that of the form

$$u = B + U\cos\omega t\,, \tag{3.51}$$

where B is a constant, when B=0, the frequency-amplitude response equation of the bistable hardening system can be obtained by using the harmonic balance method, which is expressed as

$$\frac{9}{16}b^2U^6-\frac{3}{2}b\left(m\omega^2+a\right)U^4+\left[\left(m\omega^2+\frac{F_M}{d}-\frac{3m\omega^2 H}{2L}-k\right)^2+c^2\omega^2\right]U^2-m^2g^2=0\,. \tag{3.52}$$

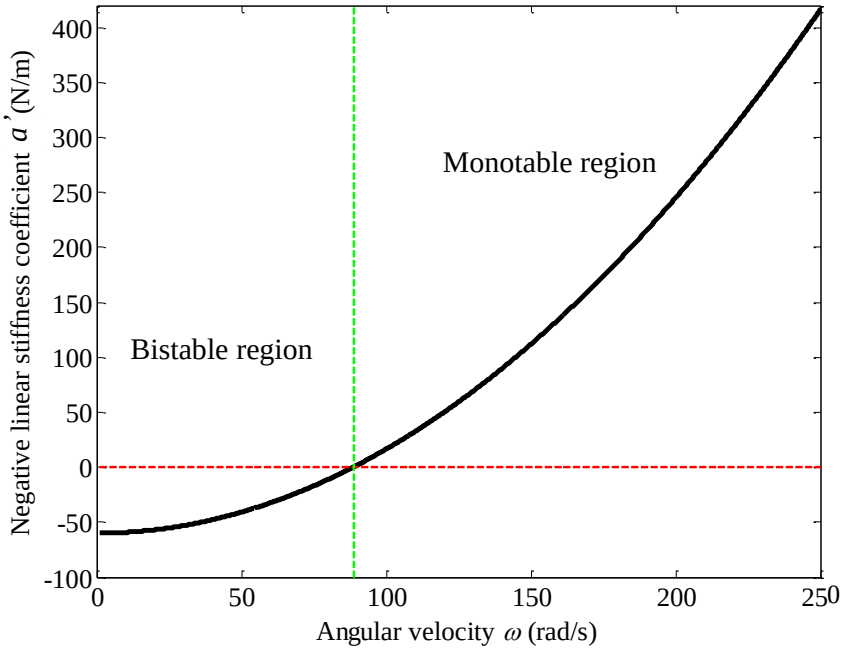

Fig. 3.12. Linear stiffness coefficient of system as a function of ω.

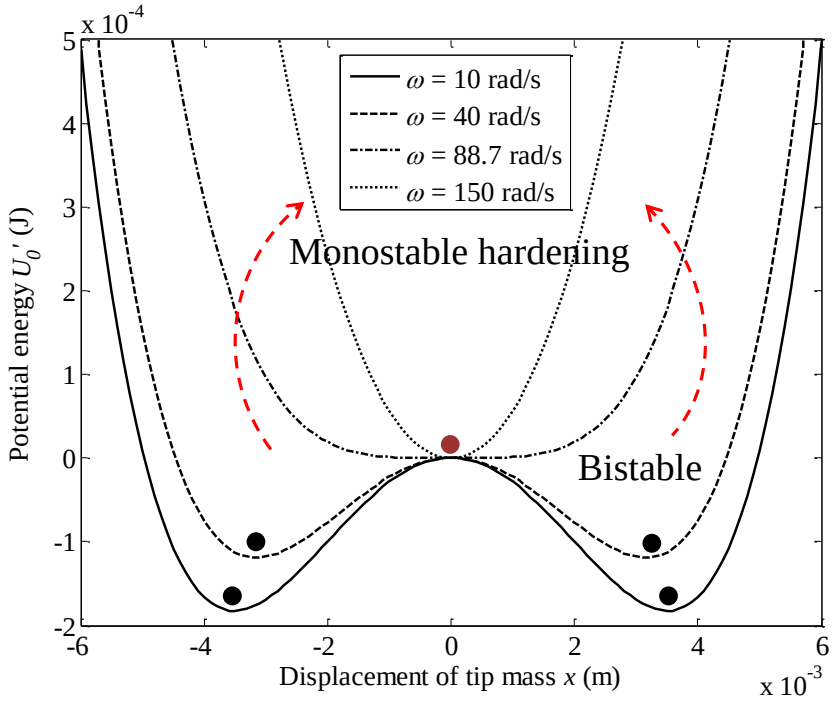

Fig. 3.13. Potential energy against the displacement of the magnetic tip mass.

Chapter 4

Numerical Analysis

4. Numerical Analysis

4.1 Responses under Stochastic Resonance

In this section, the responses under the occurrence of stochastic resonance in the cases of simulated condition, and the real measured on-road noise combined with gravitational force, are numerically analyzed.

4.1.1 Responses under Simulating Conditions

In order to confirm whether stochastic resonance can occur, and distinguish it from monostable resonance, numerical simulations were carried out under the following three conditions: (1) only road noise excitation with the bandwidth of 0 Hz–1 kHz; (2) only periodic rotational force at angular velocity of 98 rad/s; and (3) both road noise excitation and periodic rotational force at different angular velocities of tire rotation: (a) 80, (b) 90, (c) 98, (d) 110, and (e) 120 rad/s. A numerical simulation is implemented based on Equation (3.11), where $a = 220$ (N/m), $b = 6 \times 10^7$ (N/m^3), $D = 0.003$ (N), $c = 0.32$ (N/m/s), and $G = 0.1$ (N). To estimate the occurrence of stochastic resonance according to Equation (3.19), it is indicated that stochastic resonance can occur at where the rotating frequency is close to 98.2 rad/s. Meanwhile, the frequency of stochastic resonance can be adjustable by tuning one of the linear or nonlinear coefficients as shown in Figures 4.1 and 4.2.

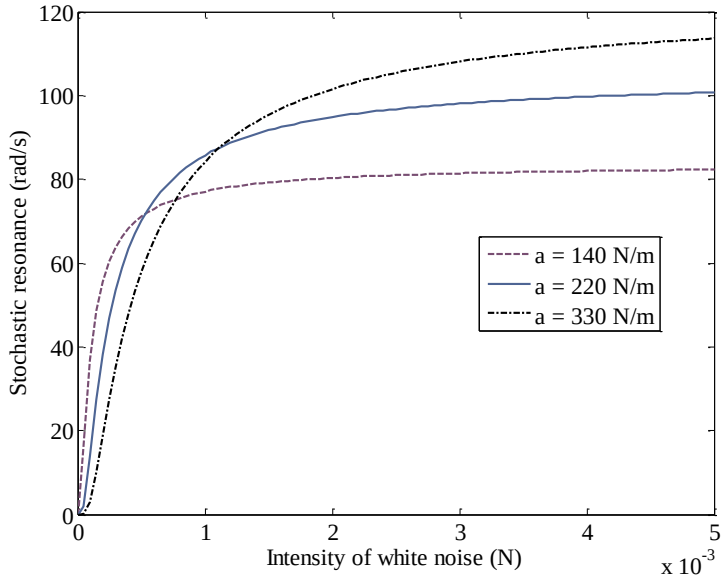

Fig. 4.1 Variation of frequency of stochastic resonance by tuning linear stiffness ($b = 6 \times 10^7$ (N/m^3)).

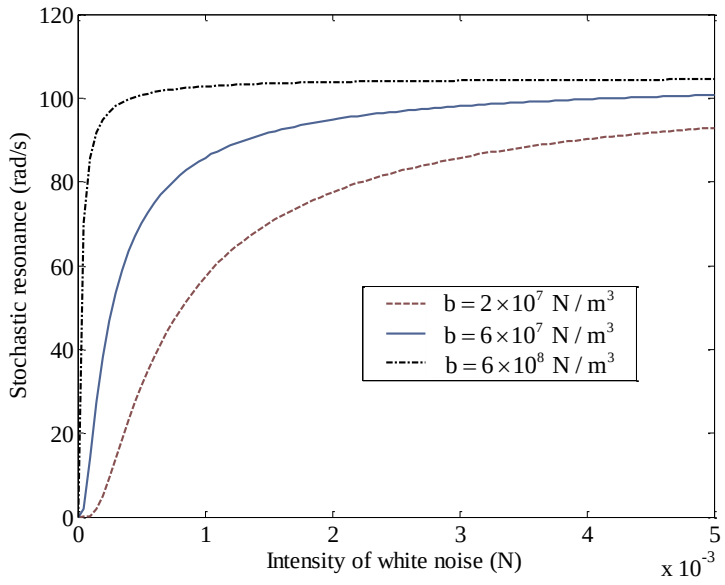

Fig. 4.2 Variation of frequency of stochastic resonance by tuning nonlinear stiffness ($a = 220$ (N/m)).

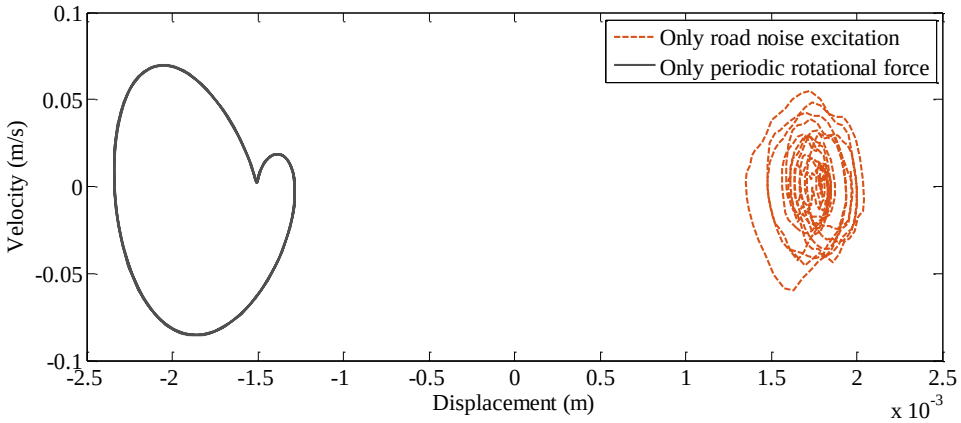

Fig. 4.3 Displacement and velocity responses under road noise excitation and periodic rotational force.

In the cases of only road noise excitation and only periodic rotational force, the displacement responses in Figure 4.3 show that the inter-well dynamics cannot be activated, and from the displacement and velocity responses under road noise excitation, the magnetic end mass disorderly fluctuates around 1.8×10^{-3} m at the maximum velocity of 0.055 m/s, which demonstrates the end mass maintains monostable motion at the position of positive value by the dashed line.

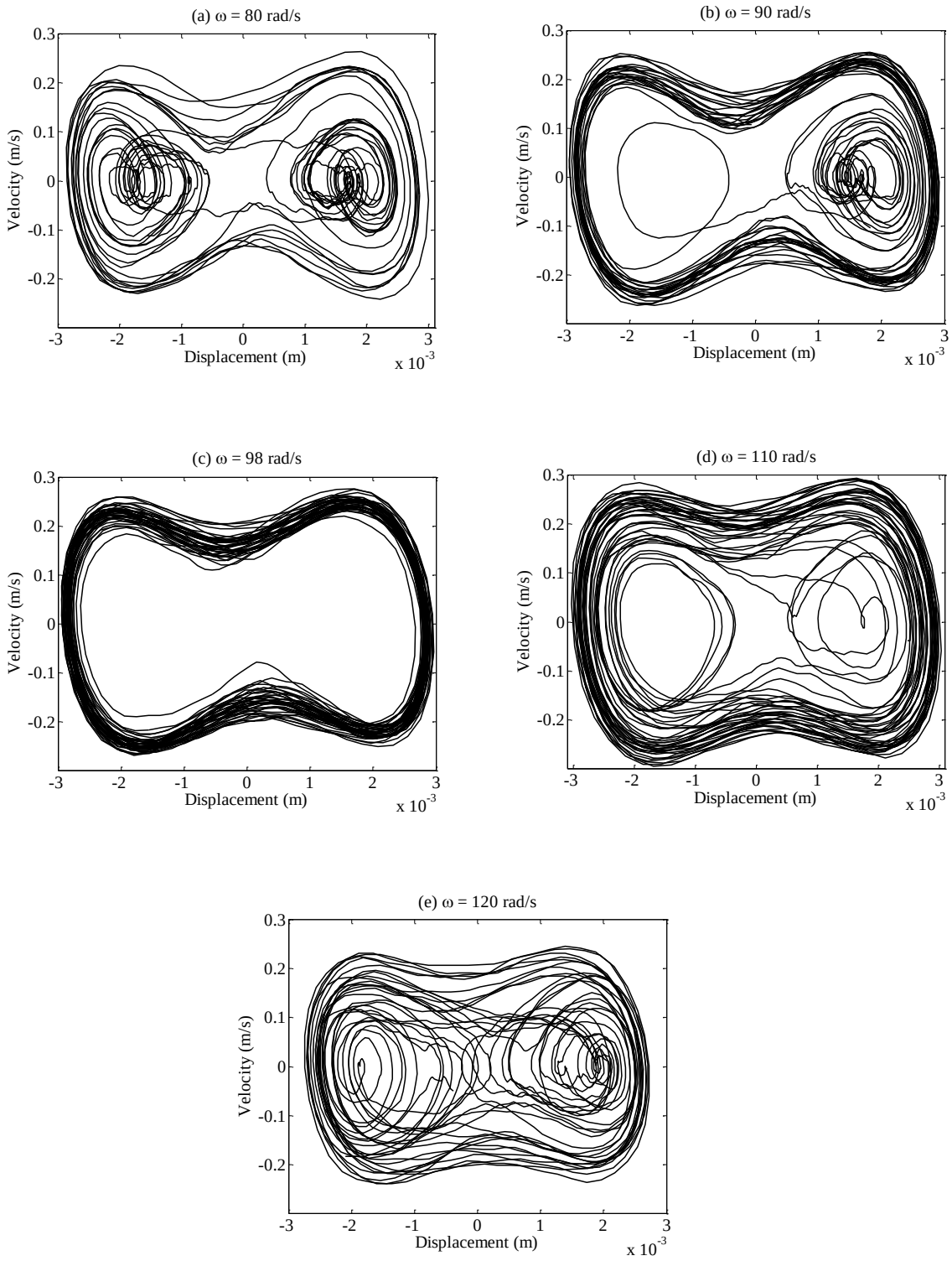

Fig. 4.4. Numerical analysis results of the displacement and velocity responses under both road noise excitation and periodic rotational force at the different angular velocities: (a) 80 rad/s; (b) 90 rad/s; (c) 98 rad/s; (d) 110 rad/s; and (e) 120 rad/s.

Meanwhile, from the responses under periodic rotational force, the end mass periodically quivers around -1.8×10^{-3} m with more bandwidth of displacement and velocity depicted as the solid line, meaning that the end mass maintains monostable vibration at the position of minus value. Therefore, this excitation alone is unable to excite the beam into bistable vibration.

From Figure 4.4, it can be seen that the cantilever beam can be induced to vibrate between two potential wells when road noise and periodic rotational excitations are applied at the same time. However, for different values of angular velocity ω, the response is seen to change. When ω is 80 rad/s, the system has the ability to vibrate between two potential wells, but most of the time maintains motion predominantly within the wells, as shown in Figure 4.4(a) although some inter-well motion is also evident. When ω is 90 rad/s, the system behaves as the bistable state in a certain period shown in Figure 4.4(b).

When the angular velocity of periodic rotational force is 98 rad/s, which is close to the value theoretically predicted by the calculated parametric excitation angular velocity for stochastic resonance, the system can maintain the inter-well motion going all the time, and the displacement and velocity response remain the strongest among the five cases as shown in Figure 4.4(c), which indicates the phenomenon of stochastic resonance. When ω exceeds 98 rad/s the displacement and velocity responses become weaker as depicted in Figures 4.4(d) and (e). Based on these results, it can be concluded that it is feasible for stochastic resonance to be used in rotational environments, and the vibration is enhanced.

4.1.2 Responses under Measured on-Road Noise

The numerical simulation was implemented under the conditions of periodic gravity force and the measured on-road noise excitation with the parametric condition as shown at Table 4.1; calculation of the Kramers rate reveals that stochastic resonance readily occurs at an angular velocity lower than 40.6 rad/s (6.5 Hz) on the basis of the intensity of the measured on-road noise $D=1.22\times10^{-4}$ (N), derived in Section 3.3.2, and the determination analysis on the frequency of stochastic resonance is presented in Figure 4.5. Obtained results are depicted in Figure 4.6. The angular velocity of the rotational tire is varied from 33 rad/s to 42 rad/s.

As shown in Figure 4.6(a), when the angular velocity is 33 rad/s, the velocity response of the cantilever beam remains at a high level for a short initial time; however, the cantilever beam subsequently fluctuates around a low velocity, which illustrates that the beam vibrates within one potential well. Figure 4.6(b) shows that there is more inter-well motion of the cantilever beam at an angular velocity of 35 rad/s than at 33 rad/s. Figure 4.6(c) shows that when ω is 38 rad/s, the velocity responses of the cantilever beam maintain a high-velocity motion. The probability of the beam jumping between two stable positions thus becomes higher as angular

velocity increases. Figure 4.6(d) and (e) show that, beyond 38 rad/s, even the velocity responses of the cantilever beam become low and inter-well motion can still be induced at shorter time periods.

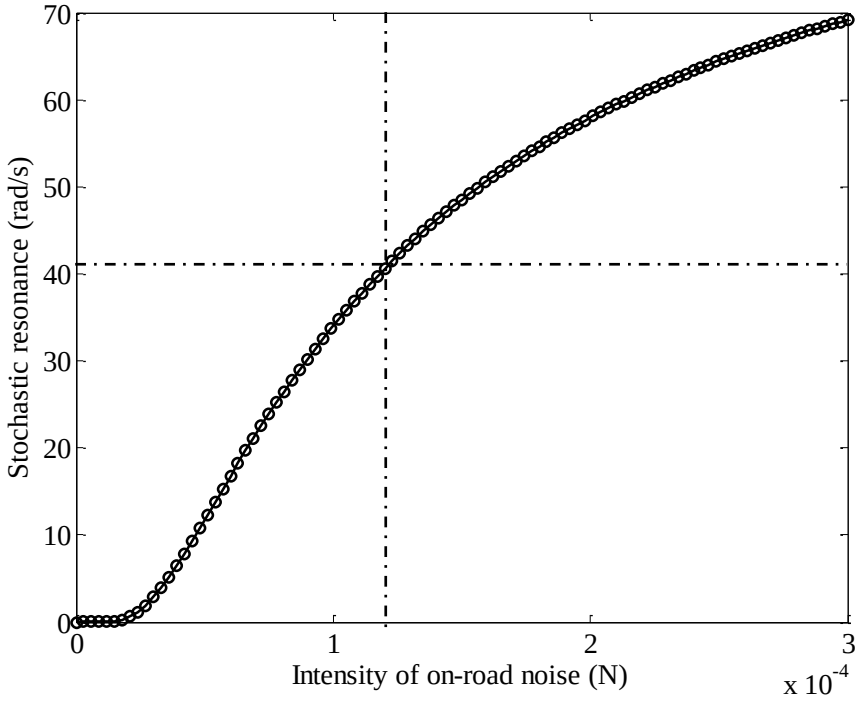

Fig. 4.5. Determination on the frequency of stochastic resonance under the on-road noise excitation.

Table 4.1. Parameters of the energy harvester.

Items	**Permeability of Free Space**	**Volume of Magnet**	**Tip Mass**	**Magnetization Amplitude**		**Coefficient**
Parameter	μ_0	v	m	M_{fx}, M_{fy}	M_{cx}, M_{cy}	k
Value	$4\pi \times 10^7$ H/m	1.07×10^{-6} m^3	8 g	-9×10^5 A/m	8.5×10^5 A/m	152.7 N/m

Thus, when the angular velocity of the rotating wheel is lower than 42 rad/s, the response of the system is enhanced by the appearance of inter-well motion. At an angular velocity of 38 rad/s, stochastic resonance is easily stimulated compared with the other four cases, which indicates that the occurrence of stochastic resonance at the angular velocity of 38 rad/s practically agrees with the result of the theoretical analysis of 40.6 rad/s as calculated in Section 3.2.2.

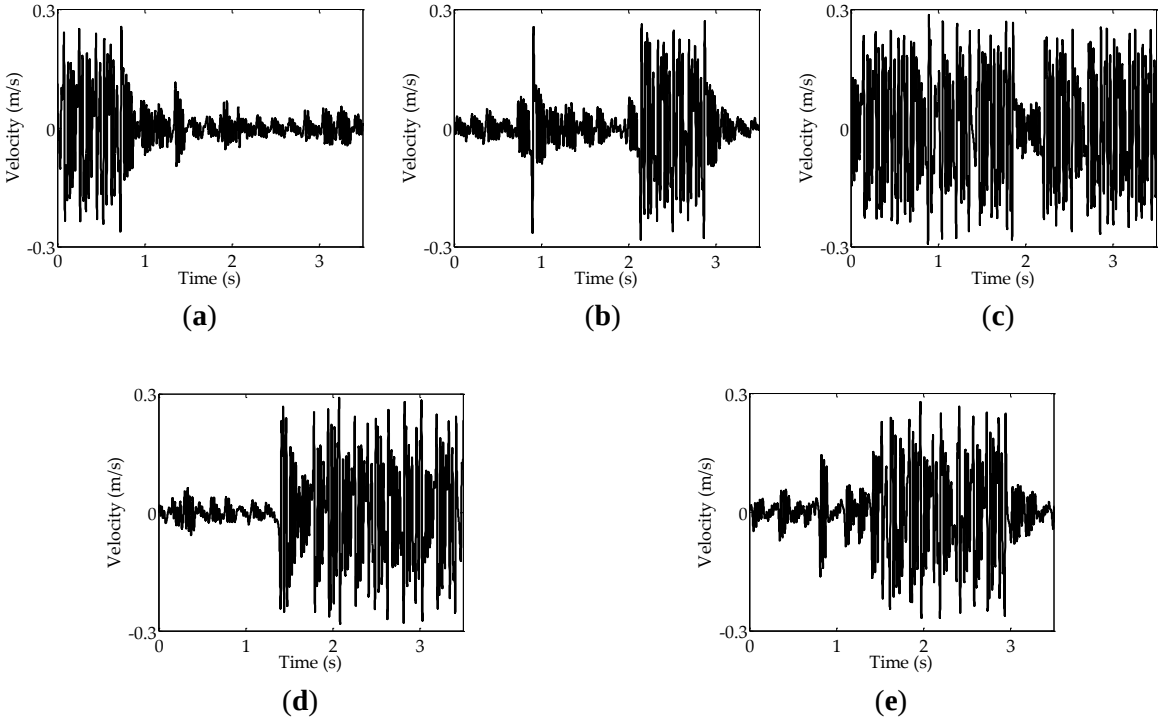

Fig. 4.6. Numerical analysis results of velocity responses under the on-road noise excitation and the periodic gravity force at the angular frequencies: (**a**) 33 rad/s; (**b**) 35 rad/s; (**c**) 38 rad/s; (**d**) 40 rad/s; (**e**) 42 rad/s.

4.2 Bandwidth Broadening by Combining Stochastic Resonance and High Energy Orbit

Because there is a one potential well motion before the beam has the ability to jump over another well. That means the beam is difficult to be stimulated the high energy orbit oscillation at the initially low frequency range as shown in Figure 3.9. From the simulation result shown in Figure 4.7, it is demonstrated that as the frequency of the excitation increases beyond 60 rad/s, the displacement response of the bistable system can be improved to a higher vibration level of the inter-well motion and the valid bandwidth is 60 rad/s–132 rad/s. In response to the weak response at low frequency, the on-road noise is exploited to activate the beam to stochastically vibrate with a higher kinetic energy than the height of the potential wells, so that the response can be enhanced owing to the occurrence of stochastic resonance.

Under the input conditions of up-sweep excitation of gravitational acceleration of 9.8 m/s^2 in conjunction with on-road noise excitation the simulation result is obtained as shown in Figure 4.8. Due to the presence of the noise energy, the vibration response is enhanced while the frequency is lower than 40 rad/s resulted from stochastic resonance and after that the phenomenon can be intermittently maintained. Therefore, the effective frequency bandwidth of

the energy harvester can be extended to a range of 31rad/s–40 rad/s by utilizing stochastic resonance. After that, the frequency exceeds the frequency of 40 rad/s, in spite of the still appearance of the intermittent inter-well motion, the phenomenon of stochastic resonance is difficult to be happened again until the occurrence of the high energy oscillating. Therefore, the effective bandwidth of the energy harvester is promising to be broadened to a wider range by combing the phenomena of stochastic resonance and high energy orbit motion of bistable.

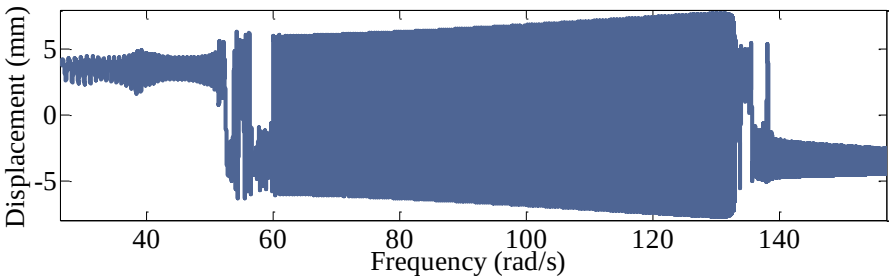

Fig. 4.7. Displacement responses under up-sweep excitation of gravitational acceleration.

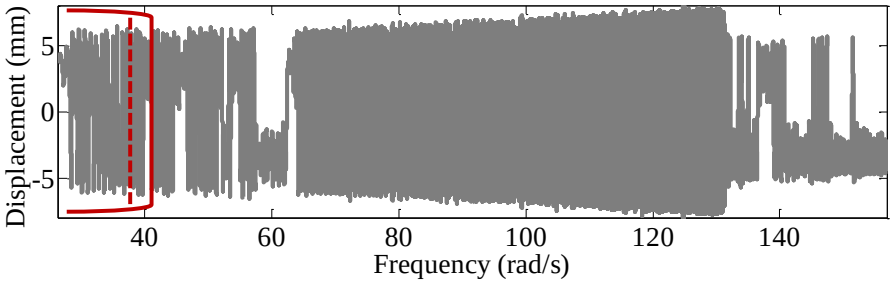

Fig. 4.8. Numerical analysis results of displacement responses under up-sweep excitation of gravitational acceleration in conjunction with the simulated on-road noise excitation.

4.3 Bandwidth Broadening by Using Centrifugal Force

4.3.1 Hardening Stiffness Tuning

In this section, a simulation study is investigated to verify that the performance characteristic under the condition of exploiting the centrifugal force and the hardening stiffness coefficient is tunable along with the change of rotational frequency. A comparison study is implemented under following three cases: (1) monostable hardening type without considering centrifugal force; (2) bistable hardening type in the absence of centrifugal force; (3) bistable hardening type in the existence of centrifugal force.

$$A = Z\sin\omega t\,,\ (0 < \omega < 250\ \text{rad/s},\ 0 < t < 400\ \text{s}). \tag{4.1}$$

(**a**) Side view

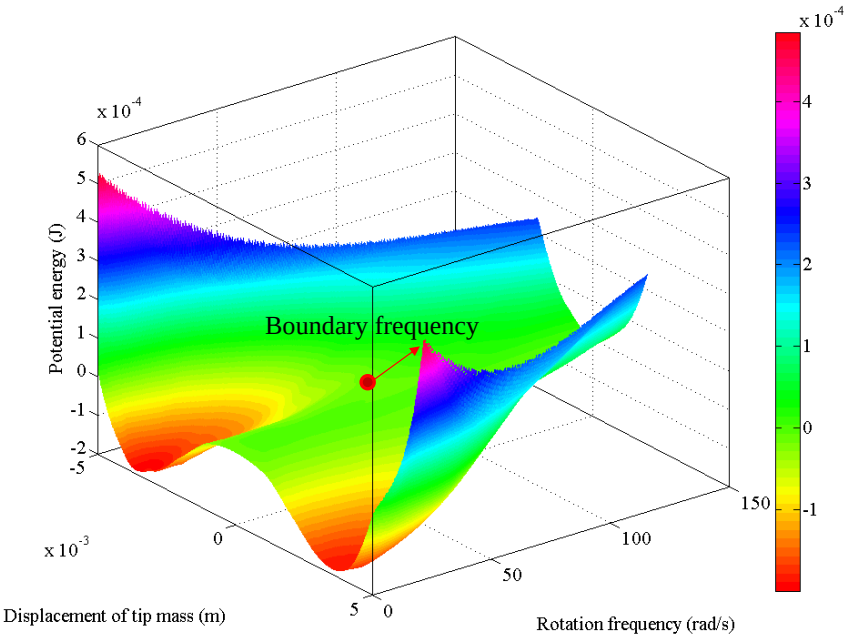

(**b**) Top view

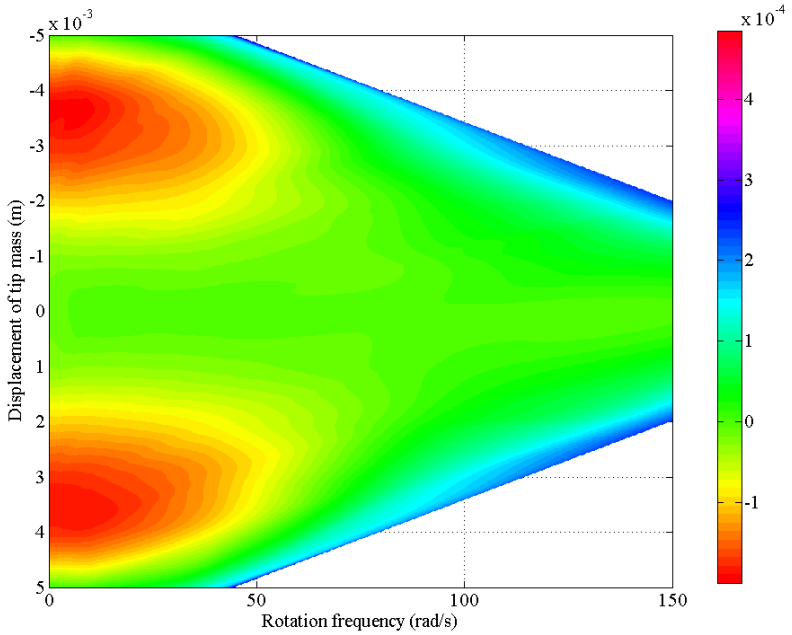

Fig. 4.9. Variation of the potential energy along with the incensement of the rotation frequency: (**a**) side view, (**b**) top view.

Table 4.2. Parameters of the energy harvesters.

Types	*m*	*a*	*b*	*c*	*k*	*L*
Monostable	8 g	60 N/m	4.8×10^6 N/m^3	0.08 N/m/s	500 N/m	4.2 cm
Bistable	8 g	60 N/m	4.8×10^6 N/m^3	0.08 N/m/s	152.7 N/m	4.2 cm

The system parameters is given in Table 4.2, from the three-dimensional figures of the potential wells shown in Figure 4.9, it can be seen that the potential wells gradually become shallow along with the increasing rotational frequency, and the system is altered from the original bistable state to the monostable state, where the system tending to be transformed is defined as boundary frequency. Assuming the amplitude of the equivalent linear stiffness which is expressed in Equation (3.48) is equal to zero, which cases the relationship of $\Delta k = F_M / d$, and then the boundary frequency of the transformation can be governed as

$$\omega_b = \sqrt{\frac{2aL}{3mH}}, \quad \left(a = \frac{F_M}{d} - k\right). \tag{4.2}$$

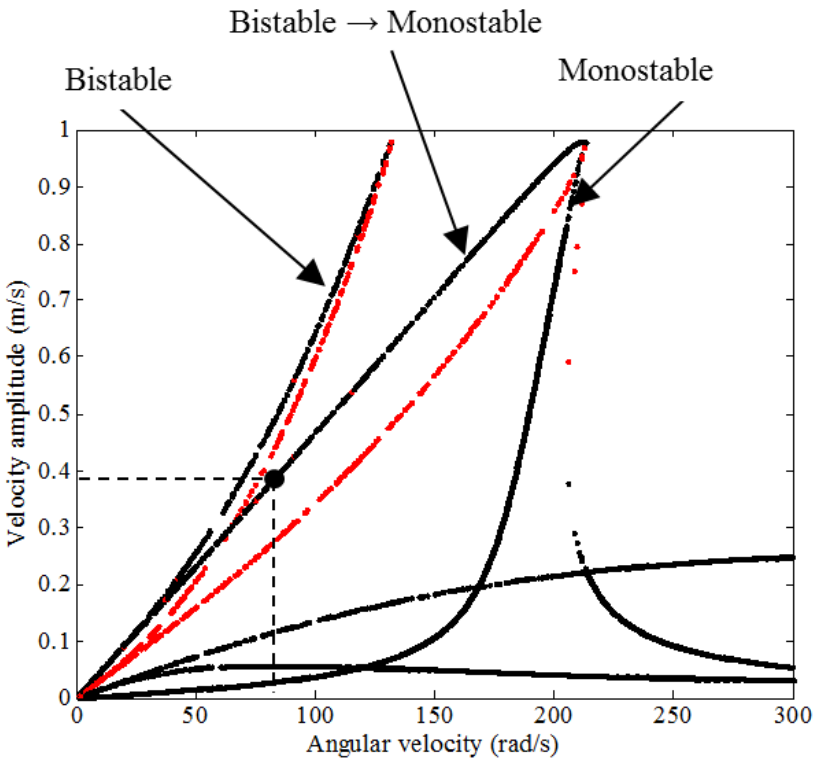

Fig. 4.10. Comparison of frequency response curves under the three different conditions.

Also from the Figure 4.10, the oscillating point can continue maintaining high energy motion from the high energy orbit of bistable system to high energy orbit of monostable system after 88.7 rad/s due to the existence of jump down point which is regarded as the resonance frequency of linear system. As gray linear shown in Figure 4.11, the centrifugal force increases slowly, rotational frequency can keep up with the frequency of jump down until 215 rad/s. That is reason that the high energy oscillating can be maintained within frequency of 215 rad/s.

Furthermore, as expressed in Equation (4.1), the investigation of linearly increasing sweep with gravitational acceleration amplitude of Z is implemented, it is confirmed that the high energy orbit motion can be maintained for a longer period of time shown in Figure 4.12, and the effective broadband is widened from 26 rad/s–132 rad/s to 15 rad/s–215 rad/s by self-adjusting stiffness shown in Figure 4.13.

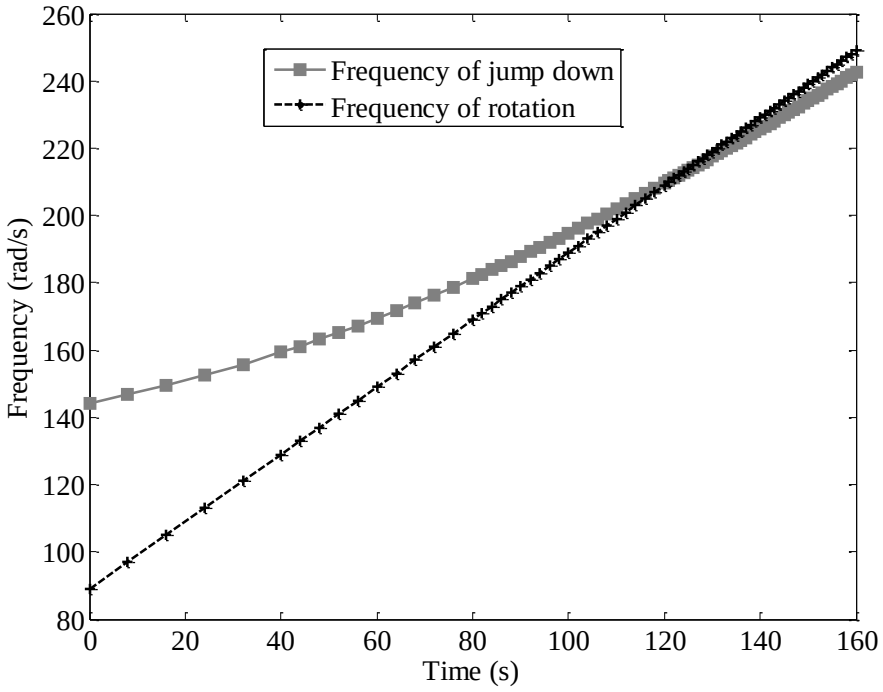

Fig. 4.11. Variability of jump down frequency against the tire rotation.

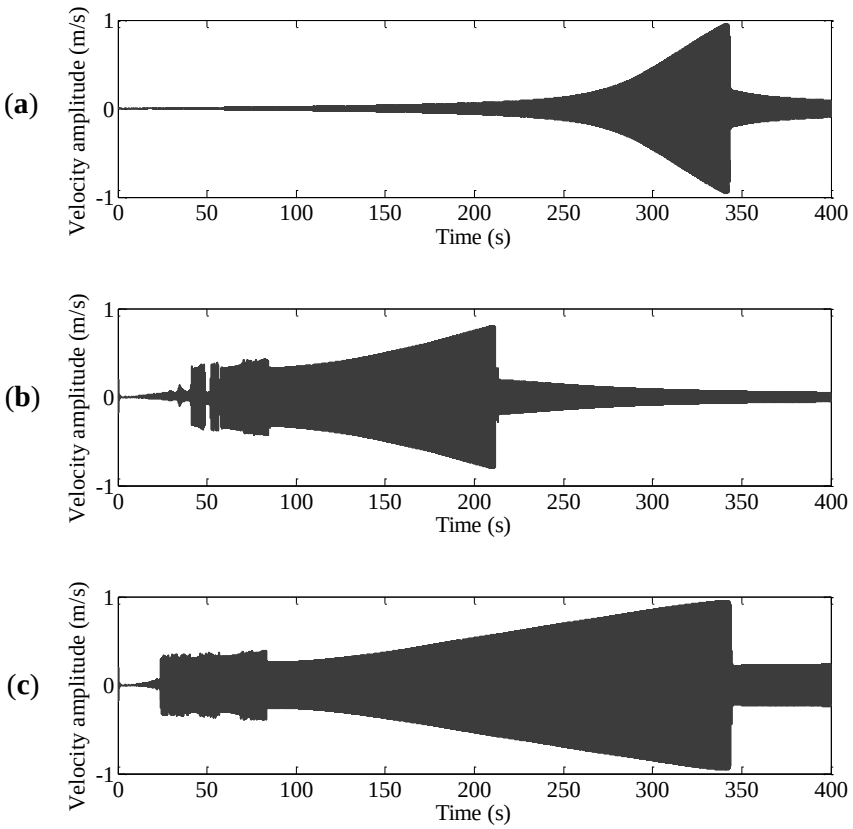

Fig. 4.12. Numerical analysis results of the time domain velocity responses of linearly increasing sweep excitation under the three conditions: (**a**) monostable hardening type without considering centrifugal force; (**b**) bistable hardening type in the absence of centrifugal force; and (**c**) bistable hardening type in the existence of centrifugal force.

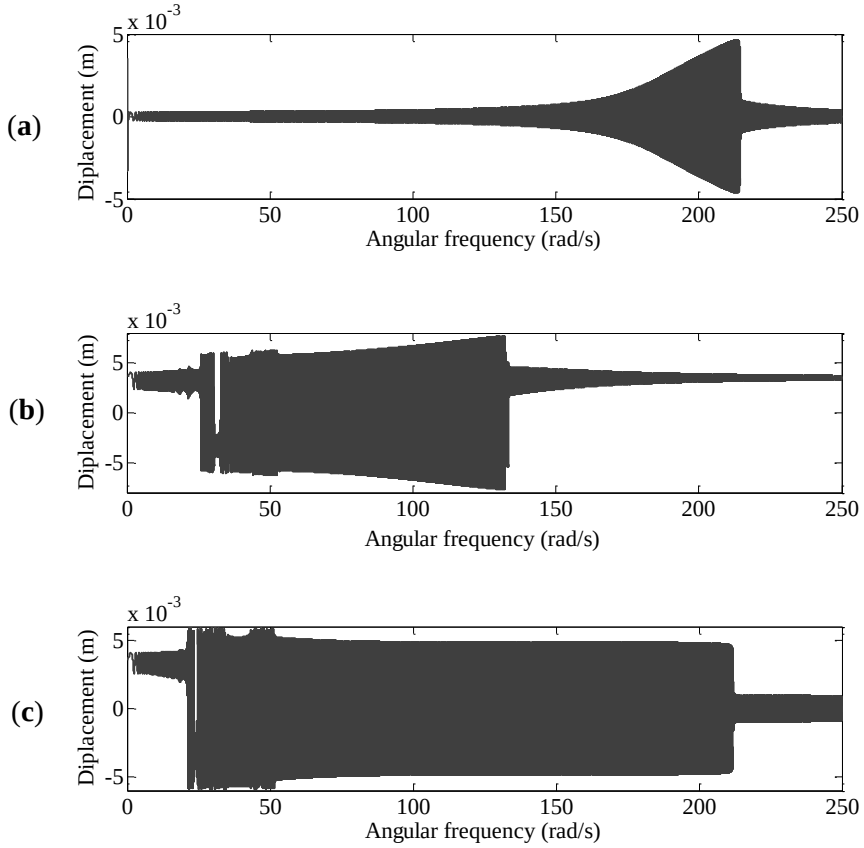

Fig. 4.13. Numerical analysis results of the relationship between the excitation angular velocity and the velocity responses of the linearly increasing sweep excitation under the three conditions: (**a**) monostable hardening type without considering centrifugal force; (**b**) bistable hardening type in the absence of centrifugal force; and (**c**) bistable hardening type in the existence of centrifugal force.

4.3.2 Softening Stiffness Tuning

In order to validate the effectiveness of the centrifugal effect on improving the operational bandwidth of bistable energy harvester, the maximum rotating angular frequency of 38.2 rad/s which corresponds to the driving speed of 40 km/h is licensed. The key task is that to reduce the boundary frequency to 25 rad/s–35rad. If the boundary frequency is too low, the effect of the high energy obit on the velocity response is crippled, which results in discontinuing of the high energy orbit oscillation, even the system is transferred; Otherwise, if the boundary frequency is higher than 40 rad/s, it is impossible to demonstrate the advantage of the centrifugal effect by carrying out the actual-vehicle experiment, due to the limitation of the maximum driving speed.

Therefore, the softening stiffness k is determined as 30 N/m, also the linear stiffness and nonlinear stiffness are reduced respectively. The specific parameters are decided as Table 4.3.

According to the relationship between boundary frequency and centrifugal distance as shown in Figure 4.14, the suitable installing position can be placed at where the centrifugal distance of proof mass is around 2.5 cm–6 cm from the rotating center of tire.

Table 4.3. Parameters of the energy harvesters.

Types	*m*	*a*	*b*	*c*	*k*	L
Bistable	8 g	10 N/m	2×10^4 N/m^3	0.08 N/m/s	30 N/m	4.6 cm

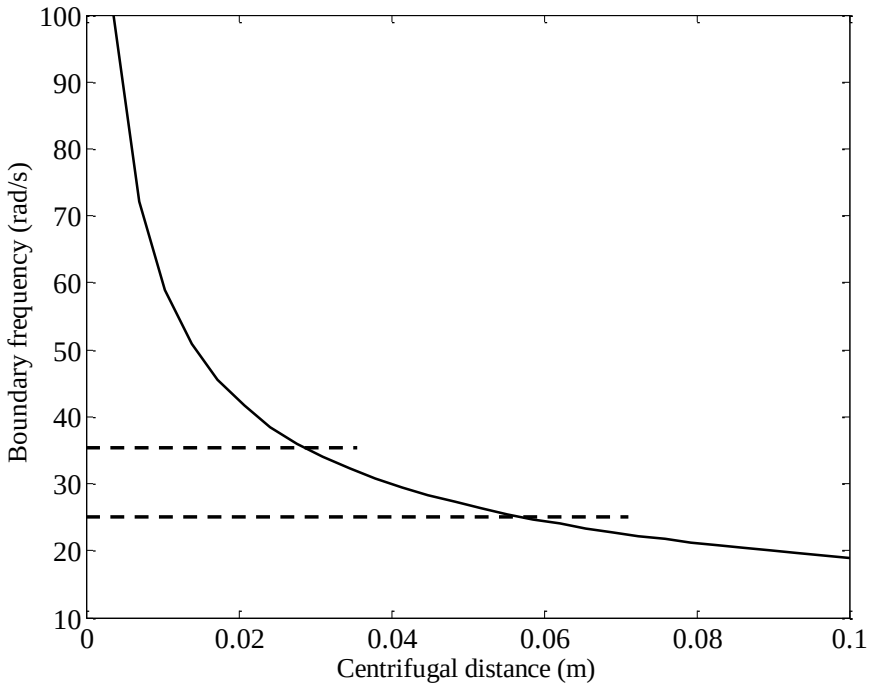

Fig. 4.14. Variation of boundary frequency as a function of centrifugal distance.

4.3.3 Performance of Varying Centrifugal Distance

In this section, the influence of the centrifugal distance on the response performance is investigated. As derived in Section 3.5, the frequency-amplitude expression is expanded through considering the stiffness adjustable term. The investigations are carried out under several cases, in which the centrifugal distances is considered to be the range of 0 cm–8 cm, and specifically decided to 0 cm, 2 cm, 3.6 cm, 4 cm, 5 cm, 7 cm, 8 cm. As the frequency amplitude result shown in Figure 4.15, in the centrifugal condition of 0 cm, which is actually treated as without the effect of the centrifugal force, the high energy orbit motion can be continued by the

frequency of 29.1 rad/s.

Along with the increment of distance to 2 cm, the high energy oscillating can be stabilized for a slightly wider bandwidth, and the system is still retained with the bistable type within the frequency of 40 rad/s by referring to Figure 4.14. Then with the increasing of the centrifugal distance, the high energy orbit tends to be gradually moved to a broader frequency, and it can be invariably maintained over the whole frequency range of 0 rad/s–40 rad/s until the position of 3.6 cm placed from the center of rotating. By comparison with other conditions of closer distance, this case the velocity amplitude can be enhanced over the maximum frequency of 40 rad/s, and the boundary frequency of transferring from bistable to monostable is found to be 31.6 rad/s, which is satisfied to the required transformation frequency range of 25 rad/s–35 rad/s.

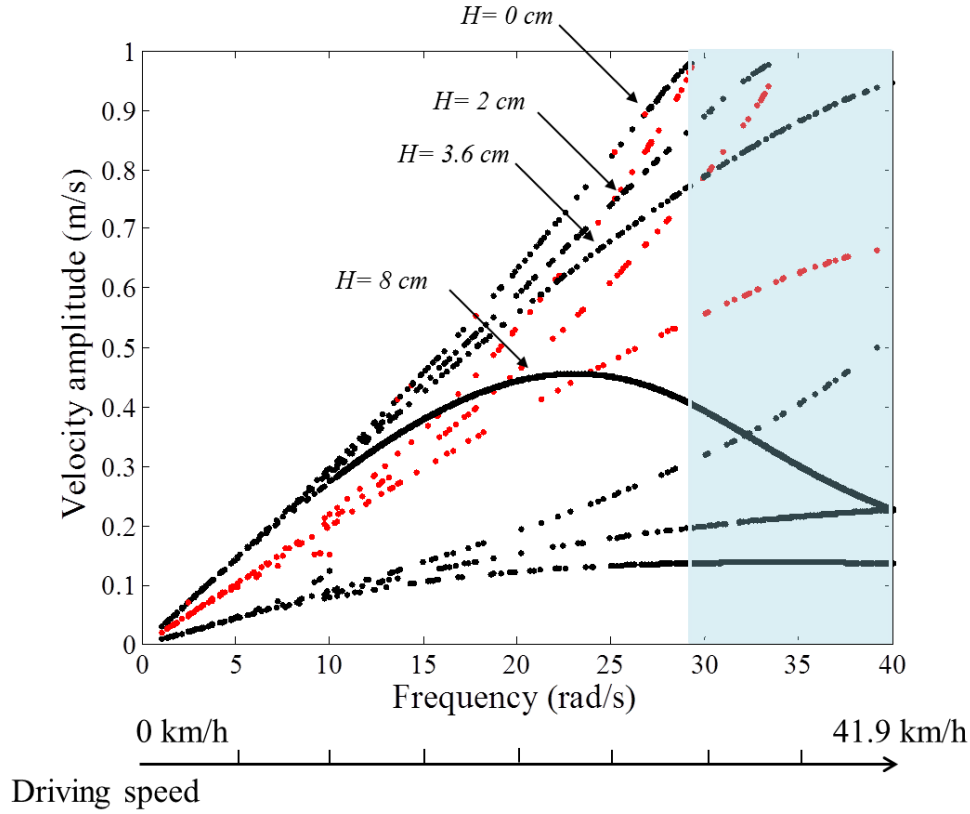

Fig. 4.15. Frequency-amplitude response under a rotating frequency domain of 40 rad/s.

Figure 4.16 demonstrates that the frequency-amplitude response under a rotating frequency domain of 100 rad/s while the centrifugal distances are longer than the distance of 3.6 cm. It is obviously known that the system is altered to monostbale system after 31.6 rad/s in the case of centrifugal force of 3.6 cm due to the existence of jump down point which can be regarded as the resonance frequency of linear system.

As green linear shown in Figure 4.17, the centrifugal force increases slowly, rotational frequency can keep up with the frequency of jump down until 46 rad/s. That is why the high energy oscillating can be maintained within frequency of 40 rad/s. After exceeding the distance of 3.6 cm, since the far distance results in that the increasing rate of centrifugal force is much rapider than that of the tire rotating as analyzed in Figure 4.17, that makes the rotating frequency can never math the jump down frequency of monostable system. Meanwhile, owing to the effect of the bistable system, as shown in figure 4.16, the high energy orbit motion can be stimulated over a low frequency range. However, the increasing centrifugal distances resulting in the decreased boundary frequencies makes the responses tend to become weaken with the initially bistable system.

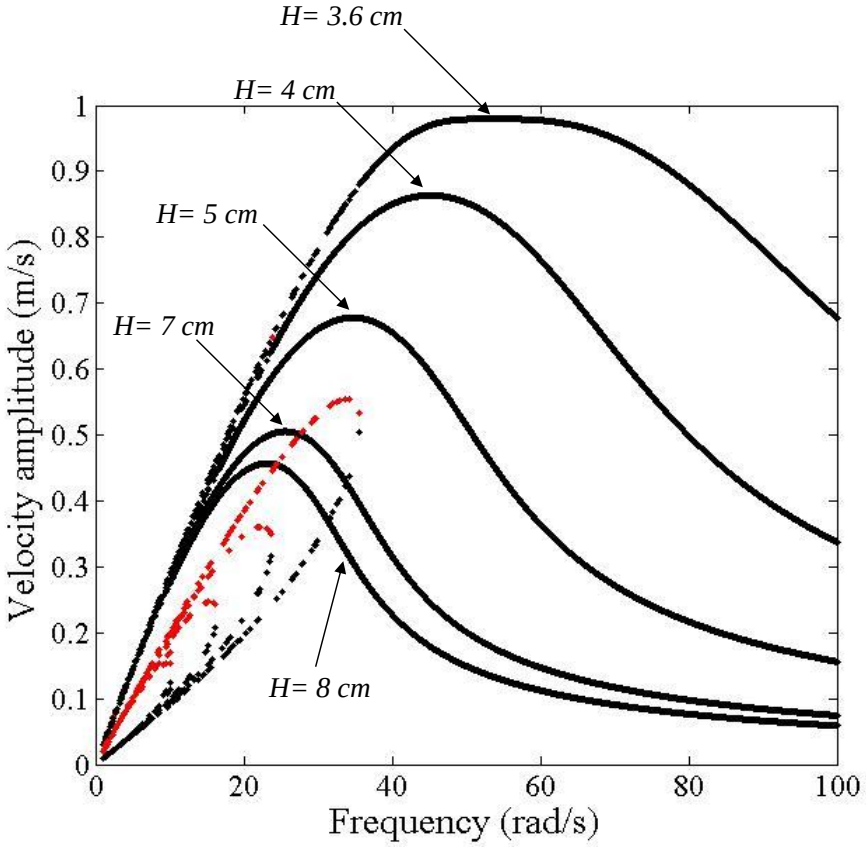

Fig. 4.16. Frequency-amplitude response under the rotating frequency domain of 100 rad/s.

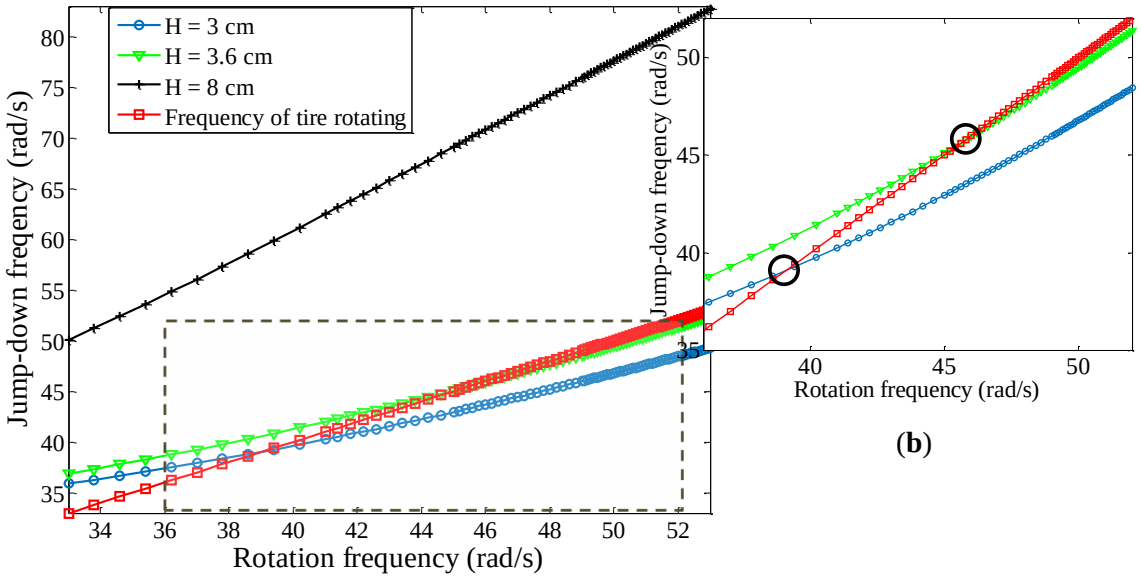

Fig. 4.17. (**a**) Variation of jump down with the rotating frequency increasing; (**b**) partial enlarged drawing.

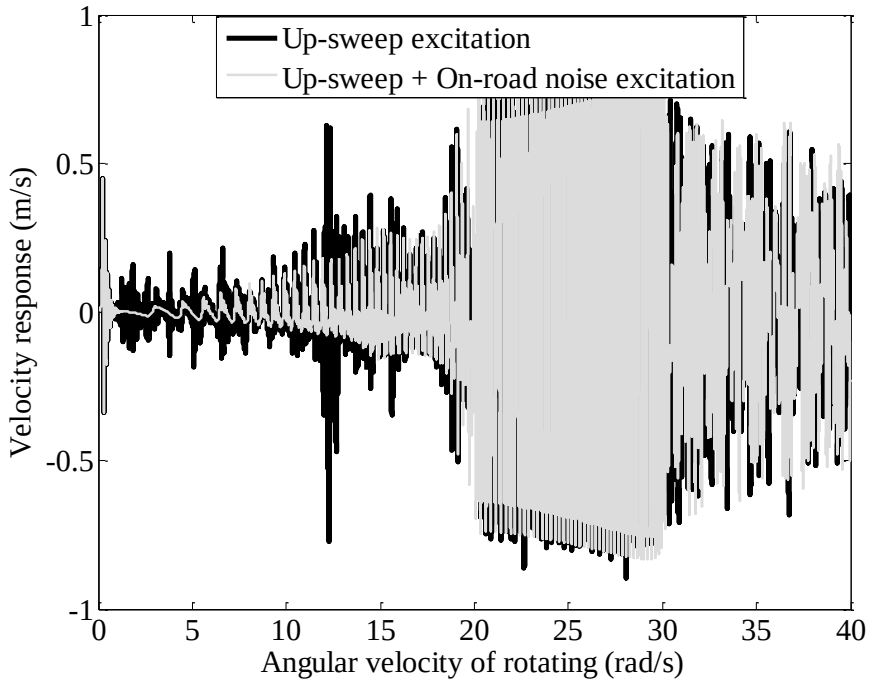

Fig. 4.18. Numerical analysis results of velocity responses under the excitations of up-sweep and up-sweep applied with on-road noise excitation at distance of 0 cm (rotating center).

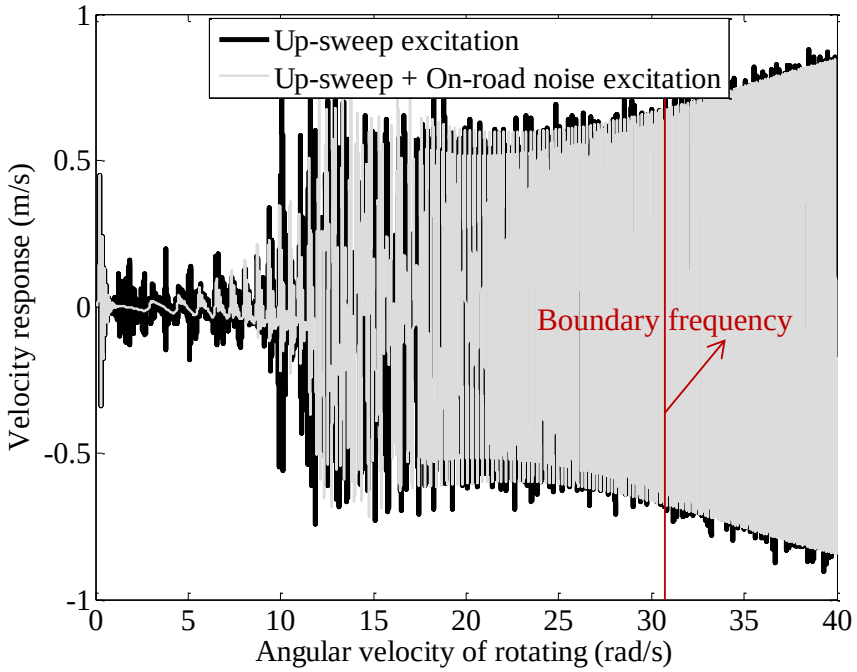

Fig. 4.19. Numerical analysis results of velocity responses under the excitations of up-sweep and up-sweep applied with on-road noise excitation at distance of 3.6 cm.

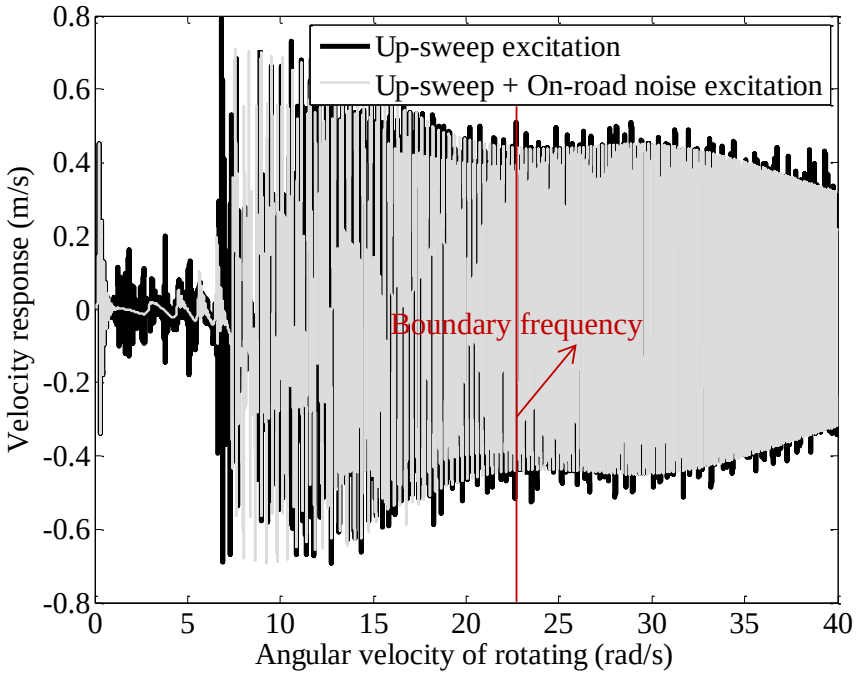

(c)

Fig. 4.20. Numerical analysis results of velocity responses under the excitations of up-sweep and up-sweep applied with on-road noise excitation at distance of 7 cm.

With the purpose of validating the apparently active effect of centrifugal force on the cantilever beam for improving the ability of harvesting energy, the spring constant and the linear as well as nonlinear coefficients of the magnets must be tuned to be awfully lesser for reflecting the advantages under the driving speed limitation of 40 km/h. Therefore, by calculation of the Kramers rate the occurring probability of stochastic resonance is obtained around an insignificant value of frequency. It can be calculated that the frequency of stochastic resonance can just match the value of rotating around the frequency of 8×10^{-4} rad/s. Figures 4.18, 4.19 and 4.20 show the detail comparisons of the input conditions of with and without on-road noise excitation.

It demonstrates the comparisons of numerical results of the velocity response while the centrifugal distance is decided to three positions of, rotating center, 3.6 cm, and 7 cm, under two different input conditions which are the up-sweep excitation and up-sweep excitation applied with on-road noise excitation. From Figures 4.18, 4.19, and 4.20, by comparing the response curves under considering on-road noise and without considering it, all of which reveal the consistent response characteristics under the two different input conditions without observing the phenomenon of stochastic resonance. Meanwhile, the best performance among these three situations can be found at the distance of 3.6 cm.

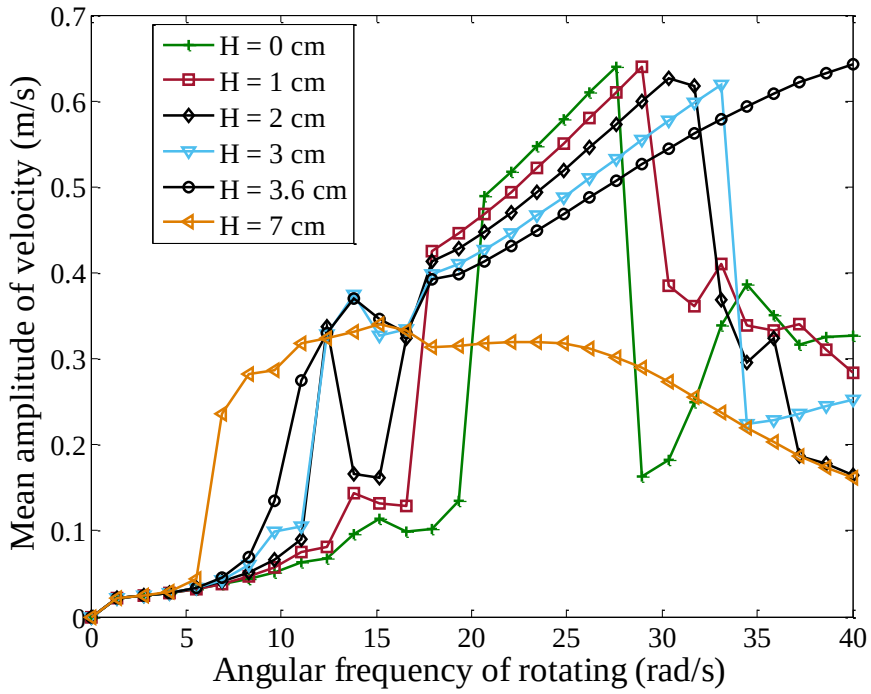

Fig. 4.21. Numerical analysis for the validation of efficient bandwidth under different centrifugally rotating distances.

Furthermore, the simulation investigations of the mean velocity under different centrifugal distances are performed. For each distance the simulations are carried out for thirty times, therefore, one point represents one time implementation of system simulation and calculation of the mean output velocity. By comparison of the different distances, the widest bandwidth is found under the frequency range of 40 rad/s when it is adjusted to 3.6 cm as shown in Figure 4.21, which is very close to the result of frequency-amplitude curve as derived in Figure 4.15.

Chapter 5

Experimental Study

5. Experimental Study

5.1 Laboratory Experiment

5.1.1 Laboratory Apparatus

In order to generate both road noise excitation and a periodic rotational force a vibrator (m060, IMV Corporation) driven by a powerful controller board (dSPACE1103, dSPACE Corporation) was used to provide the necessary conditions for the experiment. To activate the cantilever beam to alternate between stable points, a unimorph piezoelectric film, which produced small damping force, was selected as a harvester. Meanwhile, it was installed near the fixed point, where the bending stress was the highest. By mounting the proposed energy harvester on a vibrator, a high-precision laser displacement measuring system (IL-300, IL-1000, KEYENCE Corporation) could be used to judge whether the system becomes bistable, by investigating the displacement of the magnetic end mass. A high-speed, 16-bit resolution date logger (GL900, GRAPHTEC Corporation) was used to record voltage from the unimorph piezoelectric film. The coupled structure which was investigated in this paper is shown in Figure 5.1.

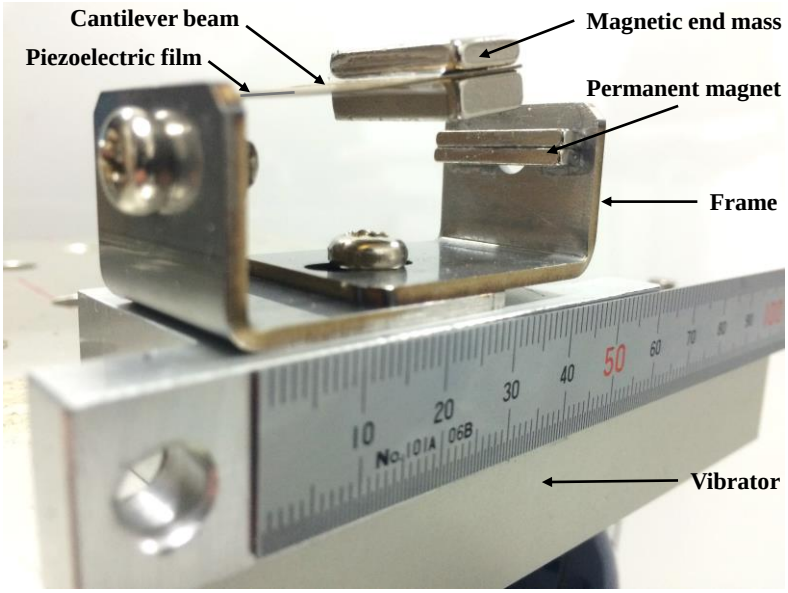

Fig. 5.1. Prototype of the proposed energy harvesting device mounted on a vibrator.

The energy harvester consists of a 42 mm × 10 mm × 4 mm aluminum cantilever beam and an adjustable screw rod for adjusting the distance between two magnets. The magnetic tip mass comprises two identical neodymium magnets (NSC0010, Miyagi, Japan) with dimensions of 15

mm × 10 mm × 3 mm and a permanent magnet (NS0093, Miyagi, Japan) with dimensions of 15 mm × 10 mm × 2 mm. Ultrathin unimorph ceramic piezoelectric material (K2512U1, THRIVE Corporation, Saitama, Japan) with dimensions of 22.9 mm × 10 mm × 0.1 mm was selected to paste on the root segment of the beam, and its electrostatic capacitance is 115 nF. The N/S pole of the magnets is still kept in the x-axis, which is the same arrangement with the model in Figure 3.6. The piezoelectric layer can only bend along the thickness direction of the cantilever, which maximizes the stress on the piezoelectric layer and thus improves power generation. The net volume of the energy harvester is 15.75 cm^3 (70 mm × 15 mm × 15 mm), as shown in Figures 5.2 and 5.3 presented the experimental setups.

The energy harvester system is fixed on the shaker table, displacement sensors 1 and 2 are set to measure the vibrational amplitudes of the magnetic end mass and shaker table, respectively, and the acceleration sensor is assembled to detect the vibration acceleration of the shaker table. An overview of the experimental setting is shown in Figure 5.4. A shaker (F-08000BDH/SLS16/Z02, EMIC Corporation, Tokyo, Japan) is used to generate periodic and noise vibration with peak-to-peak amplitude up to 50 mm. In addition, the response frequency with a range of 0Hz–2000 Hz can act as the external input for wheel rotation.

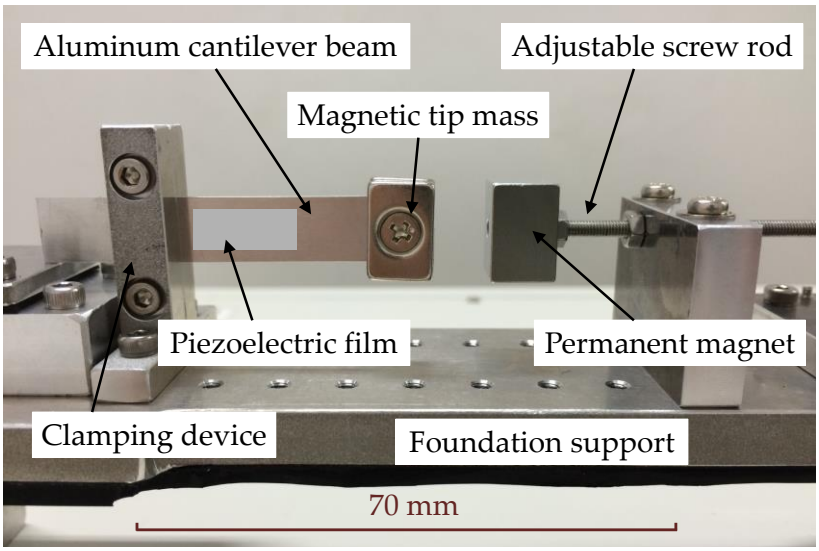

Fig. 5.2. Diagram of the macro-scale energy harvester.

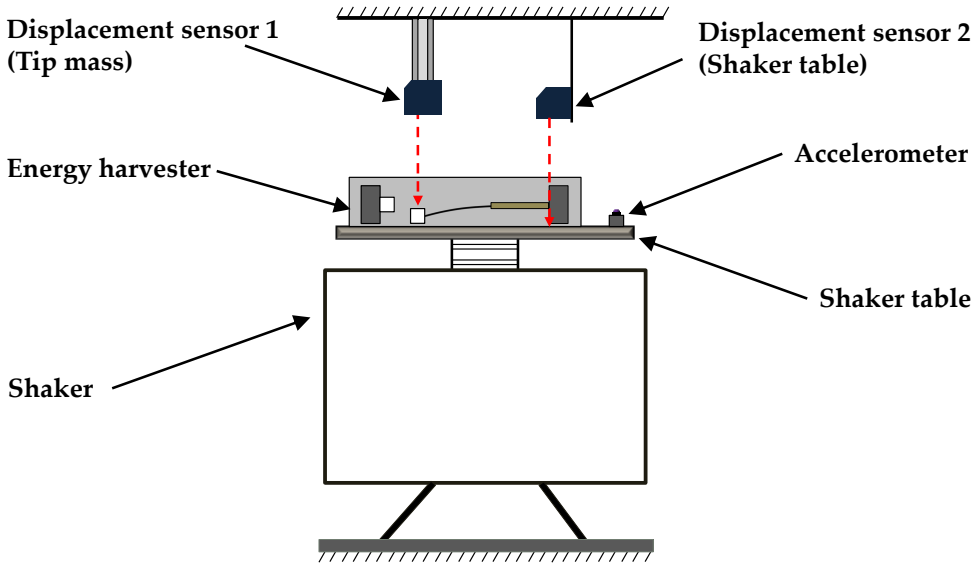

Fig. 5.3 Schematic diagram of the experimental setup.

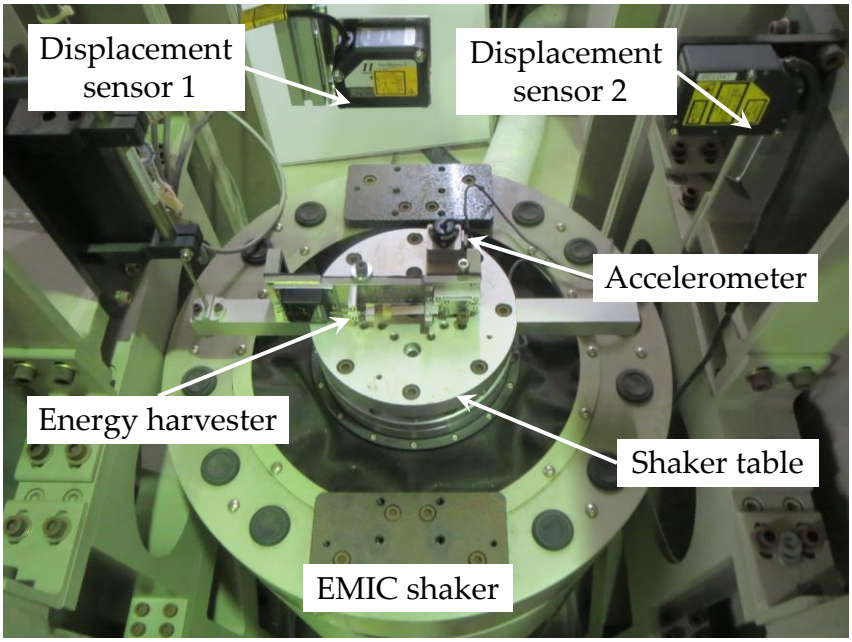

Fig. 5.4. Overview setting of experiment apparatus.

5.1.2 Responses Performance

In order to confirm whether stochastic resonance can occur in such a system and to distinguish the difference between stochastic resonance and monostable vibration experiments were carried out under three conditions as follows: (1) only road noise excitation with the broad bandwidth of 0 Hz–1 kHz, (2) only periodic rotational force at angular velocity of 98 rad/s, and (3) both

road noise excitation and periodic rotational force, respectively.

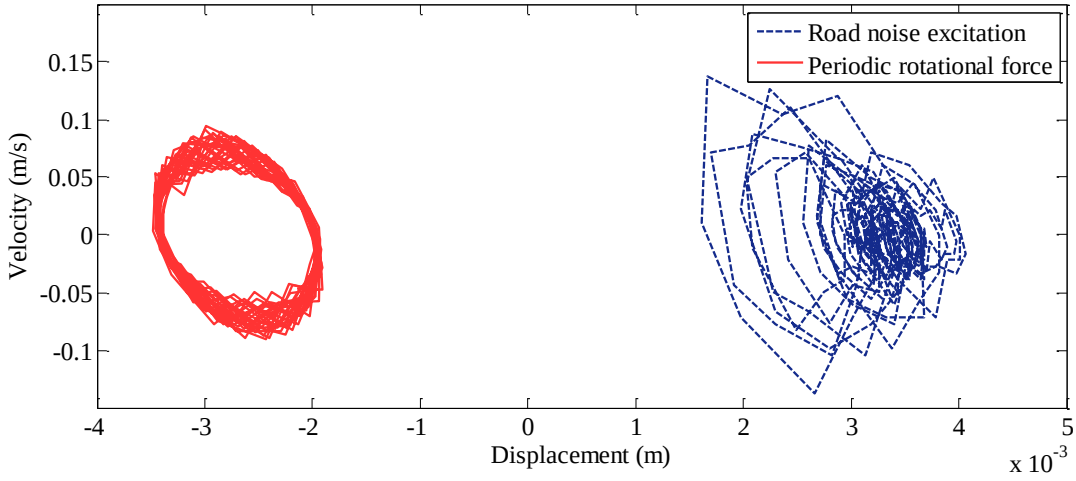

Fig. 5.5. Experimental results of displacement and velocity responses under road noise excitation and periodic rotational force.

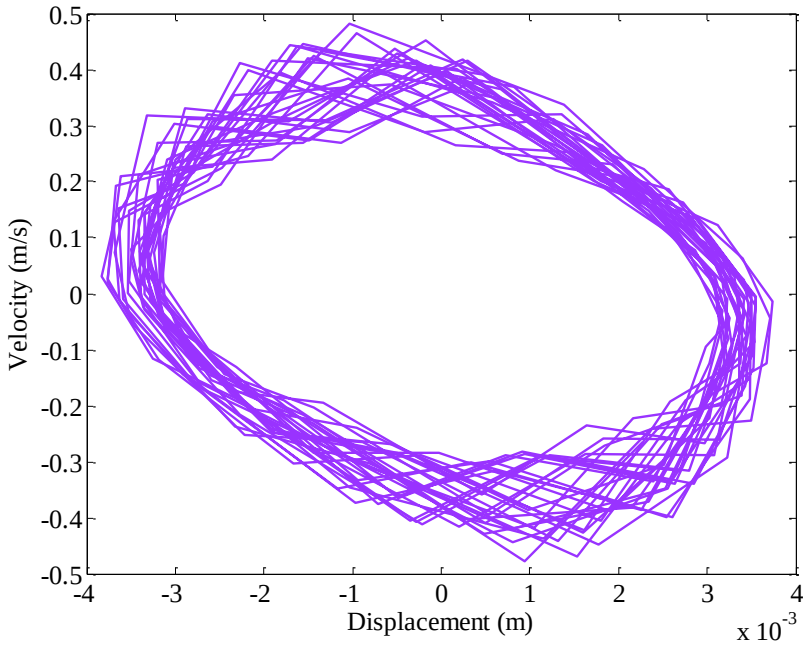

Fig. 5.6. Experimental results of displacement and velocity responses under both road noise excitation and periodic rotational force.

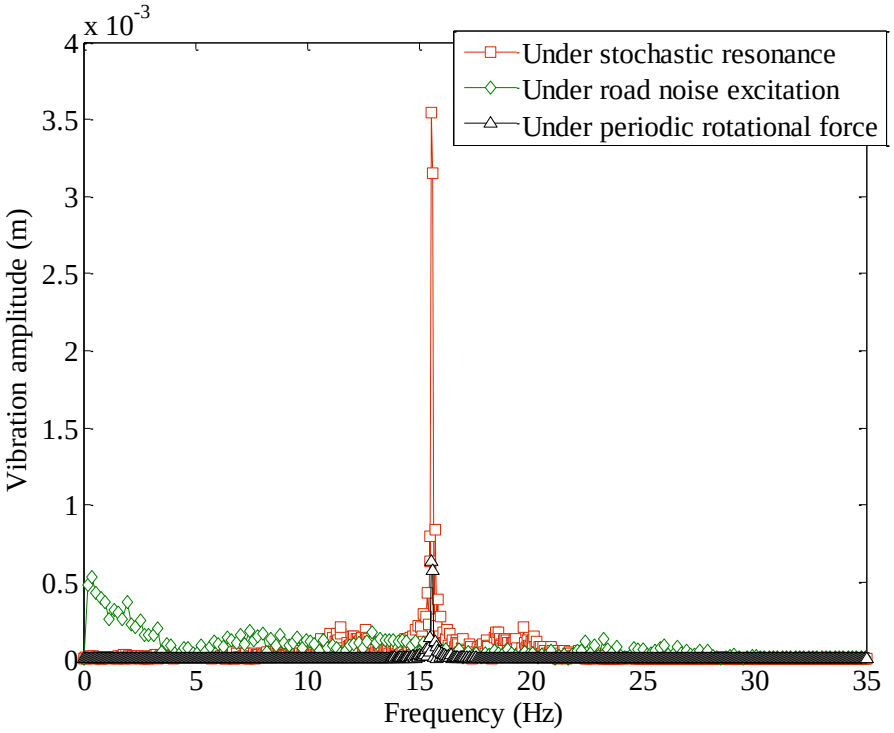

Fig. 5.7. Comparison of amplitude spectrum under three different conditions.

The displacement and velocity responses of the magnetic end mass are demonstrated in Figure 5.5, only under the road noise excitation or periodic rotational force, and it can be observed that the cantilever beam is unable to jump between the potential wells. The red solid line represents the response with reference to the periodic rotational force, operating around the angular velocity of 98 rad/s, which indicates that the cantilever beam fluctuates within another potential well. Nevertheless after both the road noise excitation and periodic rotational force are input into the vibrator, the magnetic end mass can maintain the inter-well motion, as depicted in Figure 5.6, and this is consistent with the theoretically predicted parametric excitation angular velocity of 98 rad/s for this system for stochastic resonance. From this result it can be concluded that the vibration response is enhanced by stochastic resonance. At the same time, on the basis of the comparison of amplitude spectrum under three different conditions as shown in Figure 5.7, it appears that the occurrence of large motion is increased under the condition of stochastic resonance at the frequency of 15.6 Hz and it is significant that the phenomenon of stochastic resonance has the ability to harvest energy from a rotating automobile tire.

Because the shaker provides the velocity control input, integration of the measured road surface acceleration signal into the velocity signal is essential for the accurate regeneration of the on-road noise excitation. Simultaneously, to eliminate the nondetectable low-frequency

effect below 1 Hz, with reference to the literature [95], a composite filter is designed as shown in Figure 5.8; the transfer function $G(s)'$ is derived as

$$G(s)' = \frac{s^2 + 2\omega_{cc}s}{s^3 + 2\omega_{cc}s^2 + 2\omega_{cc}{}^2 s + \omega_{cc}{}^3}, \tag{5.1}$$

where ω_{cc} is the determination coefficient for eliminating the effect of the low-frequency region. This is done instead of employing the traditional integral method, which can produce accumulative errors, as shown in Figure 5.9.

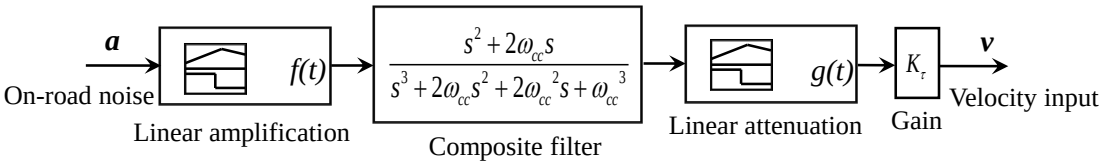

Fig. 5.8. Block diagram of the composite filter

By using this kind of filter, the acceleration signal is calculated above 1 Hz as

$$f(t) = \begin{cases} t, & (0 \le t \le 1) \\ 1, & (1 < t \le \tau) \end{cases}, \quad g(t) = \begin{cases} 1, & (0 \le t \le \tau - 1) \\ t, & (\gamma - 1 < t \le \tau) \end{cases}. \tag{5.2}$$

Here, t and τ are respectively the real time and total experiment time, $f(t)$ is the linear amplification for gradually increasing the vibrational amplitude of the shaker within 1 s of the start time, and $g(t)$ is the linear attenuation for weakening the vibration in the final second before the shaker completely stops shaking.

When the vehicle travels at low speed, with the purpose of regenerating the on-road noise indicated by the black solid line in Figure 5.10, the power spectral density of the measured on-road acceleration is further analyzed in Figure 5.11 [42]; it shows that the energy from paved road noise excitation is mainly restricted to the frequency bandwidth of 1 Hz –60 Hz while the vehicle travels at low speed. In Figure 5.10 and 5.11, the simulated vibration from the shaker is approximately consistent with the on-road noise measured using a composite filter.

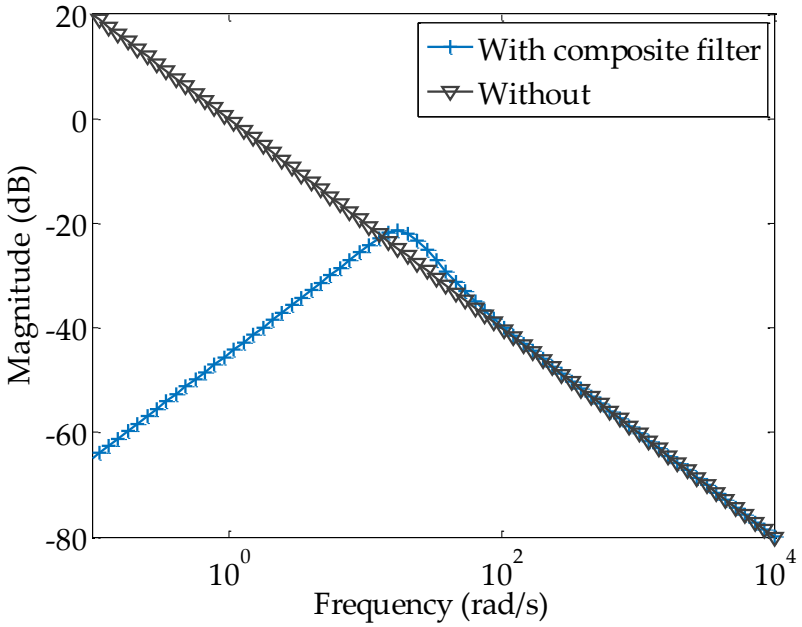

Fig. 5.9. Comparison of the frequency responses of the traditional integration method and composite filter.

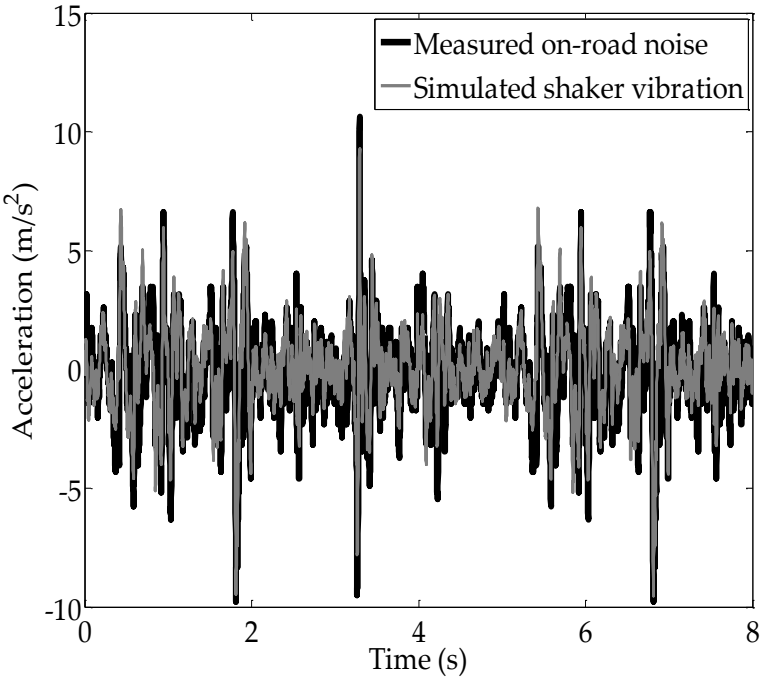

Fig. 5.10. Experimental results of acceleration regeneration of the measured on-road noise for the shaker.

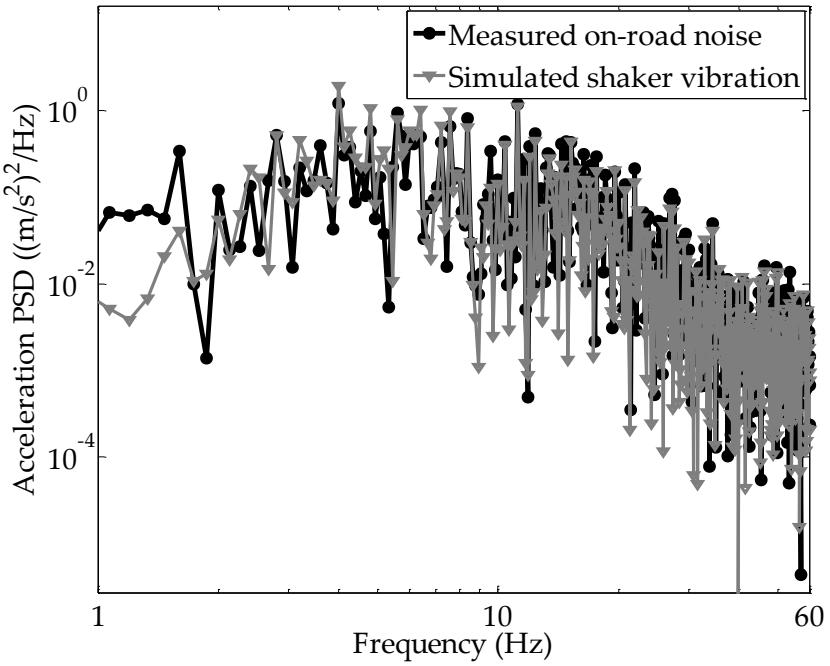

Fig. 5.11. power spectrum density comparison of the measured on-road noise and simulated shaker vibration.

The first experiment investigated the dynamic performance of the energy harvester and the collected power with a matched resistive load. The second experiment validated the sustainability of the energy harvester under a linearly increasing frequency of up-sweep excitations with constant amplitude of gravitational acceleration. The primary goal of the laboratory experiment is to verify the dynamic performance of the prototype system under three conditions: (1) on-road noise excitation, (2) periodic gravity force, and (3) wheel rotation.

As shown in Figure 5.12, the displacement responses can be observed under the above mentioned three conditions, and the two stable equilibrium positions are located at ±3.5 mm, as indicated by blue dashed lines. First, under the condition of on-road noise excitation, by suitably separating the magnets, the displacement response of the system remains at a low level, and the cantilever beam occasionally stimulates escape from one stable position to another stable position, depending on the degree of bumps in the paved road. Second, under periodic gravity force with modulation frequency of 6 Hz, the cantilever beam vibrates at a position between 2 and 4 mm with intra-well dynamic oscillation. Third, under wheel rotation, the energy harvester experiences not only excitations from its own periodic gravity force but also on-road noise excitation. The black line in Figure 5.12 shows that the system enters inter-well motion between two stable equilibrium positions, and the displacement response is strongly amplified at a

frequency of 6 Hz, which matches the simulation parameters, calculated using the Kramers rate. This demonstrates that the occurrence of stochastic resonance is feasible for real applications.

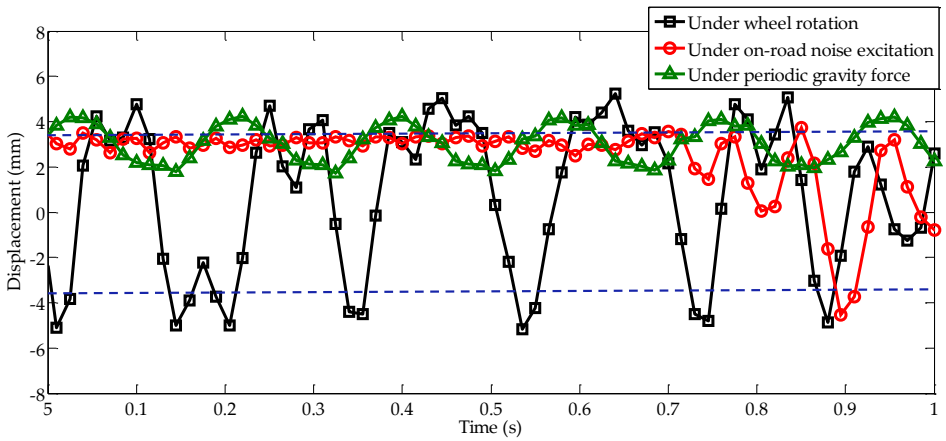

Fig. 5.12. Experimental results of displacement responses under three conditions: (1) on-road noise excitation; (2) periodic gravity force; and (3) wheel rotation combined with the on-road noise excitation and the periodic gravity force.

5.1.3 Energy Harvesting Performance

In light of the fact that the vibration is enhanced by stochastic resonance, how much power can be generated will be estimated by performing resistance tests next. The theoretical magnitude of the matching impedance is calculated to be 33.4 kΩ based on the internal impedance expression of Equation (5.3). As plotted in Figure 5.13, the maximum instantaneous power has the ability to reach 0.14 mW with a matching impedance of 33.4 kΩ, which agrees with the calculated impedance. Moreover, it is also demonstrated that it is possible to power automobile tire pressure sensors under stochastic resonance. For example, Infineon SP37 900kPa tire pressure sensors can operate under an ultra-low standby power of 1.33 μW ~2.52 μW [96].

$$R_{op} = \frac{1}{j\omega C_p}, \tag{5.3}$$

where C_p is the inner electrostatic capacitance of the piezoelectric film. The voltage response V across the internal impedance and the external load resistance can be expressed by employing the model of the piezoelectric transducer as

$$V = \frac{\theta'}{\sqrt{1 + 1/\omega^2 R^2 C_p{}^2}} x_T , \tag{5.4}$$

where $R = R_{op} + R_L$ is the total resistance of the energy harvesting circuit, R_{op} is the internal impedance, and R_L is the external load resistance. The symbol of θ' is the electromechanical coupling coefficient, which can be calculated by considering the relationship between the deflection at the tip of the beam and the deflection of the piezoelectric transducer.

Using Equation (5.4), the voltage produced across the load resistance can be written as

$$V_{op} = \frac{R_{op}}{R_{op} + R_L} \frac{\theta'}{\sqrt{1 + 1/\omega^2 (R_{op} + R_L)^2 C_p{}^2}} x_T , \tag{5.5}$$

and rearranged as

$$V_{op} = \frac{R_{op} \theta' x_T}{\sqrt{\left(R_{op} + R_L\right)^2 + 1/\omega^2 C_p{}^2}} . \tag{5.6}$$

Substituting Equation (5.3) into Equation (5.6) yields

$$V_{op} = \frac{\theta' x_T}{2 + \omega^2 C_p{}^2 R_L{}^2} . \tag{5.7}$$

For the purpose of evaluating the advantages of the phenomenon of stochastic resonance it is assumed that power generated only under road noise excitation is p_1, only under the periodic rotational force is p_2, and power obtained under both road noise excitation and periodic rotational force is p_3. Hence, the monostable vibration can harvest power by calculating the sum of p_1 and p_2, while p_3 is the power harvested by stochastic resonance respectively. Because the total instantaneous power dissipated by electrical and mechanical damping can be calculated based on the expression of $(c_e + c_m)\dot{x}_T{}^2$, then it is necessary to calculate the damping coefficient by experimental investigation.

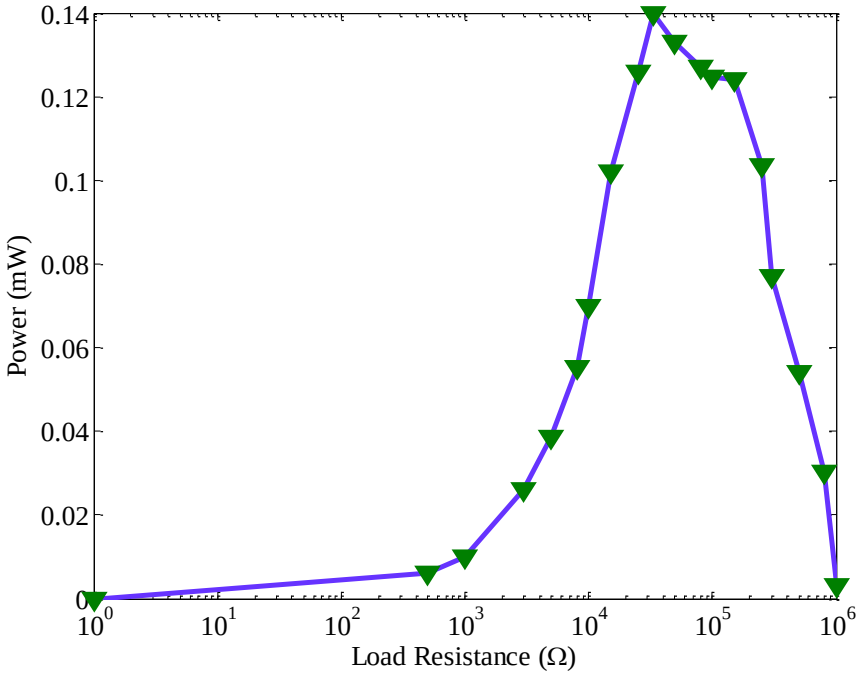

Fig. 5.13. Maximum instantaneous power with the resistor variation.

However, the electric damping coefficients are not constant in relation to different external impedances, for the reason that a piezoelectric element consists of a capacitance which would affect the process of charging or discharging as the external resistors connected to the electric circuit varies. Therefore, in order to obtain the total damping with the matching impedance, the voltage is measured as shown in Figure 5.14. By taking 20 periodical points of amplitude of maximum voltage, the total damping coefficient is calculated based on the following equation as

$$c = c_e + c_m = 2m\delta = 2m\frac{1}{p'}\ln\frac{b_{n'}}{b_{n'+p'}}, \tag{5.8}$$

where n' and p' represent the numbers of the first counting points and the last counting point, respectively, $b_{n'}$ is the amplitude of the first sampling point, and $b_{n'+p'}$ is the amplitude of the last sampling point. Then, the dissipated power can be derived by the expression of $(c_e + c_m)\dot{x}_T{}^2$. By utilizing the moving average filter the power dissipated and harvested can be depicted in Figure 5.15. Under the condition of stochastic resonance the average generated power of p_3 can reach 0.032 mW, which is nearly two fifths of the total dissipated power of 0.081 mW. Conversely, it is nearly ten times higher than the average power of $p_1 + p_2$ generated in the case of monostable vibration.

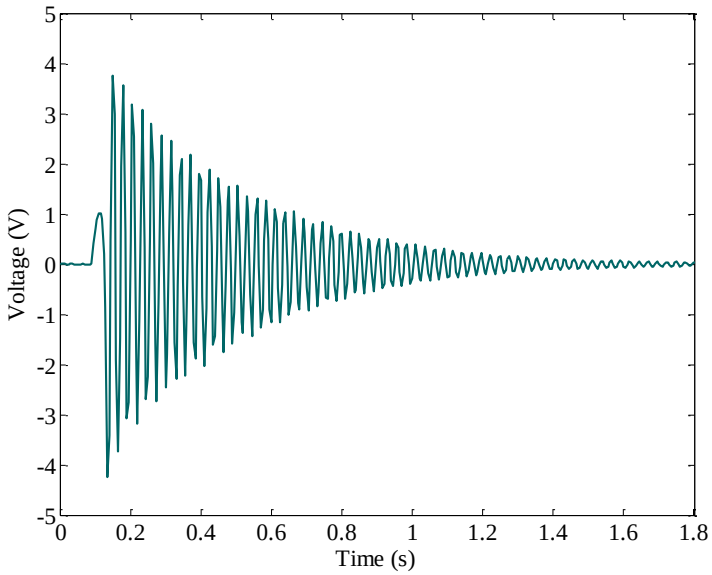

Fig. 5.14. Voltage amplitude with the matching resistor.

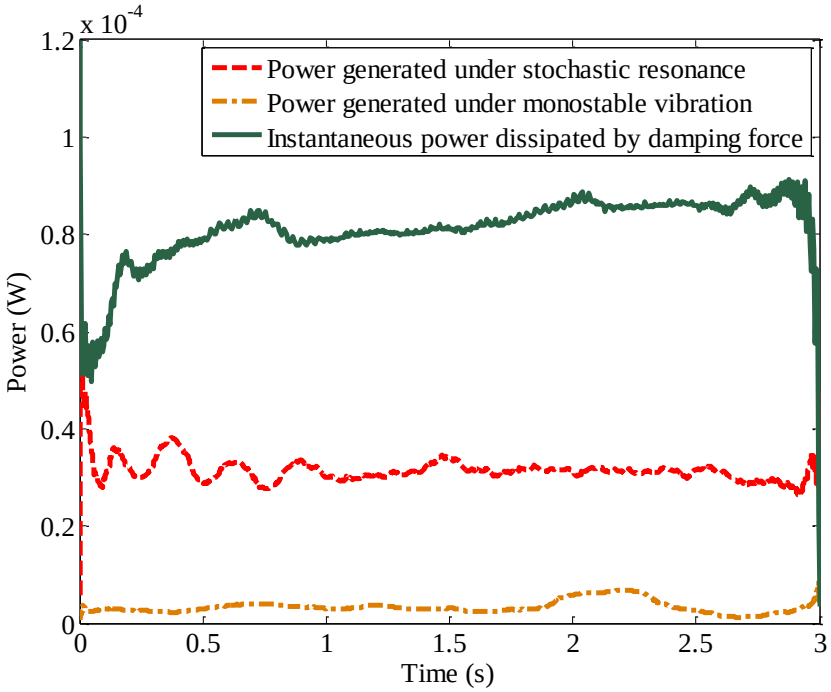

Fig. 5.15. Available power under stochastic resonance and monostable vibration.

The energy harvesting efficiency of stochastic resonance by this novel power harvester was also discussed. It is assumed that the accumulated energy during certain period of time is defined to be E_1, E_2 and E_3, respectively, which corresponds to the average generated power of p_1, p_2 and p_3. Thus, the generated energy under monostable vibration can be obtained by calculating the sum of E_1 and E_2, while the energy harvested by stochastic resonance and the

total dissipated energy by this power harvester are defined to be E_3 and E_t. By connecting the matching impedance of 33.4 kΩ as calculated above, the result of energy regenerated in three seconds is shown in Figure 5.16. The red dashed line shows that harvested energy reaches 0.0939 mJ under stochastic resonance; the orange dash-dotted line represents the fact that the obtained energy can be 0.0099 mJ from monostable vibration, and the green solid line indicates that the total dissipated energy is 0.246 mJ. In the case of stochastic resonance the energy regeneration efficiency can be calculated to 38.2 % by the expression of E_3/E_t. Nevertheless, under the condition of monostable vibration the energy harvesting efficiency can just reach 4.1 % based on the expression of $(E_1+E_2)/E_t$, which demonstrates that here stochastic resonance can enhance the generated power as well as boost the energy regeneration efficiency more effectively than the monostable vibration.

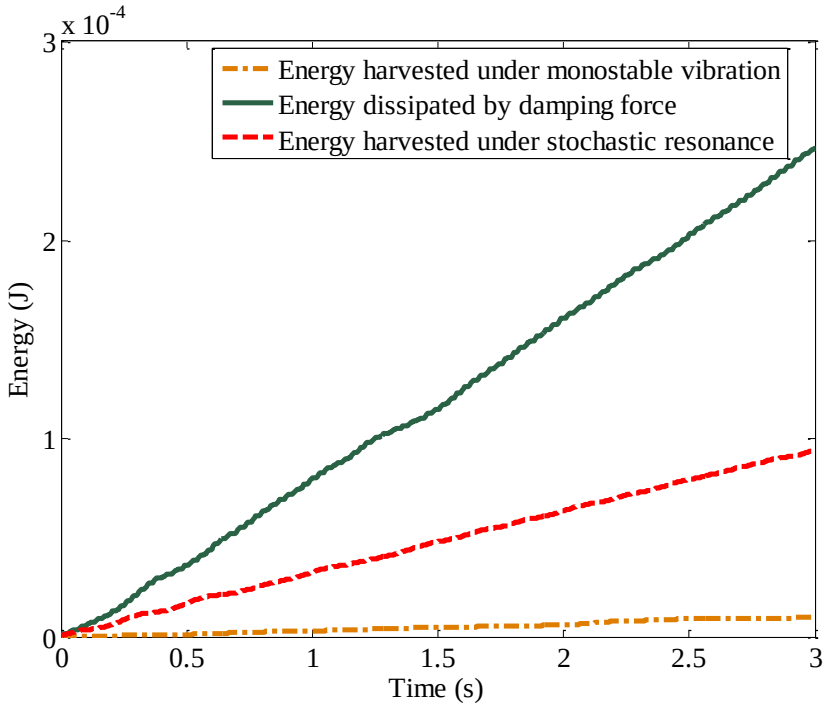

Fig. 5.16. Accumulated energy under stochastic resonance and monostable vibration.

The load resistance experiment was carried out with a matching resistor of 252 kΩ which is calculated based on the load resistance expression of $1/j\omega C_p$, to confirm performance improvement due to the occurrence of stochastic resonance under real circumstances with the periodic frequency of 37.7 rad/s.

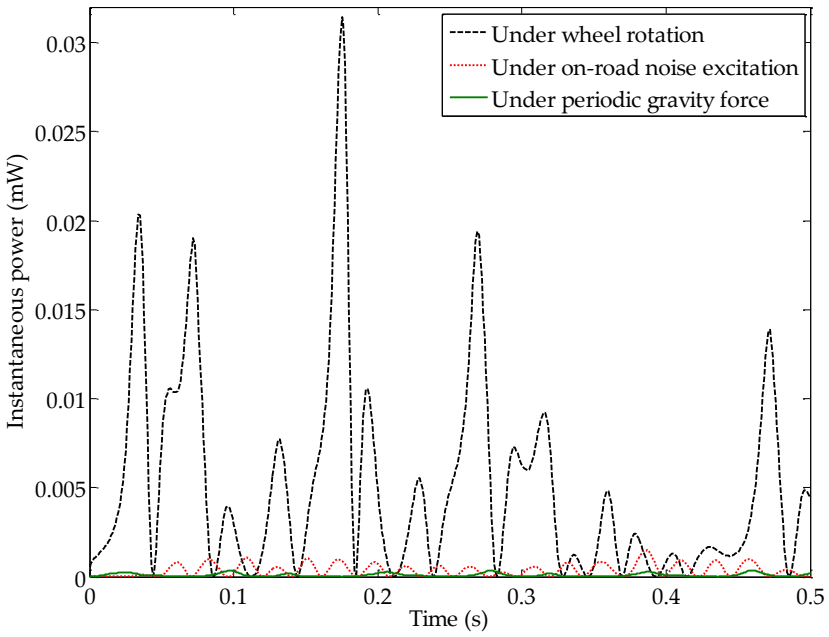

Fig. 5.17. Experimental results for the comparison of the available net power under three conditions.

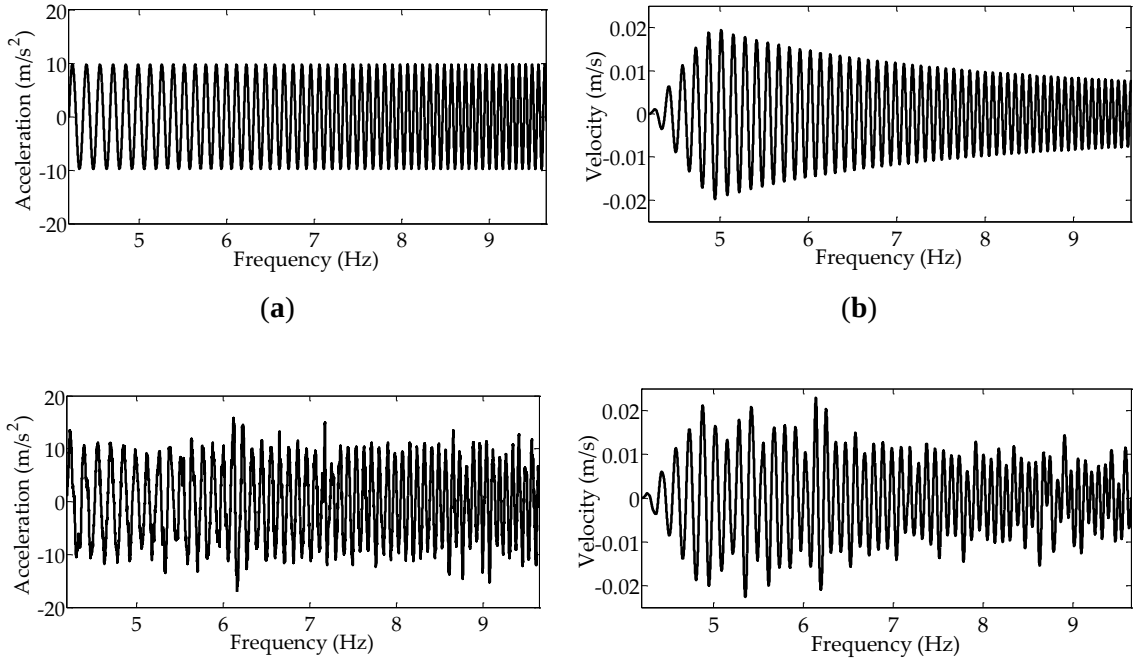

Fig. 5.18. (**a**) Up-sweep excitation curve for gravitational acceleration; (**b**) up-sweep excitation curve for the corresponding velocity; (**c**) up-sweep excitation curve for gravitational acceleration in conjunction with the simulated on-road noise excitation; (**d**) up-sweep excitation curve for the corresponding velocity in conjunction with the simulated on-road noise excitation.

Figure 5.17 shows that the harvesting system can capture a maximum power of 0.032 mW, and an average power of 0.0063 mW by using root mean square (RMS) voltage with wheel rotation. The average power is approximately 12 times that under the condition of on-road noise excitation and 50 times that under the effect of the periodic gravity force.

In the second experiment, an increasing up-sweep frequency was adopted for validation of the sustainability of stochastic resonance. Considering the amplitude limitation of the shaker and gravitational acceleration of 9.8 m/s^2, the frequency of change in acceleration and velocity was linearly increased from 4.2 to 9.7 Hz within 6.5 s. Corresponding to a vehicle speed range of 27 km/h–63 km/h, the increasing sweep frequency of the acceleration and velocity are presented in Figure 5.18(a),(b), respectively; moreover, for the case where the on-road noise excitation is interfused, the increasing sweep frequencies of the acceleration and velocity are presented in Figure 5.18(c),(d), respectively.

In Figure 5.19(a), under only the up-sweep excitation with gravitational acceleration of 9.8 m/s^2, the displacement response of the cantilever beam keeps the lower vibration level at one stable position throughout the frequency range. However, Figure 5.19(b) shows that when the up-sweep excitation and road noise are input simultaneously, the intake energy is increased to drive the high displacement response to the occurrence of stochastic resonance, owing to the presence of the additional ambient noise excitation. The vibration response is therefore enhanced with the inter-well dynamic oscillation, and even the up-sweep frequency varies during the period of 1 s–6 s which corresponds to that of the frequencies of 5 Hz–9.2 Hz. This demonstrates that the occurrence of stochastic resonance is not limited to a certain frequency, but can be maintained within a certain frequency bandwidth of 5 Hz–9.2 Hz.

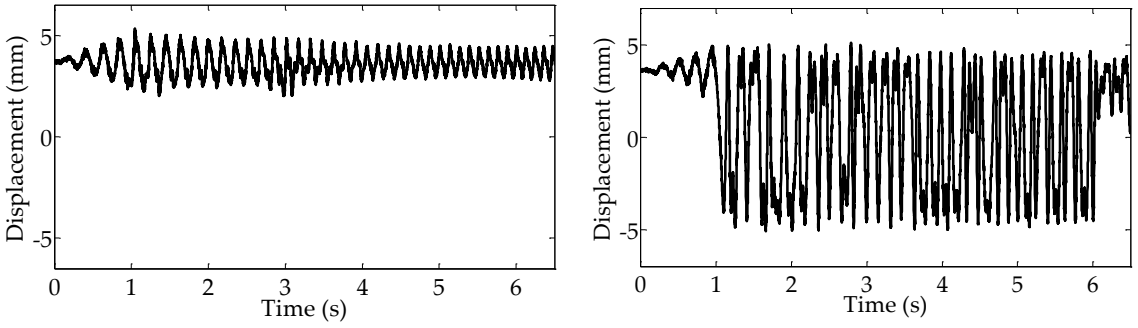

(**a**) (**b**)

Fig. 5.19. Experimental displacements: (**a**) under the up-sweep excitation; (**b**) under the combination of the up-sweep excitation and on-road noise excitation.

Figure 5.20 presents the voltages harvested at different rotational frequencies. The voltage reaches a maximum value of 1.2 V with a RMS value of 0.4 V, in Figure 5.20(a); however,

when the road noise is added to the separate periodic signal, the maximum voltage reaches 4.5 V with a higher RMS value of 1.7 V, in Figure 5.20(b). Correspondingly, as shown in Figure 5.21(b), the maximum power is 0.081 mW with average power of 0.012 mW, and the power density is obtained as 0.76 μW/cm^3 by calculating the average value of power per unit volume for the energy harvester. Apparently, the power is improved with combined excitation, and the harvesting system can be activated to high-energy motion owing to the occurrence of stochastic resonance. Importantly, the high-energy motion can be effectively maintained with the same varying rotational frequencies of 5 Hz–9.2 Hz. Consequently, the results of the experimental testing demonstrate that stochastic resonance is capable of enhancing energy harvesting over a wide range of vehicle speeds.

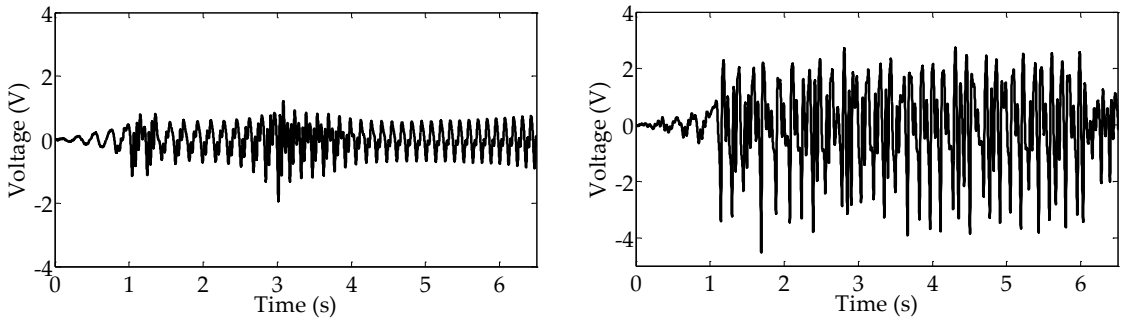

(**a**) (**b**)

Fig. 5.20. Produced voltages: (**a**) under up-sweep excitation; (**b**) under the combination of up-sweep excitation and on-road noise excitation.

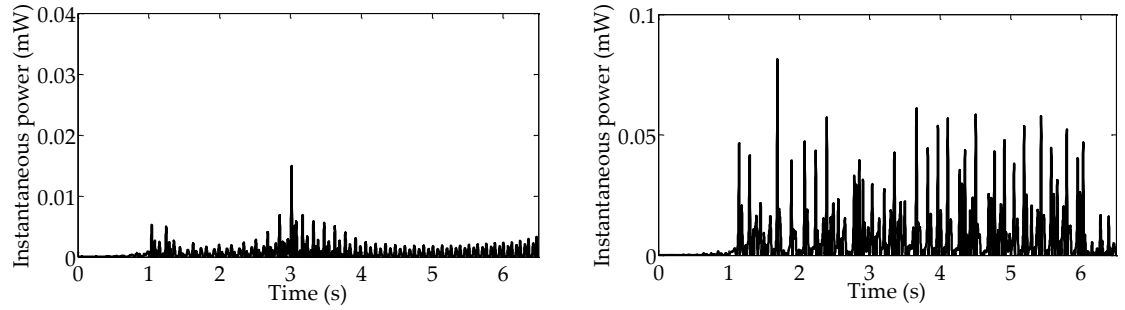

(**a**) (**b**)

Fig. 5.21. Harvested powers: (**a**) under up-sweep excitation; (**b**) under the combination of up-sweep excitation and on-road noise excitation.

5.1.4 Validation of Combining Stochastic Resonance and High Energy Orbit Oscillations

In this experiment, in order to validate the bandwidth of the frequency by using the phenomenon combination of stochastic resonance and high energy orbit oscillation under the gravitational acceleration of 9.8 m/s^2 along with on-road noise excitations. An increasing up-sweep method investigation is performed for verifying the valid frequency and the effectiveness of the energy harvester system. The frequency is gradually increased with the range of 25.1 rad/s–157 rad/s within 30 s, corresponding to the vehicle speed of 27 km/h–165 km/h.

Figure 5.22 shows the experimental data of displacement response under up-sweep excitation with 9.8 m/s^2, the cantilever beam keeps the lower vibration level within one stable position at the low frequency before 57 rad/s, and then the beam vibrates between the stable equilibrium positions of ±3.5 mm, to stimulate high energy orbit motion of nonlinear bistable system in the frequency range of 57.8 rad/s–129.4 rad/s which is approximate to the numerical analysis results obtained in Section 4.2. When the road noise along with the up-sweep excitation are applied simultaneously, as shown in Figure 5.22, due to the presence of the noise energy, that activates the system to the occurrence of the stochastic resonance while the frequency is close to 38 rad/s as validated in Section 5.1.2, then the vibration response is wholly effected under the frequency lower than 52.1 rad/s.

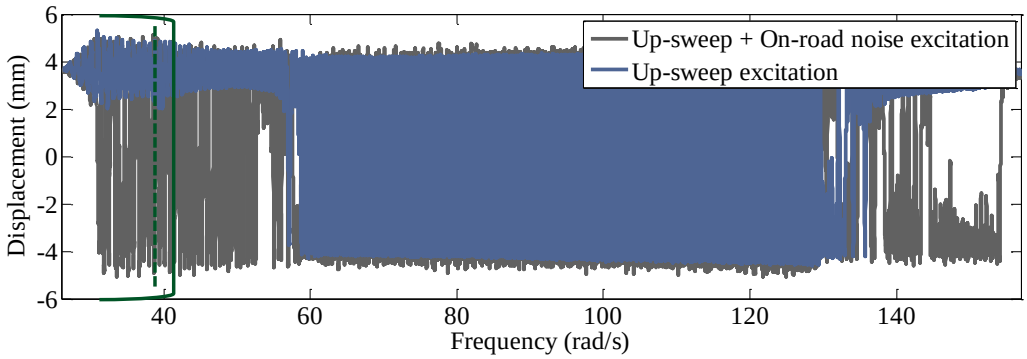

Fig. 5.22. Experimental displacements under two different cases: up-sweep excitation; and combination of up-sweep excitation and on-road noise excitation.

In order to validate the performance improvement due to the phenomenon of stochastic resonance, the power spectrums of experimental displacement responses under two kind of cases are also derived and shown in Figure 5.23, in the condition of only up-sweep excitation, before angular velocity of 57.8 rad/s due to the effect of the low energy orbit motion, the power

spectrum keep the low vibrating level. However, after considering adding the on-road noise to the system, it can be activated to appear the peak amplitude at the angular frequency near to 37 rad/s due to the high energy motion of stochastic resonance, which is approximate to the above experimental result of 37.7 rad/s. Furthermore, the power spectrum is considerably preferable to that of the only up-sweep excitation condition. Consequently, the power spectrum results demonstrate that stochastic resonance may effectively outspread the frequency range in the low frequency excitation. Therefore, the effective bandwidth of the energy harvester can be extended to 31 rad/s–129.4 rad/s; it indicates that the device is capable of boosting the vibrational response corresponding to the vehicle speed of 32.5 km/h–136 km/h.

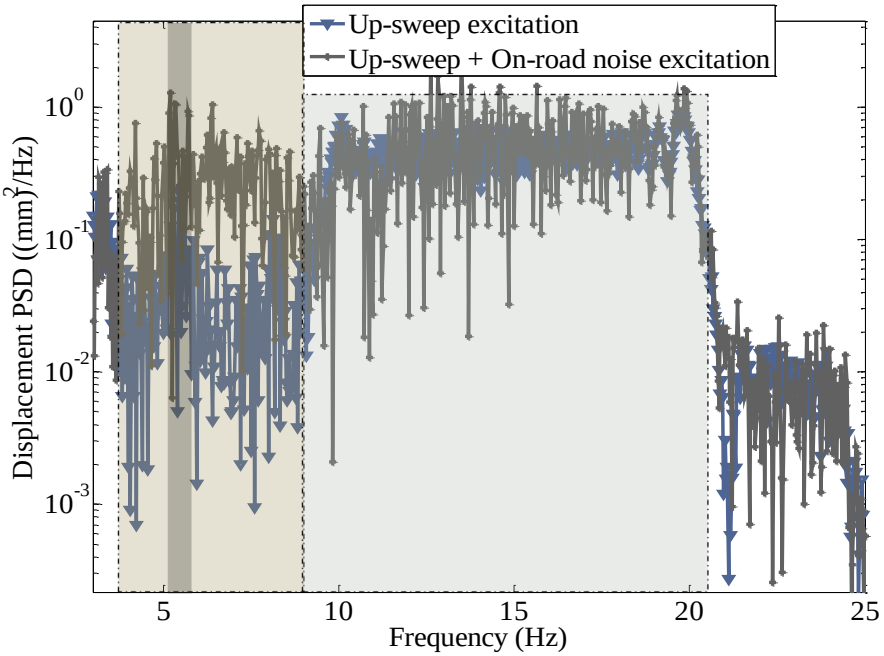

Fig. 5.23. Power spectrum density of displacement responses.

Figure 5.24 shows produced voltage at different speeds from 27 km/h–165 km/h across the matched load resister, the voltage can reach the maximum value of 6.8 V with the same valid frequency range as the displacement response, by means of adding road noise the maximum voltage achieves 7.3 V with a wider frequency bandwidth. Meanwhile, the maximum power is produced to 0.21 mW with the improved mean power density of 1.52 μW/cm^3 by making use of the net volume of the energy harvester of 15.75 cm^3 as shown in Figure 5.25.

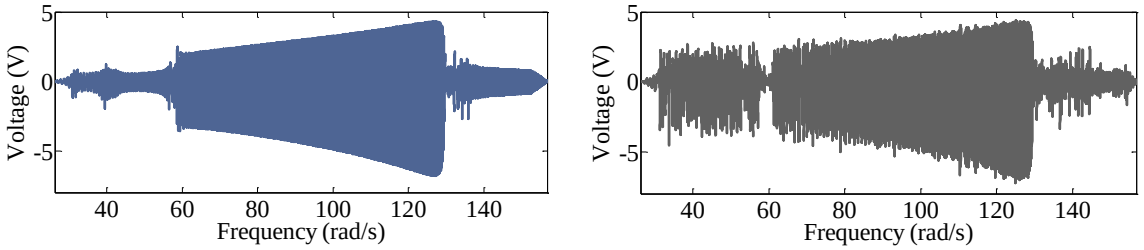

(**a**) (**b**)

Fig. 5.24. Produced voltages under two different cases: (**a**) up-sweep excitation; (**b**) combination of up-sweep excitation and on-road noise excitation.

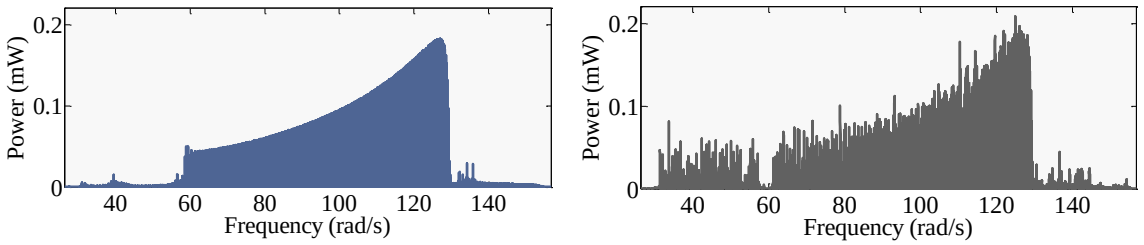

(**a**) (**b**)

Fig. 5.25. Harvested powers under two different cases: (**a**) up-sweep excitation; (**b**) combination of up-sweep excitation and on-road noise excitation.

5.2 Actual-Vehicle Experiment

5.2.1 Apparatus for on-Road Experiment

Figure 5.26(a) shows the selected types of beams for different materials of aluminum and stainless steel. The stiffness of 150 N/m is determined for validating the effectiveness of stochastic resonance, and 30 N/m is designed to perform the investigation of the positive effect of the centrifugal force experiments. Because the toughness of softening stiffness of aluminum material with 30 N/m is not excellent, the stainless steel material is preferred to be selected as the component for the fabrication. Then, the centrifugal distance is measured to 3.6cm and 7cm from the tire rotating center, which is shown in Figure 5.26(b). By making use of the determined beams the assembled energy harvester for attaching on the tire rotating center is presented in Figure 5.27.

The first vehicle driving experiment is to validate stochastic resonance as shown in the Figure 5.28. The accomplished energy harvester is attached to the front tire wheel of the electric vehicle to verify the power generation performance in real-world road environment. The center

of the cantilever tip mass is precisely located at the rotational center of the wheel to eliminate the centrifugal force's effect on the balance of the wheel and stiffness of the cantilever beam. The wireless accelerometer is mounted on the wheel for measuring the on-road noise excitation and tangential gravity acceleration, and a data acquisition system (DSO Nano v3, SeeedStudio, Shenzhen, China) is used to continuously measure real-time output voltage across a matched load resistor.

(**a**) (**b**)

Fig. 5.26. (**a**) Different types of beams for tire rotating experiments; (**b**) Determination of the centrifugal distances.

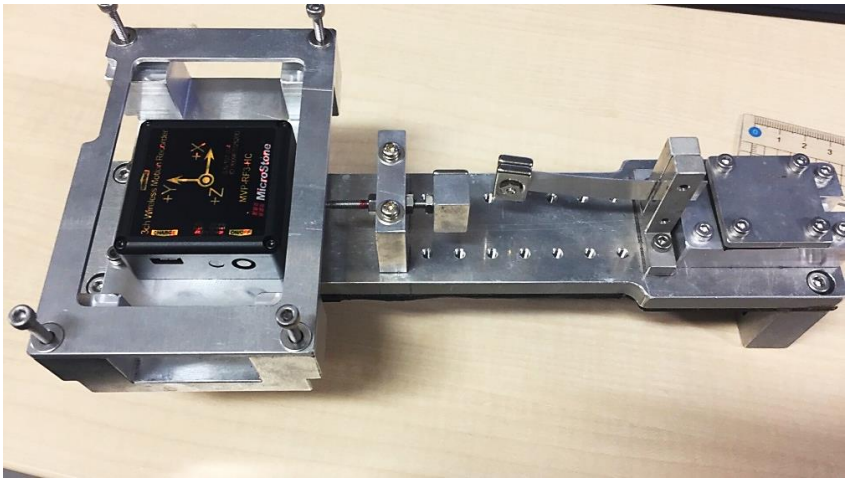

Fig. 5.27. Assembled energy harvester for attaching on the tire rotating center.

The second vehicle driving experiment is to probe the positive effect of the centrifugal force by varying the distance from rotating center. The reassembled centrifugal distance adjustable energy harvester is shown in Figure 5.30. While the centrifugal distance is at the position of rotating center, the structure as shown in Figure 5.28 can still be effectively for the reason of the balanced dynamic just by altering the hardening beam to the softening one 30 N/m as shown in Figure 5.29.

After moving the distance to 3.6 cm from tire center, because the measurement devices including voltage and acceleration acquisition systems are gathered to place on the one side of structure as shown in Figure 5.30, which generates the centrifugal force for breaking the balance of tire motion. Therefore, the same weight of dynamic balance mass is mounted on another side of structure for reducing its effect on vehicle driving dynamics as shown in Figure 5.31.

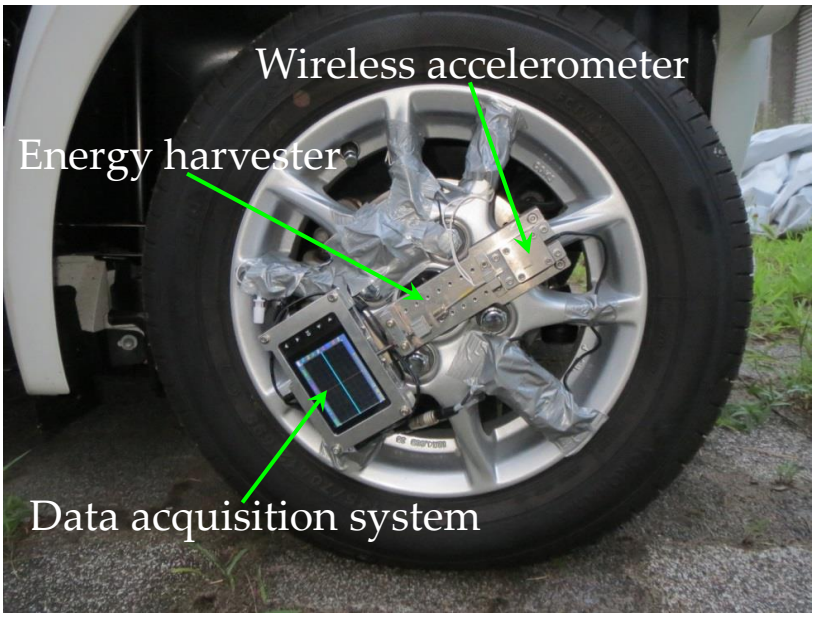

Fig. 5.28. Apparatus for the actual-vehicle experiment of stochastic resonance.

Fig. 5.29. Apparatus for the actual-vehicle experiment of centrifugal force effect under the position of rotating center.

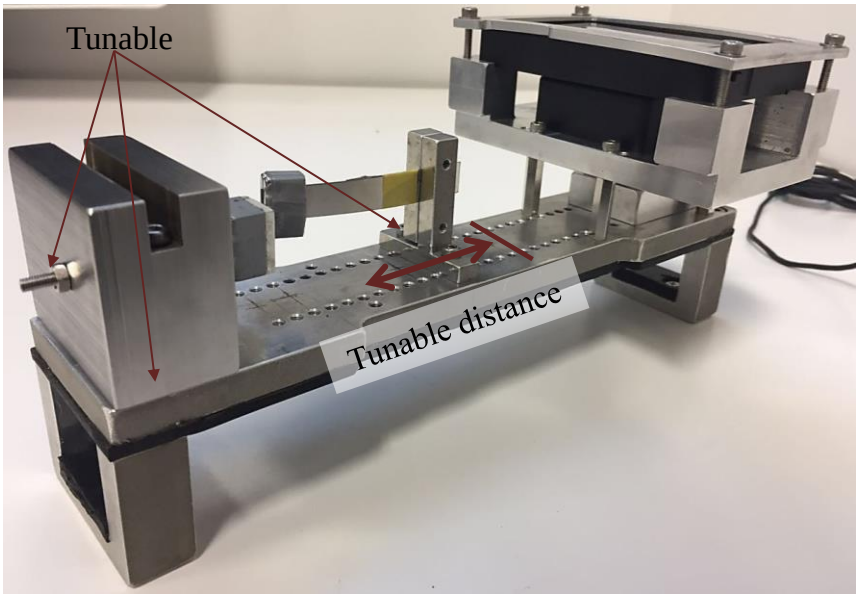

Fig. 5.30. Assembled energy harvester for adjusting the centrifugal distance.

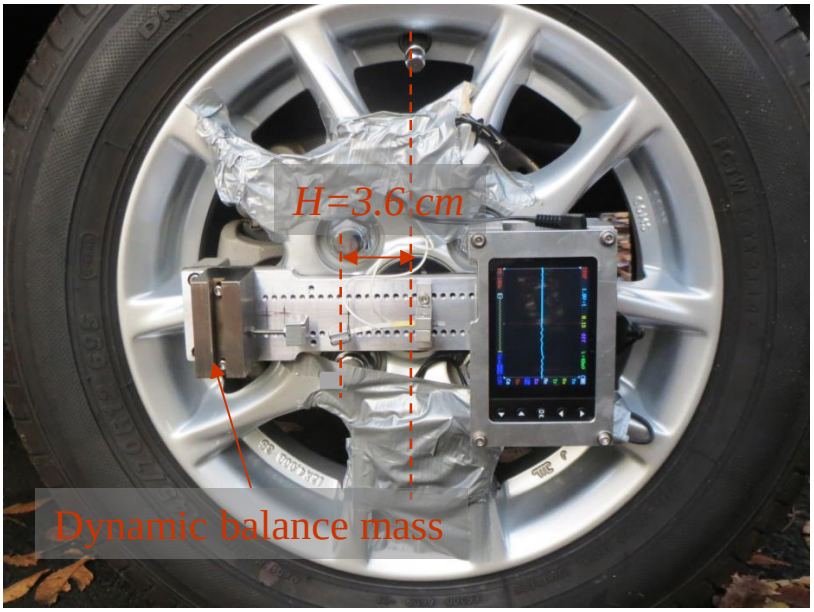

Fig. 5.31. Apparatus for the actual-vehicle experiment of centrifugal force effect under the centrifugal position of 3.6 cm.

In addition, it should be noted that the prototype of the energy harvester has to include a wireless motion recorder, accelerometer, data acquisition system, and the foundation support, to accomplish whole experimental procedure. However, in practice, without fabrication of the measurement devices, the separated energy harvester is streamlined to a concise and small-scale

model. Figure 5.32 shows the overview configuration of the actual-vehicle experiment when the centrifugal distance is located at the positon of 7 cm.

Finally, in order to compare the power generation performance of nonlinear systems with linear systems, the permanent magnet of dynamic balance mass end is removed and the comparative experiments also be performed as the details in Figure 5.33.

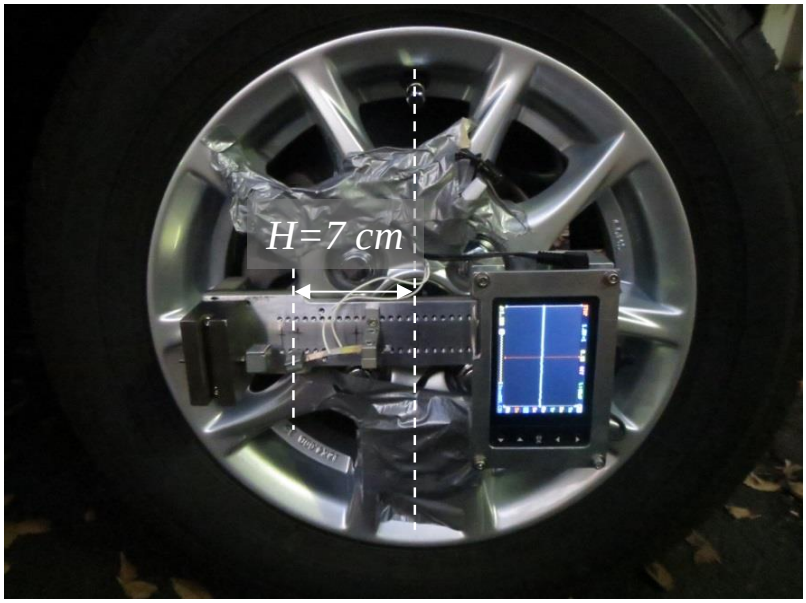

Fig. 5.32. Apparatus for the actual-vehicle experiment of centrifugal force effect under the centrifugal position of 7 cm.

Fig. 5.33. Apparatus for the actual-vehicle experiment of linear system under the centrifugal position of 3.6 cm.

5.2.2 Enhanced Energy Harvesting

It should be noted that when the energy harvester is rotating as the vehicle drives, considering the dynamic effect of rotation on the on-road noise that is forced on the cantilever, the expression of the on-road noise becomes $N(t)\sin\omega t$ instead of $N(t)$. Then the intensity of $N(t)$ is weakened to stimulate the phenomenon of stochastic resonance at an angular velocity lower than 22.5 rad/s (23.5 km/h). The validation experiment is implemented on real-world road, in which the vehicle travels at four different speeds of 10 km/h, 20 km/h, 30 km/h, and 40 km/h. According to the power spectral density of the tangentially rotational acceleration as analyzed in Figure 5.34, with the increasing in speed, the amplitude of the noise slightly increases but almost remains at the same level, which means the same ambient condition provided for the occurrence of stochastic resonance.

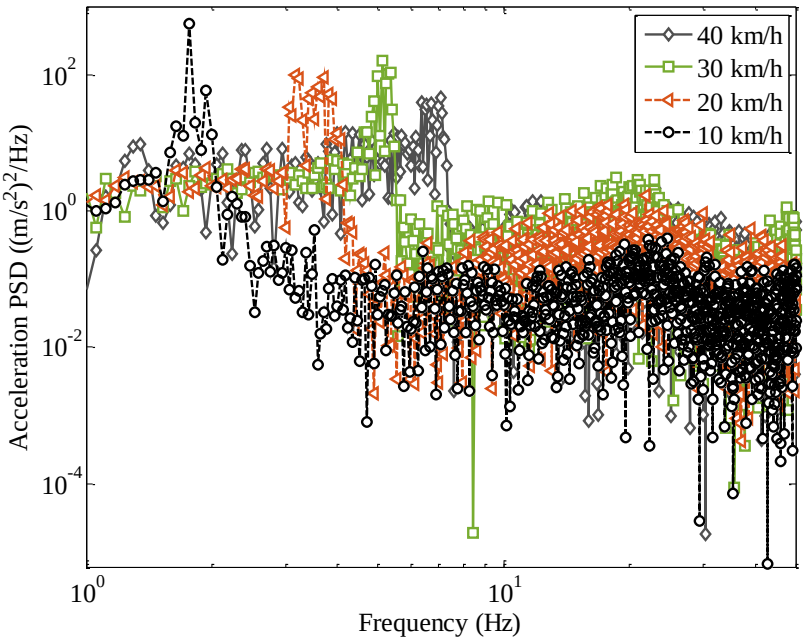

Fig. 5.34. Power spectral density of the tangentially rotational acceleration corresponding to different speeds: (**a**) 10 km/h; (**b**) 20 km/h; (**c**) 30 km/h; (**d**) 40 km/h.

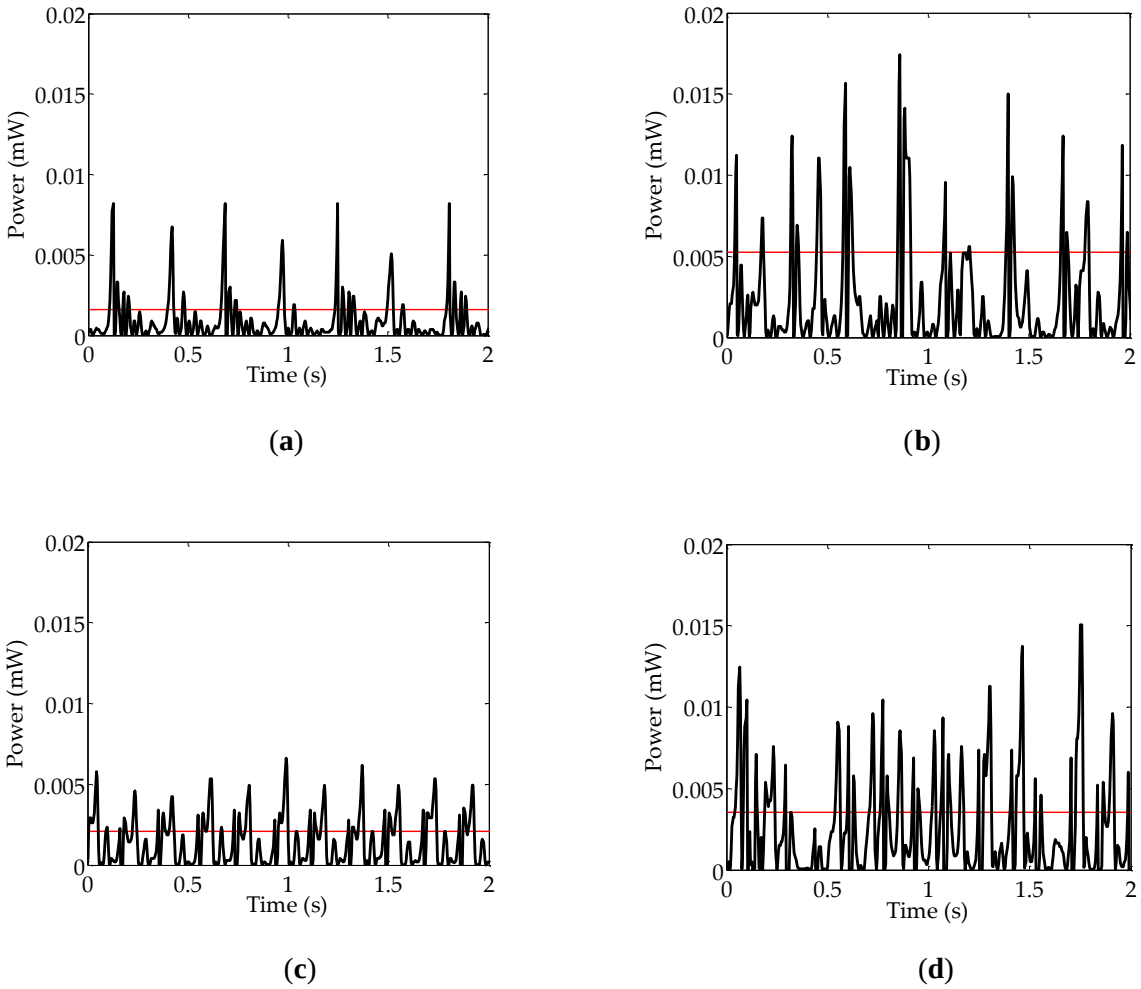

Fig. 5.35. Experimental results of power generation corresponding to different speeds: (**a**) 10 km/h; (**b**) 20 km/h; (**c**) 30 km/h; (**d**) 40 km/h.

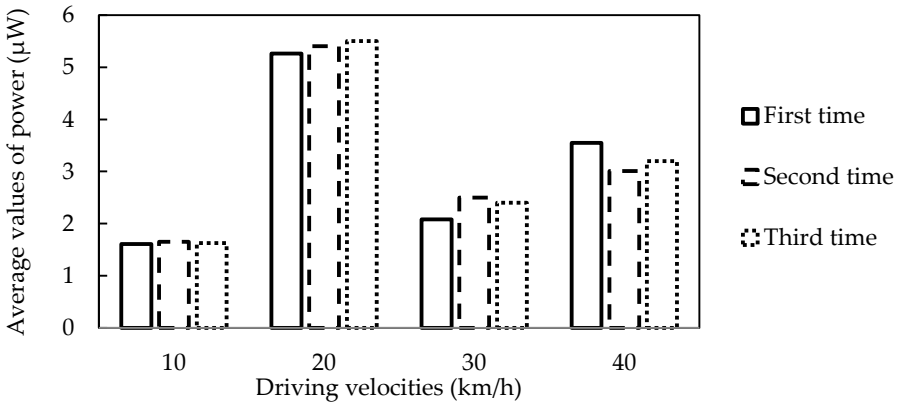

Fig. 5.36. Average values of the collected power under four different speeds.

As presented in Figure 5.35, the power generation performance are given under four different vehicle speeds, and the red solid line represents the average value of power. The experimental results indicate that the power can be boosted to a higher level with mean power of 5.5 μW at the speed of 20 km/h, due to the occurrence of stochastic resonance. It is approximated to the calculated Kramers rate value of 23.5 km/h. As presented in Figures 5.35c and d for the increasing vehicle speeds of the 30 km/h and 40 km/h, it becomes a tendency that the higher tire rotating angular velocity and on-road noise intensity resulted in the higher collected power; nevertheless, the power generation levels are still lower than that of the 20 km/h for the case of stochastic resonance. Furthermore, as presented in Figure 5.36, it is indicated that the average values of the collected power can be obviously enhanced at the velocity of 20 km/h compared to other three different driving conditions. Meanwhile, this tendency is also validated by implementing the vehicle driving of three times for every speed.

5.2.3 Further Improvement

Finally, by carrying out the experiments under different centrifugal distances and different systems, the power generation comparison results are demonstrated in this section. By the comparison of numerical analyses and experimental results; Figures 5.37, 38 and 39 show the characterized results of the mean voltage produced by the connected resister of 150 kΩ in the cases of without and with centrifugal force by setting the distances of 3.6 cm and 7 cm. It is validated that the numerical analysis can be close to the result of experiments under the three different conditions of the centrifugal distances.

Figure 5.40 exhibits the experimentally compared results in the cases of rotating center, the centrifugal distances of 3.6 cm and 7 cm. When the energy harvester is mounted on the center of the rotating, the valid bandwidth is found to be 10 km/h–25 km/h with the mean voltage around 2.1 V. However, after the energy harvester is placed at the centrifugal position far from center 3.6 cm, the voltage can be immediately improved from the driving speed of 10 km/h, meanwhile, the voltage tends to be improved as the speed increases. Even when the speed exceeds the 25 km/h, the produced voltage can still be maintained at a high level until the speed of 40 km/h. Hence, the performance of the tire-induced energy harvesting can be enhanced at the driving speed range of 10 km/h–40 km/h. Figures 5.41(a) and (b) show the real-time voltage and power responses at the speed of 40 km/h, it is indicated that the maximum voltage can reach to 6 V with the maximum power generation of 0.24 mW. The mean power is evaluated to 61 μW, which can provide the power source for around twenty sensors because of the power requirement of 3 μW per TPMS wireless sensor node, which therefore is validated as a promising way to boost the power density to 3.86 $\mu W/cm^3$, and hence improve the performance

of tire rotation-induced energy harvesting.

When the distance is increased to 7 cm, the voltage response wholly drops down a low level. All of the above results are very well agree with the numerical analysis results as derived in Section 4.3.3. Furthermore, the comparison of the linear and nonlinear systems also in implemented, the Figure 5.42 indicates that the mean voltage produced by using nonlinear system is approximately two times higher than that of the linear system. Therefore, the actual-vehicle experiments validate that the centrifugal force has the ability to further stabilize the high energy orbit oscillation and widely broaden the valid bandwidth of the nonlinear systems.

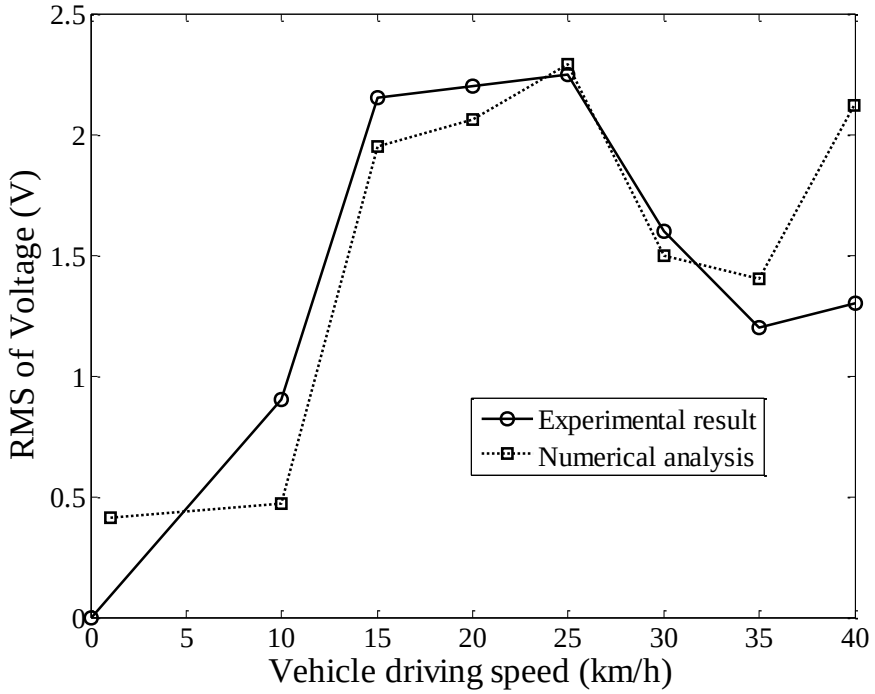

Fig. 5.37. Comparison of the experimental result and numerical analysis under the case of the centrifugal distance set around rotating center.

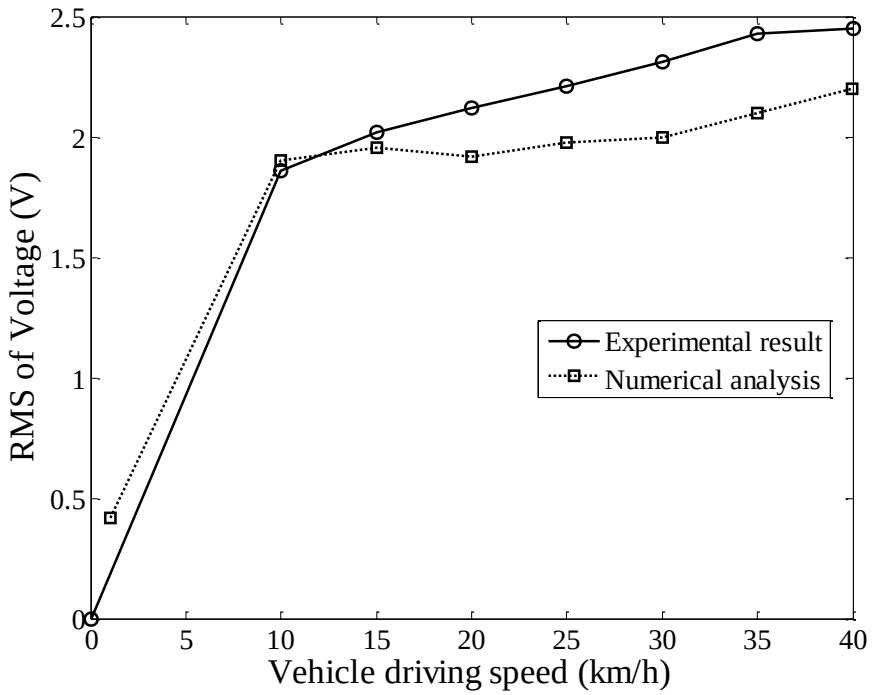

Fig. 5.38. Comparison of the experimental result and numerical analysis under the case of the centrifugal distance set at the position of 3.6 cm.

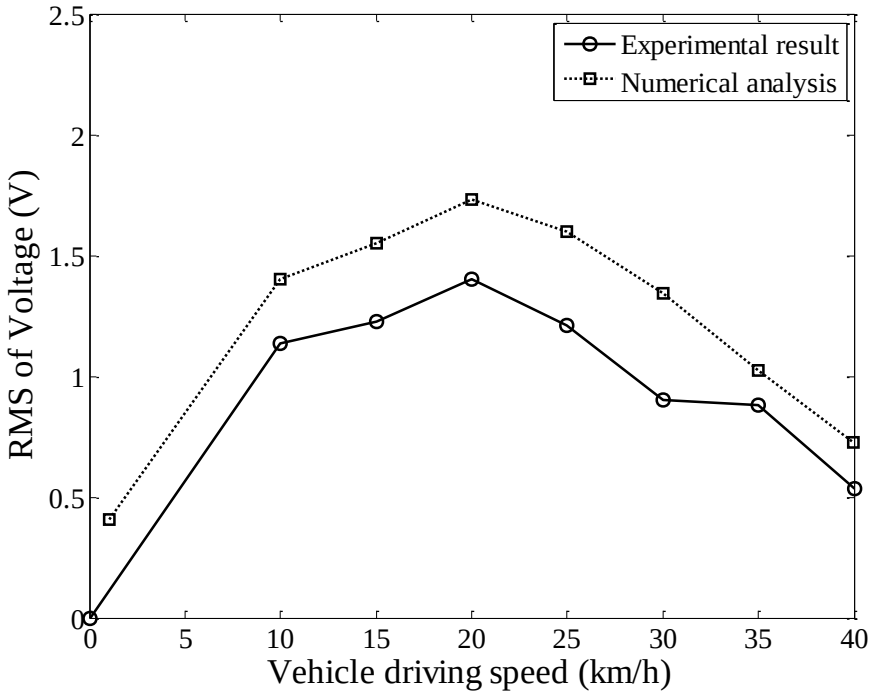

Fig. 5.39. Comparison of the experimental result and numerical analysis under the case of the centrifugal distance set at the position of 7 cm.

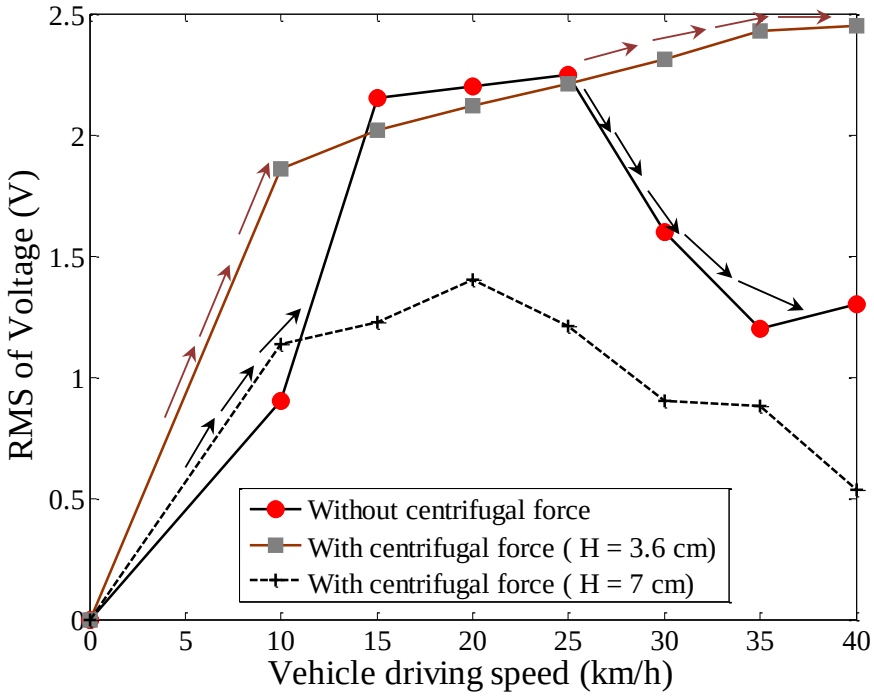

Fig. 5.40. Experimental comparison of mean values of the produced voltage under three different conditions of centrifugal distance.

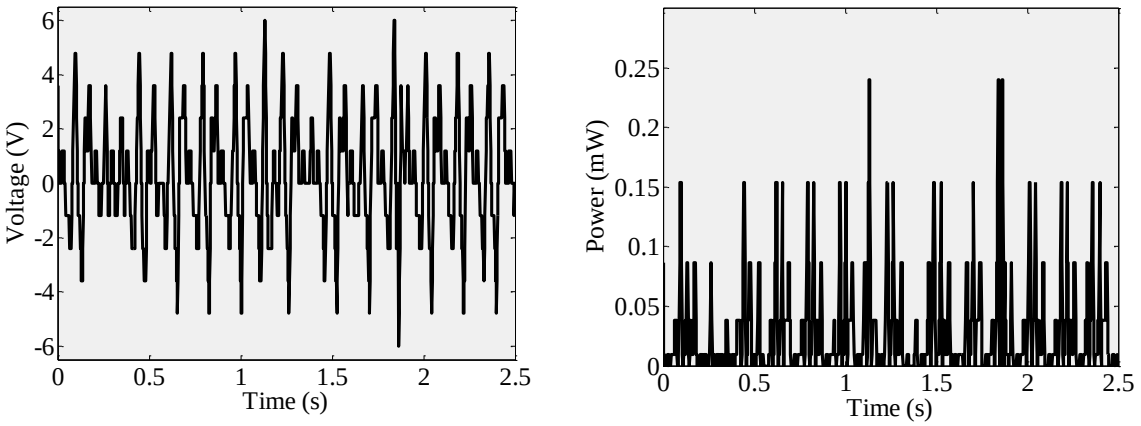

(**a**) (**b**)

Fig. 5.41. (**a**) Real-time voltage response with centrifugal distance of 3.6 under the driving speed of 40 km/h; (**b**) the corresponding power generation.

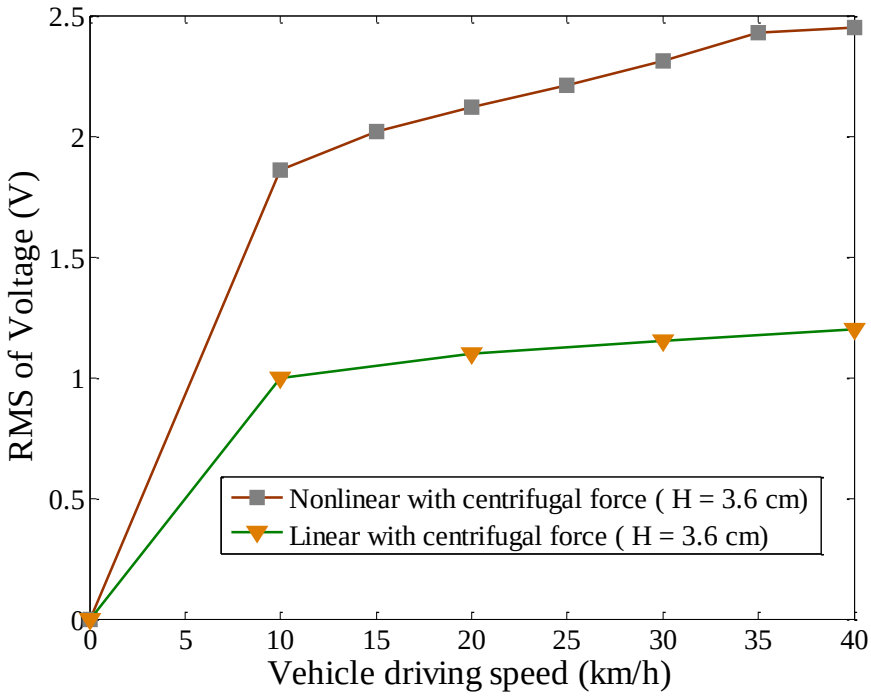

Fig. 5.42. Experimental comparison of the linear and nonlinear systems.

Chapter 6

Discussions

6. Discussions

6.1 Coexistence of Three Nonlinear Oscillating Phenomena

As described in Section 4.3.3, in the final actual-vehicle experiment, for validating the sustained phenomenon of the high energy orbit under the limited driving speed of 40 km/h, spring constant, linear as well as nonlinear coefficients of the magnets were tuned to be lesser for indicating the advantages of the dynamic characteristics under exploiting the centrifugal force. However, in order to content the actual-vehicle experimental requirements, the parameters of the harvesting system were devised as relatively small, which prompts stochastic resonance to be stimulated at an awfully insignificant value of frequency. Therefore, the investigations of the coexistence of the nonlinear oscillating phenomena of stochastic resonance, high energy orbit motion of bistable and high energy orbit motion of monostbale are carried out by the following analyses.

The parametric condition as shown at Table 6.1, the stiffness k is hardened to 350 N/m, also the linear stiffness and nonlinear stiffness are increased respectively. In order to confirm whether the three nonlinear phenomena can be coexisted under the rotating condition of considering the centrifugal effect, the investigations are carried out under three different conditions as follows: (1) rotating center in absence of on-road noise excitation, (2) centrifugal distance of 2 cm in absence of on-road noise excitation, and (3) centrifugal distance of 2 cm in presence of on-road noise excitation, respectively.

Table 6.1. Parameters of the energy harvester.

Items	**Seismeic mass**	**Linear coefficient**	**Nonlinear coefficient**	**Damping coefficient**	**Spring constant**	**Centrifugal distance**
Parameter	m	a	b	c	k	H
Value	8 g	150.5 N/m	5.2×10^{7} N/m^{3}	0.081 N/m/s	350 N/m	2 cm

As obtained in Figure 6.1, under the condition of the rotating center in absence of on-road noise excitation, it is observed that the high energy orbit oscillation occurs over the bandwidth of 78 rad/s–244.7 rad/s. Under the condition of the centrifugal distance of 2 cm in absence of on-road noise excitation, it is indicated that due to the transformed system at the boundary frequency approximated to 162 rad/s, the high energy orbit motion can be maintained for a broader bandwidth of 50 rad/s–317 rad/s as shown in Figure 6.2.

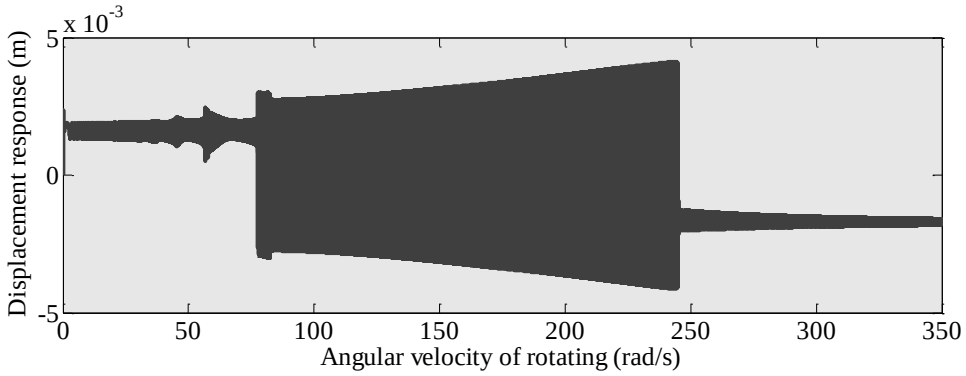

Fig. 6.1. Investigation under the position of rotating center in absence of on-road noise excitation.

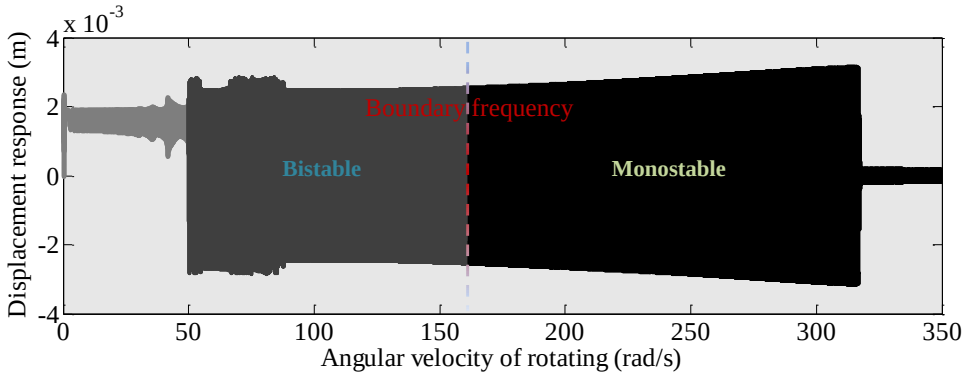

Fig. 6.2. Investigation under the centrifugal distance of 2 cm in absence of on-road noise excitation.

Based on equivalent linear stiffness expression obtained in Equation (3.48a), the positive coefficient of the beam can be expressed with respect to the rotating frequency of ω as

$$a'' = \frac{F_M}{d} - \frac{3m\omega^2 H}{2L} - k, \quad (a'' > 0). \tag{6.1}$$

Substituting Equation (6.1) into Equation (3.19) yields the modified expression of stochastic resonance by considering the effect of centrifugal force as

$$\omega_{SR}{}' < \sqrt{\frac{a''}{2m}} \exp\left(-\frac{a''^2}{4bD}\right), \tag{6.2a}$$

and

$$\omega_{SR}{}' < \sqrt{\frac{2LF_M - 3dm\omega^2 H - 2dkL}{4dmL}} \exp\left(-\left(\frac{2LF_M - 3dm\omega^2 H - 2dkL}{4dL\sqrt{bD}} \right)^2 \right). \quad (6.2b)$$

With considering of the effect of the rotating frequency on the Kramers rate on basis of Equation (6.2b), the Kramers rate is variable as a function of the angular velocity of rotating where is different from the definition of the Kramers rate under the case of inexistence of centrifugal effect. Figure 6.3 shows that the frequency characteristic of stochastic resonance is variable while the rotating frequency is increased to 100 rad/s.

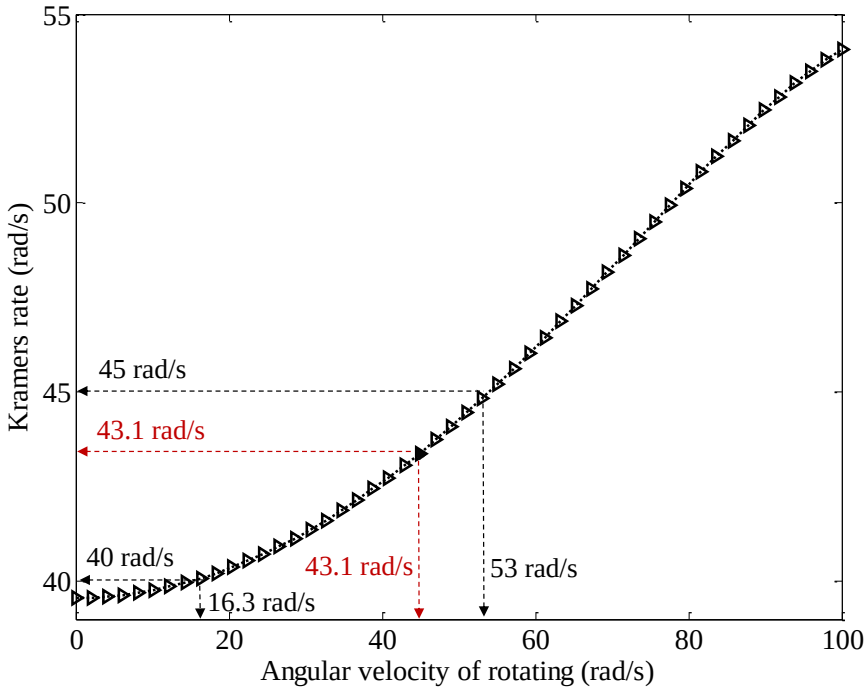

Fig. 6.3. Occurring probability of stochastic resonance with respect to angular velocity of rotating under the centrifugal distance located on the position of 2 cm.

As shown in Figure 6.3, the analyzed result of validation of the occurring probability of stochastic resonance is obtained. It can be investigated that when the rotating frequency is altered to 43.1 rad/s, the frequency can match the same value with the frequency of Kramers rate, while in the other rotating frequency, the frequencies cannot match the frequency of the calculated Kramers rate, which indicates that stochastic resonance is easy to be activated by tuning the rotational angular velocity smaller than 43.1 rad/s.

Finally, Figure 6.4(a) gives the investigation results under the centrifugal distance of 2 cm in

presence of on-road noise excitation. Due to the influence of the added on-road noise excitation, it is observed that stochastic resonance can be stimulated to improve the response of the energy harvesting system before the frequency of the 50 rad/s. The partial enlarged drawing shown in Figure 6.4(b) validates that stochastic resonance is easy to be activated by altering the rotational angular velocity smaller than 43.1 rad/s. After that, when the angular velocity of rotating exceeds 50 rad/s, the high energy orbit oscillating helps system to continue the inter-well vibration until the system is transformed to another monostable system at the boundary frequency of 162 rad/s. In conclusion, the effective operational bandwidth can be broadened to a wider range of 10 rad/s–315.2 rad/s by employing the phenomenon coexistence of stochastic resonance, high energy orbit oscillation of bistable and monostable systems.

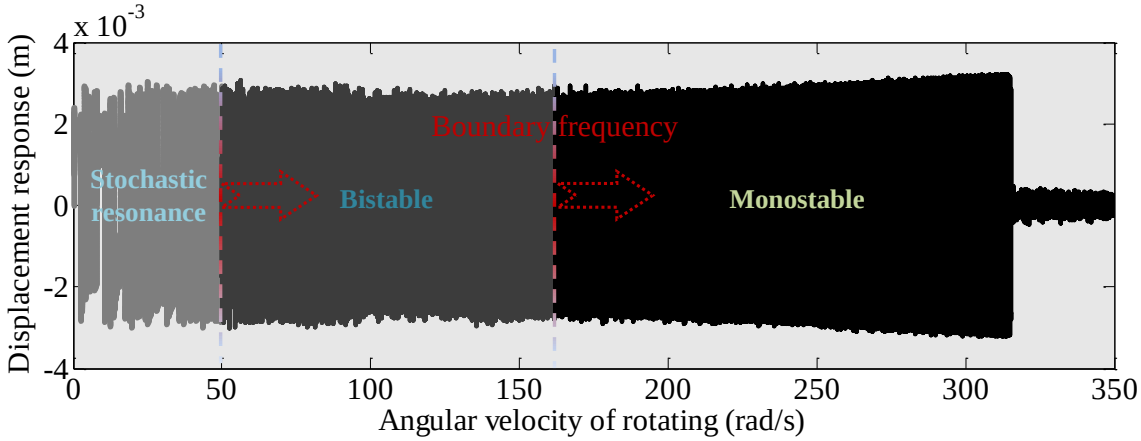

(**a**)

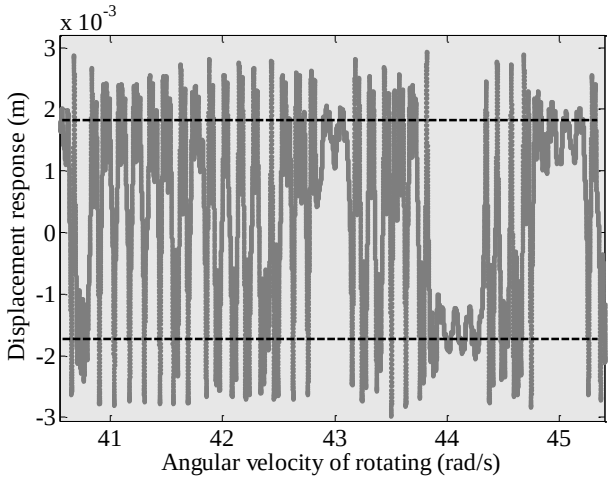

(**b**)

Fig. 6.4. Investigation under the centrifugal distance of 2 cm in presence of on-road noise excitation: (**a**) coexistence of three nonlinear oscillating phenomena; (**b**) partial enlarged drawing of stochastic resonance.

6.2 Effect of Noise Intensity on Response

As expressed in Section 2.2 Equation (2.35), the intensity of the external noise which is utilized for transmitting the inter-well motion should satisfy the conditions of:

$$\varsigma I\left(E_b\right) < D < E_b . \tag{6.3}$$

The potential energy of E_b around the angular velocity of 42 rad/s is calculated as 1.31×10^{-4} J, and the lower limit quantification is extrapolated to 1.048×10^{-5} J. However, in the cases of the intensity of noises deviation to this range which are smaller than the lower limit and higher than the potential energy E_b are quantitatively investigated as follows.

Under the weak intensity of 4.4×10^{-7} N which is lower than the lower limit quantification of 1.048×10^{-5} J, displacement responses are shown in Figure 6.5, it demonstrates that when the intensity of the noise excitation is so weak that the response of system can just maintain the monostable vibration within one potential well, even the up-sweep excitation is added to the system, the inter-well vibration cannot be activated to jump through potential barrier.

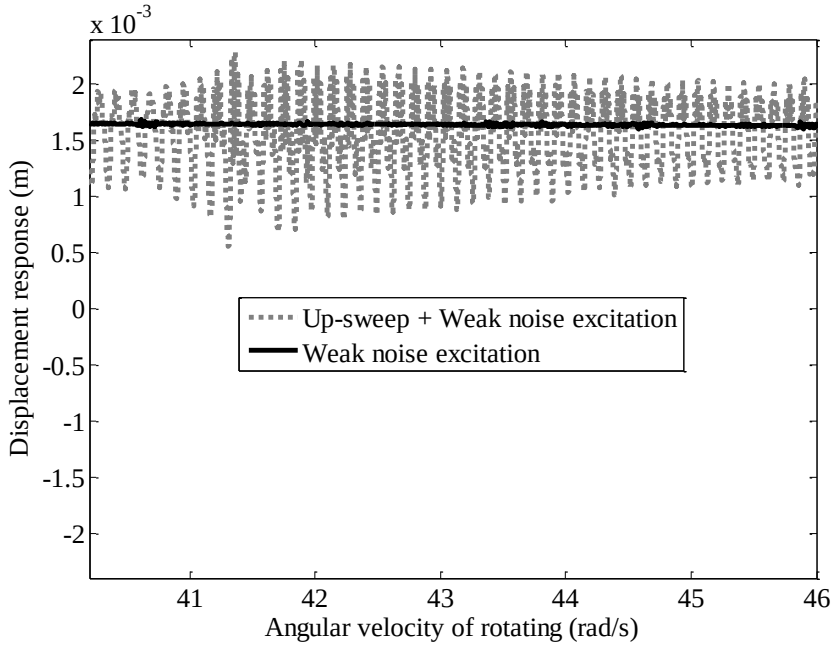

Fig. 6.5. Displacement responses: under the up-sweep excitation; under the combination of the up-sweep excitation and weak noise excitation with the intensity of 4.4×10^{-7} N.

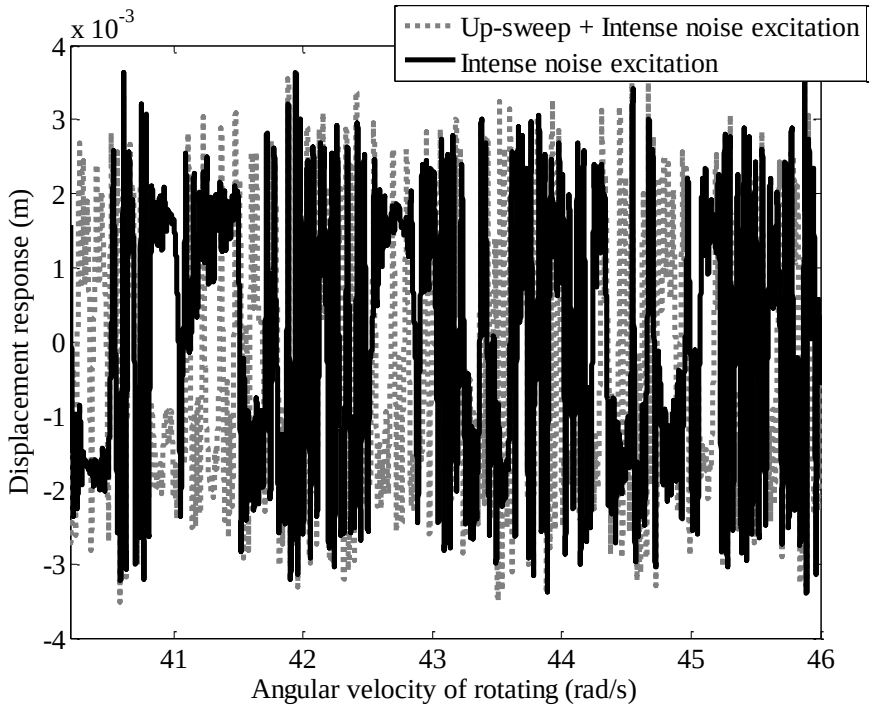

Fig. 6.6. Displacement responses: under the up-sweep excitation; under the combination of the up-sweep excitation and on-road noise excitation with the intensity of 3.14×10^{-3} N.

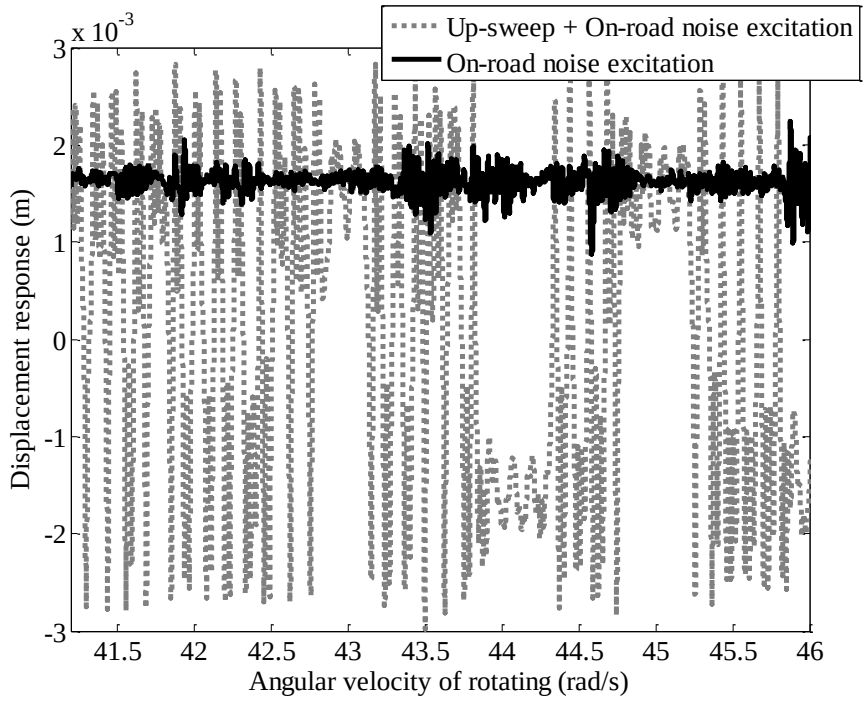

Fig. 6.7. Displacement responses: under the up-sweep excitation; under the combination of the up-sweep excitation and on-road noise excitation with the intensity of 1.22×10^{-4} N.

Under the intense intensity of 3.14×10^{-3} N which is higher than the potential energy E_b of 1.31×10^{-4} J, the displacement responses are shown in Figure 6.6; it can be observed that in the case of only noise excitation, the inter-well vibration occurs between two potential well, which can be comparable to the response under the combination of the up-sweep excitation and on-road noise excitation. Therefore, the effect of the up-sweep excitation on the response of system becomes insignificantly. Nevertheless, from tire vibration, it is still difficult to generate this kind of intense vibrating noise, which makes stochastic resonance that can be treated as a promising method for enhancing the ability of energy harvesting.

Finally, because the intensity of the on-road noise is measured as 1.22×10^{-4} N, which satisfies the intensity condition of noise for the occurrence of stochastic resonance, casing the inter-well motion can be observed under the combination of the up-sweep excitation and on-road noise excitation, and one potential well motion occurs under the only on-road noise as obtained in Figure 6.7.

6.3 Rectifier Circuit for Tire-Induced Energy Harvesting

In order to provide stable direct-current voltages to the sensors, this section proposes the specifically designed rectification method for tire-induced energy harvesting. Figure 6.8 draws the full architecture of the rectifying circuit. During the vibrational process of the energy harvesting beam, the piezoelectric transducer is subjected to tensile and compressive deformation, and these two actions results in the opposite direction of charge outflowing from transducer.

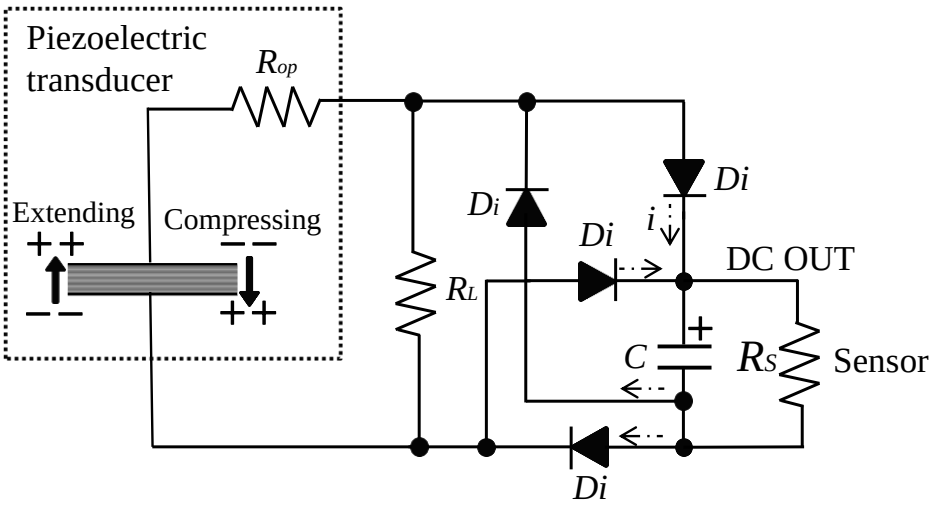

Fig. 6.8. Architecture of rectifying circuit for the full tire-induced energy harvesting setup.

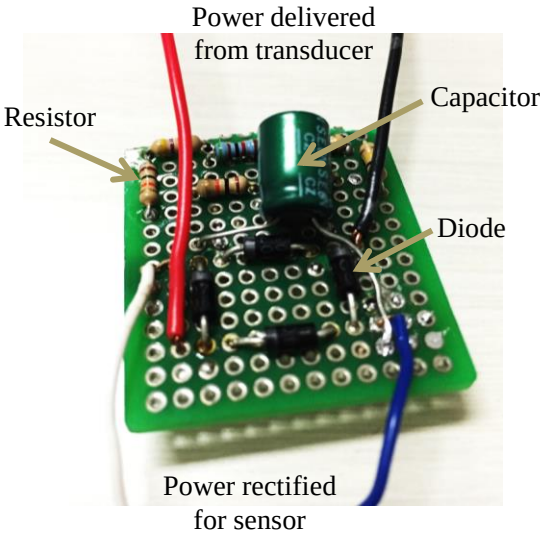

Fig. 6.9. Welded rectifier circuit board powering stable direction-current voltage for sensors.

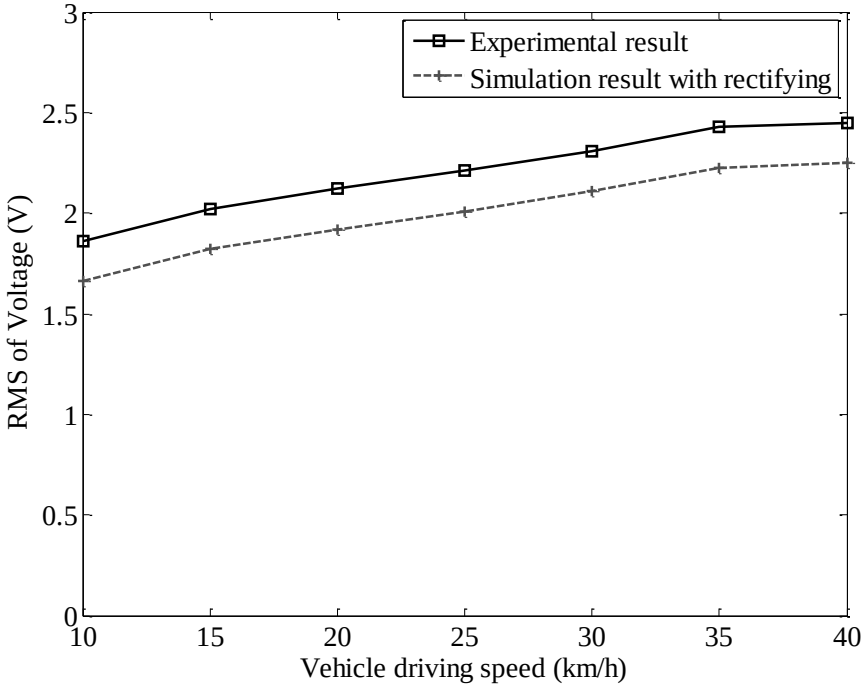

Fig. 6.10. Evaluation regarding the net voltage available for powering sensor.

In Figure 6.8, the external load resistance of R_L is optimized to be equal to the internal impedance of piezoelectric transducer R_{op} for ensuring that the output power can reach a high level. Through the use of unidirectional conductivity of the germanium diodes with the voltage

drop of 0.2 V–0.3 V, the alternating-current voltage can be rectified to direction-current style, and then stored in a capacitor C with the sufficient capacity around 10 mF. Figure 6.9 shows the Welded rectifier circuit board. Based on the experimental result of the RMS voltages without rectifying, by using them as the input condition, the simulation result with rectifying by means of utilizing the circuit shows that the net voltage powering for sensor can be evaluated as shown in Figure 6.10.

6.4 Comparison with Other Energy Harvesting Strategies

The selection and details of piezoelectric, electromagnetic and electrostatic energy harvesters from more other representative literatures utilized in the comparison are detailed in this section. The performance of energy harvesting for different methods are selected under both low frequency and high frequency excitations with the range of excitation level not limited to several m/s^2 but spreading to thousands of m/s^2. It should be note that the valid volume for the extrapolation of the mean power density is obtained by estimating the three-dimensional space of beam under the condition of vibrating, rather than the static state.

Table 6.2. Piezoelectric energy harvesters.

Reference	f (Hz)	Excitation Level (m/s^2)	Mean Power (μW)	Mean Power Density ($\mu W/cm^3$)	Method	Piezoelectric Material
Roundy, S. [97] 2003	120	2.5	375	375	MEMS: large scale	PZT
Gu, L. [54] 2010	18	10	340	4.86	Linear: self-tunable	PZT
Hu, Y. [56] 2011	10	30	0.085	35	Bending	ZnO
Cottone, F. [98] 2013	215	30	0.07	0.012	Nonlinear	PZT
Pillatsch, P. [99] 2014	4	20	10	5.4	Up conversion	PZT
Proposed approach	6	15	61	3.86	Nonlinear: tunable	PZT

*Extrapolated from data in references.

Table 6.3. Electromagnetic energy harvesters.

Reference	f (Hz)	Excitation Level (m/s^2)	Mean Power (μW)	Mean Power Density ($\mu W/cm^3$)	Method	Structure Material
Koukharenko, E. [100] 2006	1615	3.92	0.104	1.04	Resonance	Silicon
Kulah, H. [101] 2008	25	N/A	3.97	1.99	Up conversion	Styrene
Wang, Y. J. [67] 2015	6	10	30	0.94	Nonlinear	Copper

∗N/A: Not Available

Table 6.4. Electrostatic energy harvesters and other approach.

Reference	f (Hz)	Excitation Level (m/s^2)	Mean Power (μW)	Mean Power Density ($\mu W/cm^3$)	Method	Type
Arakawa, Y. [102] 2004	10	3.9	6	7.5	Electret	IPO
Lo, H. [103] 2008	50	576.6	17.98	0.36	Electret	OP
Manla, G. [104] 2012	5.55	119	3.5	0.14	Nonlinear: impact	Hybrid

∗IPO: In-Plane Overlap OP: Out-of-plane

Tables 6.2, 6.3, 6.4 demonstrate the previous works trialing to improve the harvested power utilizing different approaches. By comparison of the each table, the compact miniaturization of MEMS devices, although they have high power densities, the produced powers are still relatively low using the electret IPO type energy harvester; nevertheless, the technique of enlarging scale of MEMS device can be considered as an effective approach to improve the output power.

The method using self-tunable linear structure demonstrates a relatively high capacity of energy harvesting compared to the method of taking advantage of resonance, but it is difficult to adjust the frequency of natural resonance to match the varying frequency of the external excitation in practice. By using this proposed approach, it is no need to match the resonance of system as long as its operational frequency bandwidth is broadened to include the frequency

range of the external excitation.

Another approach of attaching the separate piezoelectric material inner tire trends to increase the power density, due to the internal attachment position of tire, it becomes inconvenient to replace the harvesting system, in other words, the replacement cost is expensive. Using this proposed approach, because the harvester is attached on the surface of tire wheel, which makes the process of replacement to be uncomplicated.

Frequency-up conversion can activate the response of vibrating around extremely high frequency to improve the power density, which although is comparable to the power density obtained in this research. Due to high-frequency vibration, the inevitable of increasing the stiffness of system to a large elasticity coefficient makes the output response not so high compared to the result of this proposed approach.

For the other mechanical strategies of utilizing nonlinear as well as nonlinear combined with impact effect, they can be treated as the potential methods to harvest the power by the simplex nonlinear vibration. However, in this research exploiting the featured approach of the tunable nonlinear characteristics to activate the coexisting of multiple nonlinear vibrations can further broaden the effective bandwidth for making efforts to improve the capacity of energy harvesting.

Chapter 7

Conclusions

7. Conclusions

Energy harvesting from ambient vibration has attracted the interest of many researchers in the last decade. Contributing to the hot topic, this thesis focused on utilizing the nonlinear phenomena covering stochastic resonance, high energy orbit oscillation of bistable systems, and high energy orbit of monostbale systems for rotation-induced vibrational energy harvester. It is worth highlighting that the operational bandwidth of rotational frequency can be significantly broadened by the combinations of stochastic resonance and high energy orbit characteristic, as well as the high energy orbit characteristics of bistable and monostable oscillator.

The detailed conclusions of each chapter are drawn, as follows:

In Chapter 2, the dynamics and its characteristics are introduced for the monostable and bistable Duffing oscillators under harmonic excitations, and stochastic resonance under the on-road noise excitation combined with gravitational effects. In the monostable case, from the frequency-amplitude response, it was demonstrated that the dynamic response can be improved at a wide frequency bandwidth of excitation, and the operational bandwidth can be further improved for energy harvesting by increasing the linear and nonlinear stiffness to stabilizing the high energy orbit motion. Another method to broaden the bandwidth is to use high energy orbit motion of bistsble. Moreover, the specific theory was also introduced for derivation process of stochastic resonance. Finally, the existing challenges were described regarding how to exploit nonlinear systems to the actual vehicle tires, which can result in excellent energy harvesting performance.

In Chapter 3, the methodologies were presented to exploit tire-rotating harvester, and a bistable energy harvester was proposed to collect energy from tire rotational environments. With the theoretical investigation, the bistable energy harvester is suitable for enhance performance of energy harvesting by application of stochastic resonance. Under the environments of tire rotation, the periodical force is autonomously self-excited by the gravitational effect of the magnetic end mass, and the noise excitation generated from the road provide the necessary conditions for the occurrence of stochastic resonance. In this work, it has been validated that there is no necessary to prepare an efficiency-reducing additional periodic modulation force, as it is now provided by the rotation of the car wheel. Therefore, the potential for the implementation of stochastic resonance is practically realizable in this particular system. The modelling analyses of energy harvester were processed under the noise and gravitational effect of tire rotations from an ideally simulating setting, as well as the real-world on-road environment, respectively. Furthermore, the bandwidth can be further broadened on the basis of combining two phenomena of stochastic resonance and high energy orbit oscillation. In addition, the centrifugally rotating dynamics was investigated to assess the influence of centrifugal force

on the rotational nonlinear energy harvester, and it was indicated that the centrifugal force might be applied as another active effectiveness to improve the harvesting performance.

In Chapter 4, by implementing the numerical simulations, it indicated that the phenomenon of stochastic resonance can occur when the tire rotates around the angular velocity of 98 rad/s under the simulated road noise excitation over a bandwidth of 0 Hz–1 kHz. The present study applied the periodic gravity force and on-road noise excitation of the rotating wheel, to validate the effectiveness of energy harvesting by the application of the phenomenon of stochastic resonance. The systematic structure was modeled under the real condition of on-road noise excitation, when a vehicle travels on a smooth paved road. Therefore, the effective frequency bandwidth of the energy harvester can be extended to a wider range by utilizing stochastic resonance combined with high energy orbit oscillating. In the last section, a simulation study was investigated to verify that the performance characteristic under the condition of exploiting the centrifugal force. In this case, the hardening and softening stiffness coefficients are tunable along with the change of rotational frequency for increasing the stiffness, in which the harvesting system can automatically transform the initial bistable into monostable oscillations, for stabilizing the high energy orbit. It was approved that the proposed method can achieve a significantly broadening bandwidth for the vibrational energy harvesting.

In Chapter 5, a series of experimental studies was carried out to validate proposed method, by the development of energy harvesting prototypes. According to the laboratory experiment, under the simulating conditions, the maximum instantaneous power was achieved to 0.14 mW under high angular velocity of 98 rad/s, while the collected energy is ten-times higher for the basis of stochastic resonance than that of the only monostable vibration. More importantly, the 38.2 % of energy harvesting efficiency was reached depending on the externally connected impedance and the electrically induced damping coefficient. Moreover, under the measured on-road noise, the experimental results revealed inter-well motion at a frequency of 6 Hz for wheel rotation, where the captured power was 12 times that under the condition of only on-road noise excitation and 50 times that under the condition of only the periodic gravity force. More importantly, it was validated that as the periodic frequency varies, the phenomenon of stochastic resonance was sustainable in terms of improving the performance of the energy harvester with a mean power density of 0.76 $\mu W/cm^3$. It demonstrates that stochastic resonance is not limited to occurring at a constant rotational frequency, but can be maintained under the variation of rotational frequencies. Finally, by the combination of the high energy orbit oscillating, the maximum power was produced to 0.21 mW, with the improved power density of 1.52 $\mu W/cm^3$.

According to actual-vehicle experiment, it validates that the present energy harvester is feasible of triggering stochastic resonance for enhancing power generation performance. As a result, the harvested mean power of 5.5 μW is sufficient for providing the electrical support for

tire pressure monitoring sensors, under the on-road noise excitation at the low driving speed of 20 km/h. Therefore, the approach is thus effective in absorbing higher energy for the application of tire pressure detection. With the further investigations, by carrying out the experiments under different centrifugal distances using the centrifugal force, the harvested power can be further enhanced to a maximum power generation of 0.24 mW with mean power of 61 μW, and boosted power density of 3.86 $\mu W/cm^3$, even under the low driving speeds. Therefore, this study validated in practice that the proposed method is a promising way to improve the performance of tire rotation-induced energy harvesting.

In Chapter 6, it is comprehensively discussed that the coexistence of the nonlinear oscillating phenomena of stochastic resonance, high energy orbit motion of bistable and high energy orbit motion of monostbale was confirmed in tire rotating environments. By devising the rectifier circuit, the net direct-current voltage available for powering sensor can be evaluated by the simulation result. Finally, by comparing with other energy harvesting strategies, it was found that the usage of this unique approach can bring some of the advantages for improving the capability in energy harvesting.

The contributions of this dissertation are highlighted as follows:

(1) Attempted to take advantage of the nonlinear characteristics for harvesting the vibrational energy from the source of rotating gravity combined with ambient road noise excitation on the automobile tires.
(2) Investigated the feasibility of the approaches by theoretical as well as numerical analyses.
(3) Validated the effectiveness of the proposed approaches for improving the performance of energy harvesting under a broadening bandwidth of frequency on the basis of laboratory tests.
(4) Achieved the nonlinear vibration on the application of the rotating tires by actual-vehicle experiments.

References

[1] Beeby, S. P., Torah, R. N., Tudor, M. J., Glynne-Jones, P., O'Donnell, T., Saha, C. R., and Roy, S., A micro electromagnetic generator for vibration energy harvesting. Journal of Micromechanics and microengineering, 17(7): 1257, 2007.

[2] Fang, H. B., Liu, J. Q., Xu, Z. Y., Dong, L., Wang, L., Chen, D., and Liu, Y., Fabrication and performance of MEMS-based piezoelectric power generator for vibration energy harvesting. Microelectronics Journal, 37(11): 1280-1284, 2006.

[3] Stephen, N. G., On energy harvesting from ambient vibration. Journal of sound and vibration, 293(1): 409-425, 2006.

[4] Shu, Y. C., Lien, I. C., Analysis of power output for piezoelectric energy harvesting systems. Smart materials and structures, 15(6): 1499, 2006.

[5] Kim, H., Priya, S., Stephanou, H., and Uchino, K., Consideration of impedance matching techniques for efficient piezoelectric energy harvesting. IEEE transactions on ultrasonics, ferroelectrics, and frequency control, 54(9): 1851-1859, 2007.

[6] Yang, S. M., Lee, Y. J., Interaction of structure vibration and piezoelectric actuation. Smart Materials and Structures, 3(4): 494, 1994.

[7] Sodano, H. A., Simmers, G. E., Dereux, R., and Inman, D. J., Recharging batteries using energy harvested from thermal gradients. Journal of Intelligent material systems and structures, 18(1): 3-10, 2007.

[8] Ujihara, M., Carman, G. P., and Lee, D. G., Thermal energy harvesting device using ferromagnetic materials. Applied Physics Letters, 91(9): 093508, 2007.

[9] Priya S., Inman D. J., Energy Harvesting Technologies, 1st edn. Springer, Berlin, 2009.

[10] Raischel, F., Moreira, A., and Lind, P. G., From human mobility to renewable energies. The European Physical Journal Special Topics, 223(11): 2107-2118, 2014.

[11] Rao, Y., Cheng, S., and Arnold, D. P., An energy harvesting system for passively generating power from human activities. Journal of Micromechanics and Microengineering, 23(11): 114012, 2013.

[12] Riemer, R., Shapiro, A., Biomechanical energy harvesting from human motion: theory, state of the art, design guidelines, and future directions. Journal of neuroengineering and rehabilitation, 8(1): 1, 2011.

[13] Roundy, S., Tola, J., Energy harvester for rotating environments using offset pendulum and nonlinear dynamics. Smart Materials and Structures, 23(10): 105004, 2014.

[14] Zuo, L., Scully, B., Shestani, J., and Zhou, Y., Design and characterization of an electromagnetic energy harvester for vehicle suspensions. Smart Materials and

Structures, 19(4): 045003, 2010.

[15] Li, Z., Zuo, L., Luhrs, G., Lin, L., and Qin, Y. X., Electromagnetic energy-harvesting shock absorbers: design, modeling, and road tests. IEEE Transactions on Vehicular Technology, 62(3): 1065-1074, 2013.

[16] Boisseau, S., Despesse, G., and Seddik, B. A., Electrostatic conversion for vibration energy harvesting, 2012. Available at: http://www.intechopen.com/books/ small-scale-energy-harvesting/ electrostatic-conversion-for-vibration-energy-harvesting.

[17] Lee, J., Choi, B., Development of a piezoelectric energy harvesting system for implementing wireless sensors on the tires. Energy Conversion and Management, 78: 32-38, 2014.

[18] Priya, S., Advances in energy harvesting using low profile piezoelectric transducers. Journal of electroceramics, 19(1): 167-184, 2007.

[19] Orfei, F., Neri, I., Vocca, H., Gammaitoni, L., Nolinear bi-stable vibration energy harvester at work. In Proceedings of the ASME International Design Engineering Technical Conference & Computers and Information in Engineering Conference, New York, USA, August, 2014.

[20] Nguyen, S. D., Halvorsen, E., and Paprotny, I., Bistable springs for wideband microelectromechanical energy harvesters. Applied Physics Letters, 102(2): 023904, 2013.

[21] Gammaitoni, L., Hänggi, P., Jung, P., and Marchesoni, F., Stochastic resonance. Reviews of modern physics, 70(1), 223, 1998.

[22] Lohndorf, M., Kvisteroy, T., Westby, E., and Halvorsen, E., Evaluation of energy harvesting concepts for tire pressure monitoring systems. PowerMEMS, Freiburg, Germany, November, 2007.

[23] Nakano, K., Cartmell, M. P., Hu, H., and Zheng, R., Feasibility of energy harvesting using stochastic resonance caused by axial periodic force. Strojniški vestnik-Journal of Mechanical Engineering, 60(5): 314-320, 2014.

[24] Zheng, R., Nakano, K., Hu, H., Su, D., and Cartmell, M. P., An application of stochastic resonance for energy harvesting in a bistable vibrating system. Journal of Sound and Vibration, 333(12), 2568-2587, 2014.

[25] Benzi, R., Parisi, G., Sutera, A., and Vulpiani, A., Stochastic resonance in climatic change. Tellus, 34(1): 10-16, 1982.

[26] Luchinsky, D. G., Mannella, R., McClintock, P. V., Stocks, N. G., Stochastic resonance in electrical circuits. I. conventional stochastic resonance. IEEE Transactions on Circuits and Systems II: Analog and Digital Signal Processing, 46(9): 1205-1214, 1999.

[27] Xu, B., Duan, F., Bao, R., and Li, J., Stochastic resonance with tuning system parameters: the application of bistable systems in signal processing. Chaos, Solitons & Fractals, 13(4): 633-644, 2002.

[28] Lee, I. Y., Liu, X., Kosko, B., and Zhou, C., Nanosignal processing: Stochastic resonance in carbon nanotubes that detect subthreshold signals. Nano Letters, 3(12): 1683-1686, 2003.

[29] Dai, D., HEquation., Multiscale noise tuning stochastic resonance enhances weak signal detection in a circuitry system. Measurement Science and Technology, 23(11): 115001, 2012.

[30] Russell, D. F., Wilkens, L. A., and Moss, F., Use of behavioural stochastic resonance by paddle fish for feeding. Nature, 402(6759): 291-294, 1999.

[31] McDonnell, M. D., Abbott, D., What is stochastic resonance? Definitions, misconceptions, debates, and its relevance to biology. PLoS Comput Biol, 5(5): e1000348, 2009.

[32] Lu, Q., Tian, J., Synchronization and stochastic resonance of the small-world neural network based on the CPG. Cognitive neurodynamics, 8(3): 217-226, 2014.

[33] Danziger, Z., Grill, W. M., A neuron model of stochastic resonance using rectangular pulse trains. Journal of computational neuroscience, 38(1): 53-66, 2015.

[34] Rallabandi, V. S., Enhancement of ultrasound images using stochastic resonance-based wavelet transform. Computerized medical imaging and graphics, 32(4): 316-320, 2008.

[35] Yang, Y., Jiang, Z., Xu, B., and Repperger, D. W., An investigation of two-dimensional parameter-induced stochastic resonance and applications in nonlinear image processing. Journal of Physics A: Mathematical and Theoretical, 42(14): 145207, 2009.

[36] Jha, R. K., Biswas, P. K., and Chatterji, B. N., Contrast enhancement of dark images using stochastic resonance. IET image processing, 6(3): 230-237, 2012.

[37] Han, J., Liu, H., Sun, Q., and Huang, N., Reconstruction of pulse noisy images via stochastic resonance. Scientific reports,5(10616): 1-8, 2015.

[38] McInnes, C. R., Gorman, D. G., and Cartmell, M. P., Enhanced vibrational energy harvesting using nonlinear stochastic resonance. Journal of Sound and Vibration, 318(4): 655-662, 2008.

[39] Kawano, M., Zhang, Y., Zheng, R., Nakano, K., and Kim, B., Design and manufacture of perpendicular bi-stable cantilever for vibrational energy harvesting on the basis of stochastic resonance. Journal of Physics: Conference Series, 660(1): 012104, 2015.

[40] Mann, B. P., Sims, N. D., Energy harvesting from the nonlinear oscillations of magnetic levitation. Journal of Sound and Vibration, 319(1): 515-530, 2009.

[41] Stanton, S. C., McGehee, C. C., and Mann, B. P., Nonlinear dynamics for broadband energy harvesting: investigation of a bistable piezoelectric inertial generator. Physica D: Nonlinear Phenomena, 239(10): 640-653, 2010.

[42] Daqaq, M. F., Masana, R., Erturk, A., and Quinn, D. D., On the role of nonlinearities in vibratory energy harvesting: a critical review and discussion. Applied Mechanics Reviews, 66(4): 040801, 2014.

[43] Harne, R. L., Wang, K. W., A review of the recent research on vibration energy harvesting via bistable systems. Smart materials and structures, 22(2), 023001, 2013.

[44] Erturk, A., Inman, D. J., Broadband piezoelectric power generation on high-energy orbits of the bistable Duffing oscillator with electromechanical coupling. Journal of Sound and Vibration, 330(10): 2339-2353, 2011.

[45] Stanton, S. C., McGehee, C. C., and Mann, B. P., Reversible hysteresis for broadband magnetopiezoelastic energy harvesting. Applied Physics Letters, 95(17): 174103, 2009.

[46] Masana, R., Daqaq, M. F., Relative performance of a vibratory energy harvester in mono-and bi-stable potentials. Journal of Sound and Vibration, 330(24): 6036-6052, 2011.

[47] Gu, L., Livermore, C., Passive self-tuning energy harvester for extracting energy from rotational motion. Applied Physics Letters, 97(8): 081904, 2010.

[48] Gu, L., Livermore, C., Pendulum-driven passive self-tuning energy harvester for rotating applications. Power MEMS, Leuven, Belgium, December, 2010.

[49] Gu, L., Livermore, C., Compact passively self-tuning energy harvesting for rotating applications. Smart materials and structures, 21(1): 015002, 2010

[50] Velupillai, S., Guvenc, L., Tire pressure monitoring [applications of control]. IEEE Control Systems, 27(6): 22-25, 2007.

[51] Wei, C., Zhou, W., Wang, Q., Xia, X., & Li, X., TPMS (tire-pressure monitoring system) sensors: Monolithic integration of surface-micromachined piezoresistive pressure sensor and self-testable accelerometer. Microelectronic Engineering, 91: 167-173, 2012.

[52] Kubba, A. E., Jiang, K., A comprehensive study on technologies of tyre monitoring systems and possible energy solutions. Sensors, 14(6): 10306-10345, 2014.

[53] Löhndorf, M., Kvisterøy, T., Westby, E., Halvorsen, E., Evaluation of energy harvesting concepts for tire pressure monitoring systems. Power MEMS, Freiburg, Germany, November, 2007.

[54] Gu, L., Livermore, C., Passive self-tuning energy harvester for extracting energy from rotational motion. Applied Physics Letters, 97(8): 081904, 2010.

[55] Elfrink, R., Matova, S., De Nooijer, C., Jambunathan, M., Goedbloed, M., Van de

Molengraft, J., Van Schaijk, R., Shock induced energy harvesting with a MEMS harvester for automotive applications. In proceedings of the 2011 IEEE International Electron Devices Meeting (IEDM), Washington, USA, December, 2011.

[56] Hu, Y., Xu, C., Zhang, Y., Lin, L., Snyder, R. L., and Wang, Z. L., A Nanogenerator for Energy Harvesting from a Rotating Tire and its Application as a Self‐Powered Pressure/Speed Sensor. Advanced Materials, 23(35): 4068-4071, 2011.

[57] Van den Ende, D. A., Van de Wiel, H. J., Groen, W. A., and Van der Zwaag, S., Direct strain energy harvesting in automobile tires using piezoelectric PZT? polymer composites. Smart materials and structures, 21(1): 015011, 2011.

[58] Mak, K. H., McWilliam, S., and Popov, A. A., Piezoelectric energy harvesting for tyre pressure measurement applications. Proceedings of the Institution of Mechanical Engineers, Part D: Journal of Automobile Engineering, 227(6): 842-852, 2013.

[59] Singh, K. B., Bedekar, V., Taheri, S., and Priya, S., Piezoelectric vibration energy harvesting system with an adaptive frequency tuning mechanism for intelligent tires. Mechatronics, 22(7): 970-988, 2012.

[60] Roundy, S., Tola, J., Energy harvester for rotating environments using offset pendulum and nonlinear dynamics. Smart Materials and Structures, 23(10): 105004, 2014.

[61] Bouendeu, E., Greiner, A., Smith, P. J., and Korvink, J. G., A low-cost electromagnetic generator for vibration energy harvesting. IEEE Sensors Journal, 11(1): 107-113, 2011.

[62] Yang, B., Lee, C., Xiang, W., Xie, J., He, J. H., Kotlanka, R. K., and Feng, H., Electromagnetic energy harvesting from vibrations of multiple frequencies. Journal of Micromechanics and Microengineering, 19(3): 035001, 2009.

[63] Lee, S., Kim, D. H., Durable and sustainable strap Type electromagnetic harvester for tire pressure monitoring system. Journal of Magnetics, 18(4): 473-480, 2013.

[64] Kubba, A. E., and Jiang, K., A comprehensive study on technologies of tyre monitoring systems and possible energy solutions. Sensors, 14(6): 10306-10345, 2014.

[65] Chen, C., Wang, Y., Li, C., Wang, S., and Sung, C., A novel energy harvesting device embedded in a rotating wheel. PowerMEMS and microMEMS, Sendai, Japan, November, 2008.

[66] Haroun, A., Yamada, I., and Warisawa, S., Micro electromagnetic vibration energy harvester based on free/impact motion for low frequency–large amplitude operation. Sensors and Actuators A: Physical, 224: 87-98, 2015.

[67] Wang, Y. J., Chen, C. D., Lin, C. C., and Yu, J. H., A nonlinear suspended energy harvester for a tire pressure monitoring system. Micromachines, 6(3): 312-327, 2015.

[68] Tornincasa, S., Repetto, M., Bonisoli, E., and Di Monaco, F., Energy harvester for

vehicle tires: Nonlinear dynamics and experimental outcomes. Journal of Intelligent Material Systems and Structures, 23(1), 3-13, 2012.

[69] Roundy, S., Wright, P. K., and Pister, K. S., Micro-electrostatic vibration-to-electricity converters. In ASME 2002 International Mechanical Engineering Congress and Exposition, New Orleans, USA, January, 2002.

[70] Frey, A., Seidel, J., and Kuehne, I., System design of a piezoelectric MEMS energy harvesting module based on pulsed mechanical excitation. Power MEMS, Leuven, Belgium, November, 2010.

[71] Manoli, Y., Energy harvesting–from devices to systems. In Proceedings of the ESSCIRC, Seville, Spain, September, 2010.

[72] Eichhorn, C., Tchagsim, R., Wilhelm, N., and Woias, P., A smart and self-sufficient frequency tunable vibration energy harvester. Journal of Micromechanics and Microengineering, 21(10): 104003, 2011.

[73] Miller, L. M., Pillatsch, P., Halvorsen, E., Wright, P. K., Yeatman, E. M., and Holmes, A. S., Experimental passive self-tuning behavior of a beam resonator with sliding proof mass. Journal of Sound and Vibration, 332(26): 7142-7152, 2013.

[74] Eichhorn, C., Goldschmidtboeing, F., Porro, Y., and Woias, P., A piezoelectric harvester with an integrated frequency-tuning mechanism. Power MEMS, Washington, USA, December, 2009.

[75] Ayala, I. N., Zhu, D., Tudor, M. J., and Beeby, S. P., Autonomous tunable energy harvester. Power MEMS, Washington, USA, December, 2009.

[76] Wu, X., Lin, J., Kato, S., Zhang, K., Ren, T., and Liu, L., A frequency adjustable vibration energy harvester. Power MEMS, Sendai, Japan, November, 2008.

[77] Shahruz, S. M., Design of mechanical band-pass filters for energy scavenging. Journal of Sound and Vibration, 292(3): 987-998, 2006.

[78] Shahruz, S. M., Design of mechanical band-pass filters for energy scavenging. Journal of Sound and Vibration, 292(3): 987-998, 2006.

[79] Jung, S. M., Yun, K. S., Energy-harvesting device with mechanical frequency-up conversion mechanism for increased power efficiency and wideband operation. Applied Physics Letters, 96(11): 111906, 2010.

[80] Rastegar, J., Pereira, C., and Nguyen, H. L., Piezoelectric-based power sources for harvesting energy from platforms with low-frequency vibration. SPIE Proceedings, 6171: 617101, 2006.

[81] Mann, B. P., Sims, N. D., Energy harvesting from the nonlinear oscillations of magnetic levitation. Journal of Sound and Vibration, 319(1): 515-530, 2009.

[82] Gammaitoni, L., Neri, I., and Vocca, H., Nonlinear oscillators for vibration energy harvesting. Applied Physics Letters, 94(16): 164102, 2009.

[83] Masana, R., Daqaq, M. F., Electromechanical modeling and nonlinear analysis of axially loaded energy harvesters. Journal of vibration and acoustics,133(1): 011007, 2011.

[84] Zhou, S., Cao, J., Inman, D. J., Lin, J., Liu, S., and Wang, Z., Broadband tristable energy harvester: Modeling and experiment verification. Applied Energy, 133: 33-39, 2014.

[85] Sebald, G., Kuwano, H., Guyomar, D., and Ducharne, B., Experimental Duffing oscillator for broadband piezoelectric energy harvesting. Smart materials and structures, 20(10): 102001, 2011.

[86] Magnus, K., Vibrations, Blackie and Son, London, 1965.

[87] Hagedorn, p., Non-linear oscillations (Translated and edited by Wolfram Stadler), Clarendon Press, Oxford, 1981.

[88] Kramers, H. A., Brownian motion in a field of force and the diffusion model of chemical reactions. Physica, 7(4): 284-304, 1940.

[89] Hänggi, P., Talkner, P., & Borkovec, M., Reaction-rate theory: fifty years after Kramers. Reviews of modern physics, 62(2),:251, 1990.

[90] McNamara, B., Wiesenfeld, K. Theory of stochastic resonance. Physical review A, 39(9): 4854, 1989.

[91] Risken, H., The Fokker-Planck Equation, Berlin, 1984.

[92] Zwanzig, R. W., Contribution to the theory of Brownian Motion. Physics of Fluids (1958-1988), 2(1): 12-19, 1959.

[93] Mann, B. P., Owens, B. A., Investigations of a nonlinear energy harvester with a bistable potential well. Journal of Sound and Vibration, 329(9): 1215-1226, 2010.

[94] Su, D., Nakano, K., Zheng, R., and Cartmell, M. P., On electrical optimization using a Duffing-type vibrational energy harvester. Proceedings of the Institution of Mechanical Engineers, Part C: Journal of Mechanical Engineering Science, 0954406214563736, 2014.

[95] Stoten, D. P., Fusion of kinetic data using composite filters. Energy harvesting from vehicle tires using stochastic resonance. Proceedings of the Institution of Mechanical Engineers, Part I: Journal of Systems and Control Engineering, 215(5): 483-497, 2001.

[96] Available at: http://www.infineon.com/dgdl/SP37_900kPa_PB.pdf?folderId=db3a30431ce5fb52011d52c72ab131a4&fileId=db3a3043382e8373013847cfd97d78a9

[97] Roundy, S., Wright, P. K., and Rabaey, J., A study of low level vibrations as a power source for wireless sensor nodes. Computer communications, 26(11): 1131-1144, 2003.

[98] Cottone, F., Gammaitoni, L., Vocca, H., Ferrari, M., and Ferrari, V., Piezoelectric buckled beams for random vibration energy harvesting. Smart materials and structures, 21(3): 035021, 2012.

[99] Pillatsch, P., Yeatman, E. M., and Holmes, A. S., A piezoelectric frequency up-converting energy harvester with rotating proof mass for human body applications. Sensors and Actuators A: Physical, 206: 178-185, 2014.

[100] Koukharenko, E., Beeby, S. P., Tudor, M. J., White, N. M., O'Donnell, T., Saha, C., and Roy, S., Microelectromechanical systems vibration powered electromagnetic generator for wireless sensor applications. Microsystem technologies, 12(10-11): 1071-1077, 2006.

[101] Kulah, H., Najafi, K., Energy scavenging from low-frequency vibrations by using frequency up-conversion for wireless sensor applications. IEEE Sensors Journal, 8(3): 261-268, 2008.

[102] Arakawa, Y., Suzuki, Y., and Kasagi, N., Micro seismic power generator using electret polymer film. PowerMEMS, Tokyo, Japan, November, 2004.

[103] Lo, H. W., and Tai, Y. C., Parylene-based electret power generators. Journal of Micromechanics and Microengineering, 18(10): 104006, 2008.

[104] Manla, G., White, N. M., and Tudor, M. J., Numerical model of a non-contact piezoelectric energy harvester for rotating objects. IEEE Sensors journal, 12(6): 1785-1793, 2012.

List of Publications

Published Academic Journals (With Reviewing)

(1) Yunshun Zhang, Rencheng Zheng, Tsutomu Kaiuka, Dongxu Su, Kimihiko Nakano, and Matthew P. Cartmell, Broadband vibration energy harvesting by application of stochastic resonance from rotational environments, The European Physical Journal, 224(14): 2687-2701, 2015, DOI: 10.1140/epjst/e2015-02583-7 (Copyright @2015 EDP Sciences and Springer).

(2) Yunshun Zhang, Rencheng Zheng, Kenji Ejiri, Dongxu Su, and Kimihiko Nakano, Modelling analysis for vibration energy harvesting excited by low-speed sutomobile tires, Transactions of the JSME, 82(840): 1-11, 2016, DOI: 10.1299/transjsme.15-00645. (In Japanese) (Copyright @2016 The Japan Society of Mechanical Engineers).

(3) Yunshun Zhang, Rencheng Zheng, Keisuke Shimono, Tsutomu Kaizuka, and Kimihiko Nakano, Effectiveness testing of a piezoelectric energy harvester for an automobile wheel using stochastic resonance, Sensors, 16(10): 1727, 2016, DOI: 10.3390/s16101727 (Copyright @2016MDPI AG).

Proceeding of Academic Conferences (With Reviewing)

(1) Yunshun Zhang, Rencheng Zheng, and Kimihiko Nakano, Feasibility of energy harvesting from a rotating tire based on the theory of stochastic resonance, Journal of Physics: Conference Series PowerMEMS 2014, 557(1): 012097, Hyogo, Japan, 2014, DOI: 10.1088/1742-6596/557/1/012097 (Copyright @2014 IOP Publications).

(2) Yunshun Zhang, Rencheng Zheng, Tsutomu Kaizuka, and Kimihiko Nakano, Study on tire-attached energy harvester for low-speed actual vehicle driving, Journal of Physics: Conference Series PowerMEMS 2015, 660(1): 012126, Boston, USA, 2015, DOI: 10.1088/1742-6596/660/1/012126 (Copyright @2015 IOP Publications).

(3) Yunshun Zhang, Kimihiko Nakano, Rencheng Zheng, and Matthew P. Cartmell, Adjustable nonlinear mechanism system for wideband energy harvesting in rotational circumstances, Journal of Physics: Conference Series MOVIC & RASD, 744(1): 012079, Southampton, UK, 2016, DOI: 10.1088/1742-6596/744/1/012079 (Copyright @2016 IOP Publications).

Proceeding of Academic Conferences (Without Reviewing)

(1) Yunshun Zhang, Rencheng Zheng, Kimihiko Nakano, and Matthew P. Cartmell, Energy harvesting from vehicle tires using stochastic resonance, The 4th Korea-Japan Joint Symposium on Dynamics and Control, pp. 106-109, Busan, Korea, May, 2015.

(2) Yunshun Zhang, Rencheng Zheng, Dongxu Su, and Kimihiko Nakano, Modelling analysis for vibration energy harvesting excited by low-speed automobile tires, Dynamics and Design Conference 2015, No.15-7, Hirosaki, Aomori, August, 2015. (In Japanese)

Proceeding of Academic Conferences (With Reviewing as Second Author)

(1) Michitaka Kawano, Yunshun Zhang, Rencheng Zheng, Kimihiko Nakano, and Beomjoon Kim, Feasibility of energy harvesting using vertical bi-stable cantilever with tip mass based on stochastic resonance, 2015 JSME-IIP/ASME-ISPS Joint Conference on Micromechatronics for Information and Precision Equipment, Kobe, Japan, 2015.

(2) Michitaka Kawano, Yunshun Zhang, Rencheng Zheng, Kimihiko Nakano, and Beomjoon Kim, Modelling and fabrication of perpendicular bi-stable cantilever for vibrational energy harvesting grounded on stochastic resonance, Micro and Nano Engineering 2015, Hague, Netherlands, 2015.

(3) Michitaka Kawano, Yunshun Zhang, Rencheng Zheng, Kimihiko Nakano, and Beomjoon Kim, Design and manufacture of perpendicular bi-stable cantilever for vibrational energy harvesting on the basis of stochastic resonance, Journal of Physics: Conference Series PowerMEMS 2015, 660(1): 012104, Boston, USA, 2015, DOI: 10.1088/1742-6596/660/1/012104 (Copyright @2015 IOP Publications).